

Behaviour and Stability of Shallow Underground Constructions

Jimmy Töyrä

Luleå University of Technology
Department of Civil and Environmental Engineering
Division of Mining and Geotechnical Engineering

2006:76 | ISSN: 1402-1757 | ISRN: LTU-LIC -- 06/76 -- SE

LICENTIATE THESIS

Behaviour and Stability of Shallow Underground Constructions

Jimmy Töyrä

Division of Mining and Geotechnical Engineering

Luleå University of Technology

SE - 971 87 Luleå

PREFACE

The research presented in this thesis was carried out at the Division of Mining and Geotechnical Engineering at Luleå University of Technology. It was performed during the years 2003-2006, under the supervision of Professor Erling Nordlund. The financial support for the project has been provided by SveBeFo, SBUF and Banverket.

First of all I would like to thank Prof. Erling Nordlund for giving me the chance to do this work here at the university and for making time for me in his tight schedule. I also want to thank my reference group, Johnny Sjöberg at Vattenfall Power Consultant AB, Tomas Franzén Managing Director of SveBeFo, Olle Olofsson at Banverket, Anders Fredriksson at Golder Associates AB, Beatrice Lindström at WSP Group and Bengt Niklasson and Björn Stille at Skanska for pointing me in the right direction.

All the people who helped me along the way deserve thanks. Lars Malmgren, David Saiang, Tomas Villegas, Alexander Bondarchuk and Fredrik Perman have helped me with numerical modelling. Catrin Edelbro, Kristina Larsson and Andreas Eitzenberger who got me through all the bureaucracy, Magnus Westblom for playing pool with me, and for all the co-workers at the institution for the interesting discussions during coffee breaks.

I would like to thank the Trailer Park Boys, Mattias, Jonas and Arvid for the adventures in the mountains. Kloot has been moved, long live Kloot.

Hotel Tellus, for staying put. It feels like home. The Mattsson family (Inger, Pär, Ida and Otto) for their support.

Haluan myös kiittää tätejäni Marjattaa, Kirstiä ja Riittaa heidän loppumattomasta avustaan.

My family for giving me the opportunities in life, for the never ending-support, care and love.

Finally, I want to thank my beloved Sara. I'm looking forward to all the adventures that lie ahead of us.

Luleå, December 2006

Jimmy Töyrä

SUMMARY

Due to lack of space on the surface in urban areas there is an increased need for underground constructions. These constructions are often situated at shallow depth. With a better understanding of which parameters that control the behaviour and stability of shallow underground constructions the cost efficiency of pre-investigations and the tunnel construction will be improved.

The objective of this thesis is to identify and describe the important factors that control the behaviour and the stability of shallow seated tunnels. This knowledge will make it possible to determine data which needs to be collected and the accuracy necessary to be able to make reliable analyses. Shallow tunnels are in this work defined as tunnels that have an overburden of less than 0.5 times the tunnel diameter. This thesis consists of a literature review that contains studies of the mechanics and design of shallow tunnels. Furthermore, it contains conceptual numerical analyses as well as numerical analyses of a real case.

The conceptual analyses included factors such as rock mass strength, virgin state of stress, the location of the tunnel in the rock mass and geological structures. The results show that the most important factor concerning the stability is large geological structures. Other factors that can be considered as important are the virgin state of stress and rock mass strength especially the tensile strength, since failure was primarily in the form of tensile yield. From these results, a check list was compiled. It is based on how sensitive the behaviour and stability are to variations of the different factors.

The case study in this thesis is a section of Arlandabanan, Shuttle station 2. It is a shallow tunnel that is seated underneath Terminal 5 of Arlanda airport. The geology of the rock mass was characterised by a clay filled structure, and a mica schist with weaker layers. The comparison between measured deformations and results from the numerical analysis was partly contradictory. Probable reasons are overestimation of the impact of mica schist orientation, the clay filled structure, the load from Terminal 5 as well as the conclusions of the virgin stress drawn from the stress measurements. It also shows that steep structures may be vulnerable combined with surface loads and low horizontal stresses.

SAMMANFATTNING

I takt med ökad urbanisering minskar möjligheten att nyttja markytan och behoven av konstruktioner under jord ökar. Genom bättre förståelse av vilka parametrar som kontrollerar beteendet och stabiliteten för en underjordskonstruktion går det att förbättra kostnadseffektiviteten i förundersökningar och under tunnelbyggnationen.

Målet med detta projekt är att identifiera och beskriva de faktorer som styr beteendet och stabiliteten för en ytlig tunnel. Denna kunskap ska göra det möjligt att bestämma vilka indata som behöver samlas in och vilken noggrannhet som behövs för att kunna göra en relevant analys. Ytliga tunnlar har i denna rapport definierats som tunnlar vars bergtäckning är 0.5 gånger tunnelns diameter. Denna rapport består av en litteraturstudie som behandlar det mekaniska beteendet och design av ytligt belägna tunnlar. Rapporten innehåller dessutom konceptuella numeriska analyser samt numeriska analyser av ett verkligt fall.

I de konceptuella analyserna studerades faktorer såsom bergmassans hållfasthet, det primära spänningstillståndet, tunnelns placering i bergmassan samt geologiska strukturer. Resultaten visade att den viktigaste faktorn att ta hänsyn till vid en stabilitetsanalys är stora geologiska strukturer. Andra faktorer som anses vara viktiga är det primära spänningstillståndet och bergmassans hållfasthet. Eftersom de brott som förekom i bergmassan var dragbrott, är bergmassans draghållfasthet en viktig faktor. Baserat på dessa analyser utformades en lista där faktorernas påverkan på beteendet och stabiliteten beskrevs.

Det verkliga fallet som analyserades var en sektion av Arlandabanan, Shuttle station 2. Stationen är en ytlig tunnel som ligger under Arlandas Terminal 5. Andra faktorer som fanns i detta fall var ett lerslag samt skifferplanen i glimmerskiffern som utgjorde bergmassan. Jämförelsen mellan uppmätta deformationer och resultat från de numeriska analyserna var delvis motstridiga. Troliga förklaringar till detta är överskattning av betydelsen av svaghetsplanen i glimmerskiffern, lerslaget och/eller underskattade horisontalspänningar. Analyserna visade också att branta stupningsvinklar kan vara kritiska när det finns ytlaster och horisontalspänningen är låg.

TABLE OF CONTENTS

1	INTRODUCTION.....	1
1.1	Shallow seated tunnels.....	1
1.2	Objectives and approach.....	2
1.3	Outline of thesis.....	3
2	STABILITY AND PERFORMANCE OF SHALLOW SEATED TUNNELS.....	5
2.1	Mechanics of shallow seated tunnels.....	5
2.1.1	Virgin stresses at shallow depth.....	5
2.1.2	Induced stresses at shallow depth.....	10
2.1.3	Failure modes and failure mechanisms	14
2.2	Design of tunnels at shallow depth.....	15
2.2.1	Stress and deformation analysis	15
2.2.2	Stability analysis	18
2.2.3	Empirical design.....	24
3	CONCEPTUAL NUMERICAL ANALYSES.....	33
3.1	Introduction.....	33
3.2	Conceptual model factors	34
3.3	Input data – Typical Swedish rock mass conditions.....	37
3.4	Model development	39
3.4.1	Model setup and input data	40
3.4.2	Comparison of analytical and numerical solution.....	45
3.4.3	Effect of floor inclination.....	46
3.5	Parameter study	49
3.5.1	Model setup and input data	49
3.5.2	Parameter variation	53
3.5.3	Instability indicators.....	57
3.5.4	Results – Continuum models.....	60
3.5.5	Results – Discontinuum models.....	79
4	IDENTIFICATION OF IMPORTANT FACTORS	85
5	CASE STUDY – ARLANDABANAN	91
5.1	Introduction.....	91
5.2	Model setup and input data.....	93
5.3	Focus areas of the analysis	99
5.4	Results.....	101
5.4.1	Tangential stress around the tunnel boundary.....	101
5.4.2	Deformation of the tunnel boundary	107
5.4.3	Deformation of the ground surface	111

5.4.4	The area of plasticity	115
5.4.5	Extensometer measurements	119
6	DISCUSSION	121
6.1	Conceptual analysis	121
6.2	Case Study	123
6.3	Summary	125
7	CONCLUSIONS	127
8	RECOMMENDATIONS FOR FUTURE WORK.....	129
9	REFERENCES	131

1 INTRODUCTION

1.1 Shallow seated tunnels

Urbanization leads to an increased need for underground space, for railroads, roads, sewers, telecommunication and high voltage cables. These constructions are in many cases situated in urban areas and at shallow depth. Increased environmental demands have resulted in an increased use of conventional tunnelling technique at shallow depths and a decreased use of the so-called cut-and-cover technique. Examples of recent and on-going tunnelling projects in urban areas in Sweden are Arlandabanan, Södra Länken in Stockholm, Götatunneln in Gothenburg and Citytunneln in Malmö.

The mechanical properties and the state of stress in the shallow portions of the earth's crust are much more sensitive to anomalies in the rock mass than at depth. This makes it harder to estimate and measure these properties. Since it is common to make excavations at relatively shallow depth, it is important to increase the understanding of the specific problems and the important factors governing the performance of such constructions in order to improve the design.

Many factors influence the behaviour and the stability of shallow underground constructions. Some factors, among others, are the depth at which the excavation is located, the topography of the ground surface, the reduction of strength and stiffness of the rock mass caused by weathering, geological structures (forming wedges and blocks or structures that are continuous and gently dipping which can lead to large destressed volumes of rock), damage from blasting, loads from buildings at the ground surface and the state of stress in the shallow portions of the bedrock.

Since the stress magnitude at shallow depth is low around the excavation, the risk of destressing of the rock mass in the vicinity of the excavation is large. This implies that gravitational sliding of wedges and blocks are the most probable stability problem. However, if the overburden is heavily weathered and consequently has a low strength, even a low absolute stress magnitude may induce failure and stability problems.

The excavation at shallow depth can lead to subsidence on the surface and thereby damage to buildings in the area. It is very important to minimize the subsidence in urban areas. The load induced in the rock mass by external loads from buildings above the excavation can also affect the excavation in an unfavourable way. The optimum dimension of the underground opening has a large economical and technical importance. For example, if a bearing arch is

formed, in some cases it may not be necessary to redistribute the load from overlying buildings. The need for reinforcements and the choice of excavation method is also affected by the behaviour of the rock mass around the tunnel. Some pertinent questions are:

- How accurately must the virgin state of stress be known to be able to perform realistic analyses?
- How are the results from a stability analysis affected by the precision/uncertainty of strength, stiffness, geological variations, blast damage, and loads from buildings on the ground surface?
- How are the results from an analysis of magnitude and location of subsidence affected by the precision/uncertainty of strength, stiffness, geological variations, blast damage and load from buildings on the ground surface?
- In what way will the uncertainty of the virgin state of stress, stiffness, strength, and the other factors affect the design of tunnels and rock caverns and the reinforcement of these?
- How should the pre-investigations be conducted to decrease the total costs of a project? What parameters need to be determined with highest precision.

1.2 Objectives and approach

The objective of this thesis is to identify the factors that have most impact on the stability of shallow tunnels and constructions in hard rock. This will aid in determining which data needs to be collected and the accuracy needed for a given case so that the design of the tunnel becomes as cost efficient as possible. This work will also provide understanding of which factors are important and which combinations are favourable for the stability.

These objectives were accomplished with conceptual numerical analyses, where the different factors are varied one at a time to find out the impact of each factor on the stability and behaviour of the tunnel. A case study was also carried out. A section of Shuttle station 2 of the Arlandabanan was chosen. It is a well known and well documented shallow tunnel in Sweden that includes many of the factors analysed in the conceptual modelling.

1.3 Outline of thesis

Following this introduction, a literature study is presented in Chapter 2. This will serve as a basis for the following chapters.

To gain information on how the different factors influence the stability and behaviour of shallow tunnels conceptual analyses were performed. In Chapter 3, these conceptual numerical analyses are presented. It starts with a short introduction, followed by a presentation of the input data used for the reference, or base case. The program *FLAC* 5.0 (Itasca 2005a) was used for all continuum models. *UDEC* 4.0 (Itasca 2005b) was used for some complementary analyses of discontinuum problems. *Examine^{2D}* (RocScience, 1996) was used for model development only. A model was developed in *FLAC* to optimise the computational time and minimize boundary effects. To do this, results from models with different sizes and zone sizes were examined and compared to other programs as well as an analytical solution. This is followed by the actual parameter variation analysis and results from this.

Based on the preceding chapter, the identification of important factors is presented in Chapter 4. The impact that the different factors have on the stability of a shallow seated tunnel is discussed.

The analysis of Arlandabanan tunnel section, Shuttle station 2, is presented in Chapter 5. After a short introduction, the model setup and input data is given. The results from the analysis as well as measurements conducted at the site while excavating the tunnel section ends the chapter.

Discussions on both the conceptual analyses and the case study are presented in Chapter 6 and concluded in Chapter 7. Finally, in Chapter 8, recommendations to future work are given.

2 STABILITY AND PERFORMANCE OF SHALLOW SEATED TUNNELS

2.1 Mechanics of shallow seated tunnels

Behaviour and stability of a shallow tunnel does not only include the tunnel itself, it also includes the behaviour and stability of the ground surface. Deformations on the ground surface may be of great importance for the infrastructure and buildings in the vicinity of the tunnel.

2.1.1 *Virgin stresses at shallow depth*

The state of stress at shallow depth is often complex and seldom measured and reported. This means that stress measurements reported in the literature are often from a depth greater than 50 m and the stresses for the shallower portions of the bedrock are often estimated by extrapolation.

The material properties of a rock mass are highly variable parameters. According to Leijon (1989) the random measuring error in the data obtained with overcoring corresponds to a standard deviation of ± 2 MPa in the average normal stress. Considering that the stresses may be of the same magnitude as the error near the surface it is obvious that the uncertainty in the measured stresses at shallow depths is great.

The undisturbed state of stress (virgin) at shallow depth is much more sensitive to factors like weathering, irregular topography, residual stresses, erosion and melting of land ice than at greater depth. At shallow depth irregular topography may alter both the stress directions and the stress magnitude, weathering may reduce the already low stresses, geological structures may create large destressed blocks and zones, and residual stresses can create large anomalies in the state of stress.

The ratio between the horizontal and the vertical stresses are probably greater than at greater depth. This is partly because the tectonic stresses at shallow depth represent a larger part of the total state of stress than the gravitational stresses. Furthermore, the fact that erosion and melting of the land ice affects the ratio at shallow depths contributes more to a higher horizontal to vertical stress ratio.

The stresses that exist in the rock mass are related to the weight of the overburden but also to its geological history. Knowledge of the *in situ* state of stress in a rock mass is important in civil and mining engineering. The stress magnitudes in the rock mass generally increase with

depth. Consequently, stress-related problems such as failure due to high stress magnitude also increase with depth. However, excavations at shallow depth may also be challenging, either because of high horizontal stresses or due to the lack of horizontal stresses (Amadei and Stephansson, 1997).

Rock stress can be divided into virgin stress and induced stress. The virgin (or *in situ*) stresses are those existing before any artificial disturbance, while induced stresses are created by artificial disturbances like excavation and drilling or induced by changes in natural conditions such as drying and swelling.

The virgin state of stress is normally described with one vertical stress and two horizontal stresses that are denoted σ_v , σ_h and σ_H . The vertical principal stress is usually a result of the weight of the overburden per unit area above a specific point in the rock mass and is normally assumed to be a function of depth and is defined as

$$\sigma_v = \rho g z \quad (2.1)$$

where ρ is the density of the rock mass (kg/m^3), g is the gravity acceleration (m/s^2), and z is the depth below ground surface (m).

The horizontal component due to gravitational loads depends on the rock mass properties. If the material can be considered linear-elastic and isotropic and a one-dimensional state of strain is assumed, the average horizontal stress is defined according to the theory of basic elasticity as

$$\sigma_H = \frac{\nu}{1-\nu} \sigma_v \quad (2.2)$$

where ν is Poisson's ratio ranging from 0.15 to 0.35 for most rock types, with a common value of 0.25.

Equation (2.2) assumes that the rock mass is isotropic, but this is seldom true on a larger scale. Anisotropy is common in rock and can be a result of bedding, stratification, schistose planes, or jointing. Anisotropy is often divided into transversely isotropy and orthotropic anisotropy. A transversely isotropic material is a material that has different properties in two directions, i.e., there are isotropic planes, while an orthotropic material has different properties in all three directions, i.e. there are three orthogonal planes of elastic symmetry.

Factors that affect the horizontal stresses

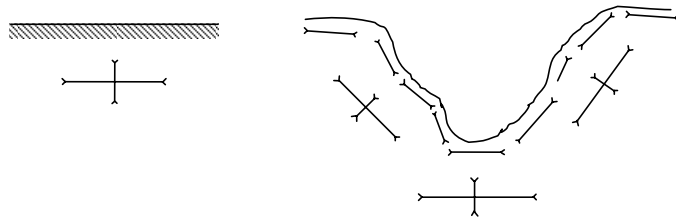
A contribution mainly to the horizontal stresses are the tectonic forces that come from the interaction of the tectonic plates, with each other and with the earth's mantle resulting in boundary forces between the plates. Two groups of forces are responsible for the tectonic stresses, namely broad-scale tectonic forces and local tectonic stresses. The broad-scale tectonic forces are forces acting in lithospheric plate boundaries such as shear tractions at the base of the lithosphere, slab pull at subduction zones, ridge push from oceanic ridges and trench suction. Local tectonic stresses are related to bending of the lithosphere due to surface loads, isostatic compensation and downbending of oceanic lithosphere. The tectonic stresses are constant in areas where the length and width are several times the thickness of the elastic part of the lithosphere (Zoback et al., 1989). Tectonic forces will give a constant contribution which means that a horizontal stress will exist that is non-zero at ground level and that the stress will increase with the depth due to the gravitational stresses. In Scandinavia it is principally the driving forces from the accretion zone (the Mid-Atlantic ridge) that contribute to the horizontal stresses.

Another form of difference in elastic constants is anisotropy in which the values of deformation modulus and Poisson's ratio may vary with direction of a homogeneous rock mass. Anisotropy can influence both the magnitude and orientation of local principal *in situ* stresses and should not be ignored in the evaluation of stress measurement data (Amadei, 1983). This is not dealt with further in this work

Under periods of time the crust has been loaded by land ice, layers of sedimentary rock and sediments, all of them several kilometres thick. The crust has been deformed plastically from the load of these layers and adjusted to the present state of stress. When the rock and the sediments erode and when the ice melts the vertical and horizontal stresses decrease. It is considered that erosion and melting of land ice results in an increase the magnitude of σ_H relative to the magnitude of σ_v .

An irregular topography affects the magnitude and direction of the virgin stresses, see Figure 2.1. The influence of the topography is large near the surface and will decrease with depth and a rough estimation can be obtained by examining hills and valleys with compressive respectively tension loads on a flat surface. The stresses that arise when a half space is loaded with a uniformly distributed or a linear varying load can be solved through integration of the solution of a linear load.

A)



B)

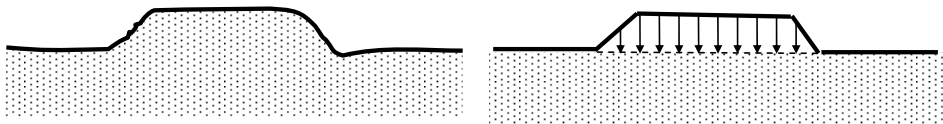


Figure 2.1 The effect of the primary stresses due to an irregular topography can be estimated by replacing hills and valleys with linear varying loads.

Rock masses are rarely uniform and variations in geology and the existence of geologic structures and heterogeneities may affect the distribution and magnitude of *in situ* stresses and contribute to the scatter often observed in field measurements (Fairhurst, 1986). Hudson and Cooling (1988) identified three cases depending on the relative stiffness of the material in the discontinuity versus the material in the surrounding rock; (1) if the discontinuity is open, the major principal stress is diverted parallel to the discontinuity, (2) if the discontinuity have similar properties as the surrounding rock, the principal stresses are unaffected, and (3) if the material of the discontinuity is rigid, the major principal stress is diverted perpendicular to the discontinuity. Geological structures are significant for the state of stress at shallow depths. An open discontinuity above a tunnel can lead to a destressed zone in the roof so that a bearing arch above the tunnel cannot be formed.

State of stress in Scandinavia

In most cases in Scandinavia, the stress field corresponds to a thrust faulting ($\sigma_H > \sigma_h < \sigma_v$) or to a strike-slip faulting ($\sigma_H > \sigma_v > \sigma_h$) with the general direction of the major horizontal stress of NW-SE. This is considered to originate from the Mid-Atlantic Ridge and from the interaction between the African and the European plate (Berg, 2005).

Stress measurements by hydraulic fracturing and overcoring in Scandinavia analyzed by linear regression of the principal horizontal stress versus depth have been summarized by Stephansson (1993) and can be seen in Table 2.1 and Figure 2.2. σ_H is the maximum horizontal stress, σ_h is the minimum horizontal stress and z is the depth.

Table 2.1 Variation of horizontal stress components with depth in Fennoscandia, Stephansson (1993)

Variation of σ_H and σ_h (MPa) with depth (m)		Type of measurement and depth range (m)
1.	$\sigma_H = 10.4 + 0.0446z$ $\sigma_h = 5 + 0.0286z$	Leeman-Hiltscher overcoring (0-700)
2.	$\sigma_H = 6.7 + 0.0444z$ $\sigma_h = 0.8 + 0.0399z$	Leeman-type overcoring (0-1000)
3.	$\sigma_H = 2.8 + 0.04z$ $\sigma_h = 2.2 + 0.024z$	Hydraulic fracturing (0-1000)

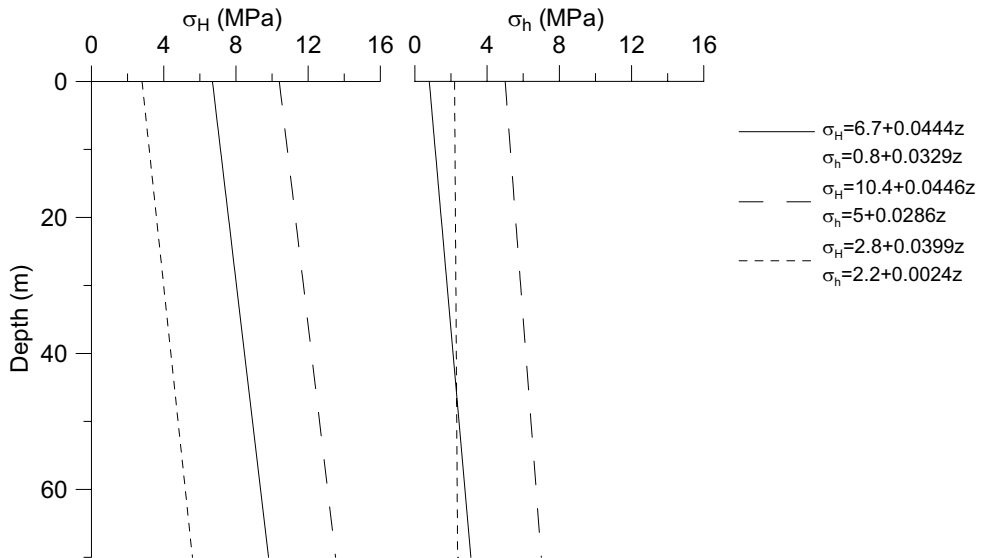


Figure 2.2 Principal states of stress for different measurement methods, compiled by Stephansson (1993).

Berg (2005) has studied results from stress measurements conducted in Sweden at shallow depth (10 – 50 m) with the overcoring technique from four different sites. The results showed that stress measurements at shallow depth give a relatively large scatter compared to stress

measurements at greater depth, both within a measurement level, between different levels and at different sites.

Furthermore, Berg (2005) compared the results from the study with the regression line presented by Stephansson (1993), see Table 2.1 (3) and Figure 2.2. This comparison showed that the regression line did not fit the shallow stress measurements very well, although it cannot be said whether it overestimates or underestimates the stress conditions at shallow depth.

2.1.2 Induced stresses at shallow depth

When a tunnel is excavated, the rock that is left around the open space has to carry more load since the support from the rock that existed earlier in the now excavated cavity has been removed. The redistributed stresses are called secondary or induced stresses.

If the horizontal stresses are assumed to be greater than the vertical stresses, the redistributed stresses will form major principal stress trajectories that will have the shape as shown in Figure 2.3.

Shape of tunnel

The low stress levels at shallow depths are particularly critical if the shape of the tunnel is badly chosen, which could lead to unnecessarily low stress levels in the tunnel roof.

“Streamlined” sections in the direction of the major principal virgin stress are preferred to minimize the risk of a destressed roof, while a tunnel section with a flat roof will redistribute the stresses away from the tunnel boundary into the rock, see Figure 2.3.

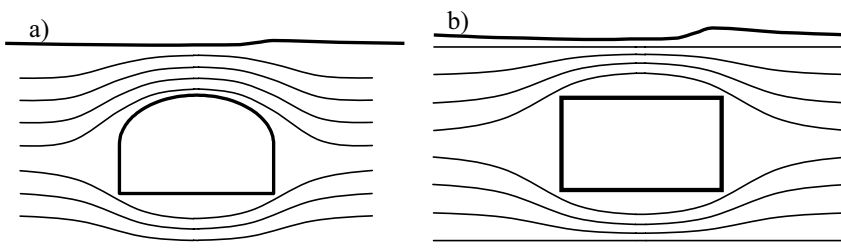


Figure 2.3 Stress trajectories around a) an arched roof and b) a flat roof.

When the virgin horizontal stress is greater than the virgin vertical stress, like it usually is at shallow depth in Scandinavia, the stress situation can lead to destressed tunnel walls. A rounded tunnel shape will decrease the risk of destressed tunnel walls.

Less overburden will in most cases result in lower stresses around the tunnel. Thus, the risk of slip along pre-existing geological structures and fallouts in the roof and walls of the excavation increases. A thin overburden could also mean that concentrations of horizontal stresses can occur above the excavation, leading to stress-induced failure.

Weathering, topography and geological structures

If the overburden is weathered and has decreased strength and stiffness, the horizontal stress trajectories will most likely be redistributed from the ground surface and be concentrated beneath the tunnel instead of in the tunnel roof. This leads to a destressed tunnel roof, see Figure 2.4.

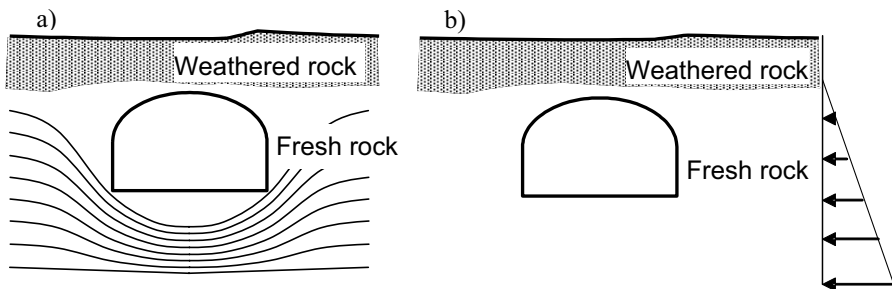


Figure 2.4 The stress situation for a shallow seated tunnel in weathered rock, a) the stress trajectories and b) the distribution of the virgin horizontal stresses.

As discussed earlier, an irregular topography affects the magnitude and direction of the virgin stresses. For example, a valley above a tunnel may result in stress concentrations above the tunnel, which can lead to stress-induced failure in the roof of the tunnel, see Figure 2.5. A hill above the tunnel may lead to larger vertical stresses and unchanged horizontal stresses compared to a flat overburden. An irregular topography can also lead to an extremely thin overburden.

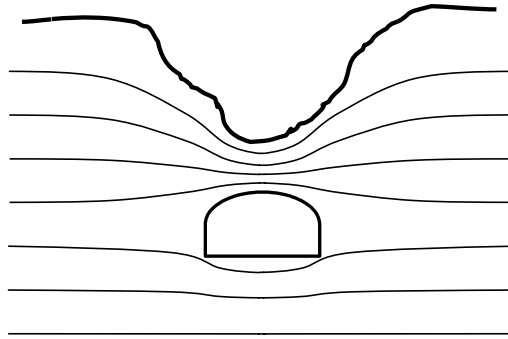


Figure 2.5 The stress trajectories of a tunnel beneath a valley.

Geological structures such as a destressed block in the form of a nappe or an open discontinuity can create a stress shadow and if larger volumes are isolated it can lead to large volumes of destressed rock, see Figure 2.6. These areas of destressed rock are very sensitive to gravitational fallouts of blocks and wedges.

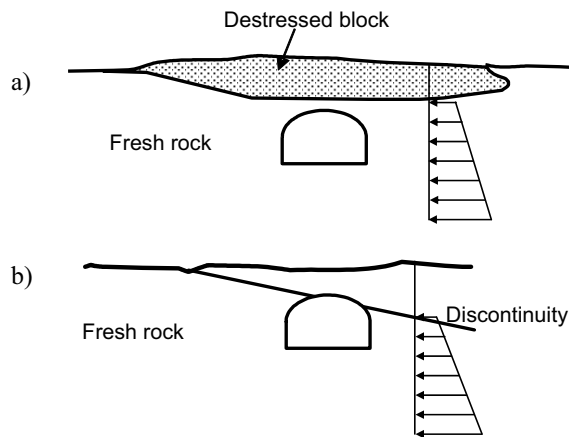


Figure 2.6 Geological structures that can lead to large volumes of destressed rock, a) a destressed block in form of a nappe, b) an open discontinuity.

Loading from foundations

The stresses in the rock caused by a load at the ground surface can be derived using linear elastic theory and the solution by Boussinesq (1883) for a point load applied to a semi-infinite body. A number of solutions for different loading situations are presented in the rock mechanics literature for isotropic as well as anisotropic rock masses (see for instance Poulos and Davis, 1974, and Gaziev and Erlikhman, 1971).

The effect of the load located on the ground surface on the stability of shallow seated underground excavations depends on whether a bearing arch can form above the roof of the tunnel or not. The effect of the surface load on the stability of the tunnel and subsidence of the ground surface, therefore, decreases with increasing virgin horizontal stress.

Damaged rock around the tunnel

The stability of an underground structure is very much dependent on the integrity of the rock immediately surrounding the excavation. Gravity driven fallouts from the roof of the tunnel are especially related to the interlocking of the blocks formed in the roof. Blast damage from unrestricted blasting can extend several meters into the rock mass and the zone of loosened rock can lead to instability problems in the rock surrounding the excavation, especially in shallow seated tunnels where the overburden is limited.

When excavating a tunnel, the rock in the immediate surrounding of the tunnel will have, in addition to the naturally existing cracks and joints, cracks that are caused by blasting and redistribution of stresses. These new cracks and joints will probably decrease the stiffness and the strength of the rock which suggests that the ability to attract stresses will also be reduced, see Figure 2.7.

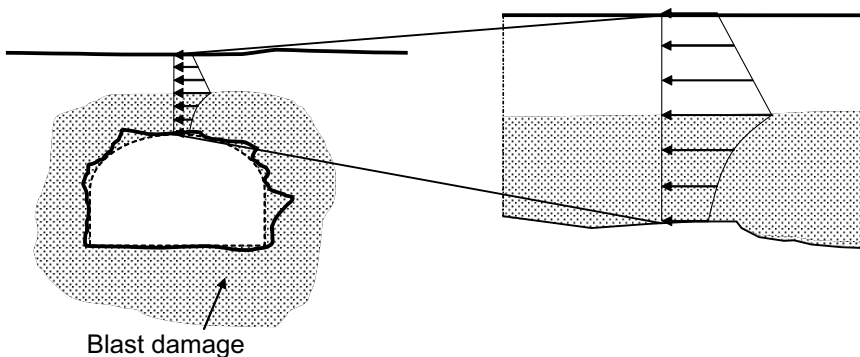


Figure 2.7 The stress and the strength of damage caused by the excavation.

The excavation damaged zone at the Underground Research Laboratory (URL) in Canada was estimated by Martino (2002) through seismic and permeability measurements. The measurements were made on two tunnels at different depths (240 and 420 m). Both tunnels showed similar patterns of excavation damage, with both tunnels having increased damage

immediately surrounding the tunnels. The most highly damaged inner zone (defined as the zone where sharp changes in the rock mass properties and visible cracks have occurred) was relatively narrow, 0.1 to 0.3 m in width. A less damaged outer zone (defined as the zone where gradual changes in the rock mass properties have occurred), where the measured values return towards background values, surrounds the inner zone. In the tunnel located at a depth of 240 m, the outer zone was smaller than for the tunnel located at a depth of 420 m. The difference is believed to be caused by the difference in the magnitude of the *in situ* stresses surrounding the two tunnels, which increases the damage around the deeper tunnel. Martino (2002) assumed that, for the tunnel at greater depth the damage is caused by both the blasting and the altered stress conditions while the damage for the shallower tunnel is only caused by blasting since the stress level is relatively low. The total damaged zone around the shallower tunnel varies between 0.2 and 0.5 m.

The typical background S-wave velocity for the upper tunnel was 3200 m/s, with a decrease of 400 m/s in the inner damaged zone. The background velocity of the P-wave around the same tunnel was 5400 - 5600 m/s and decreased from 400 – 1300 m/s in the inner damaged zone. The reductions in the seismic velocities would correspond to a reduction of 35 – 40% in Young's modulus (if the density is assumed to be constant).

Tests were also performed at the Äspö Hard Rock Laboratory (HLR) in Sweden by Emsley et al. (1997) to estimate the damage and disturbance caused by tunnel excavation. Several seismic techniques were used to measure the rock properties in the damaged zone. All seismic methods showed a significant decrease in velocity close to the tunnel excavated by drilling and blasting. The zone with reduced velocities was 0.3 m up to 1 m occasionally.

2.1.3 Failure modes and failure mechanisms

The rock mass has a complex behaviour due to the existence of natural discontinuities. The mechanical behaviour of the rock mass, therefore, depends on the mechanical behaviour of blocks and joints. Depending on the induced state of stress around the excavation different kinds of stability problems can occur.

Stability problems in jointed rock masses with low stress magnitudes are generally associated with gravity driven fallouts of wedges and blocks from the roof and sidewalls. This failure process is controlled by the three-dimensional geometry of the tunnel and the rock structure (Hoek and Brown, 1980). There must exist at least three joint surfaces that separate the wedge from the surrounding rock mass to form a wedge in an excavation, see Figure 2.8.

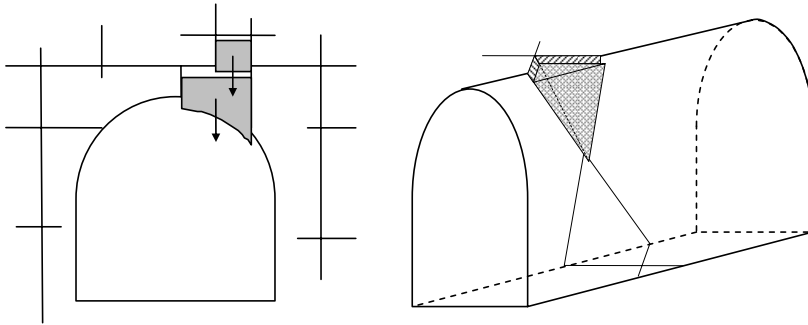


Figure 2.8 Gravity driven wedges and blocks that can form in the tunnel roof and wall.

Stress concentrations above the tunnel due to, for example, irregular topography could cause stress-induced failures. If the rock contains few joints and is brittle, spalling, and in extreme cases, rock bursts may occur.

For intermediate stress conditions, a bearing arch can be formed but the stresses may not be large enough for stress induced failure to occur. In Table 2.2 failure mechanisms for different stress magnitudes in shallow tunnelling are listed.

Table 2.2 Failure mechanisms for different states of stress in shallow tunnelling.

Low stresses and jointed rock	Intermediate stresses	High stresses, few joints and brittle rock
<ul style="list-style-type: none"> - Fallouts of wedges and blocks - Beam failure - Ravelling 	<p>Stresses are enough for a bearing arch to form.</p>	<ul style="list-style-type: none"> - Stress induced failure - Spalling - Rock burst

2.2 Design of tunnels at shallow depth

2.2.1 Stress and deformation analysis

Analytical stress analysis

General closed-form solutions for tunnels with circular cross-section at shallow depth were presented by Mindlin (1939, 1948). The solutions presented gave the expressions for the tangential stresses at the boundary of the circular opening and at the free surface. Mindlin presented solutions for the following loading cases

- a) a tunnel at shallow depth in a uniaxial state of virgin stress (1948),
- b) a tunnel excavated in a rock mass with a gravitational virgin stress state (1939).

The solutions are, however, very complex and the tangential stress is expressed in terms of infinite series and is therefore not presented here.

In 1939 Mindlin presented a solution for the tangential stress at the boundary of a tunnel with a circular cross-section excavated in a rock mass with a gravitational state of stress. He considered three different cases,

- hydrostatic state of stress
- uniaxial state of strain
- no horizontal restraints, that is, no stresses in the horizontal direction.

No numerical examples are presented here. Although the solutions are complex, they may still be used practically to calculate the tangential stresses around a circular opening. Closed-form solutions for other cross-sections have not been found in the literature.

Numerical methods

The rock mass comprising the Earth's upper crust is a discrete system and even though analytical methods may be useful for evaluating the effect of many factors, closed-form solutions do not exist for all geometries. Numerical methods must, therefore, be used to study practical problems. Even though the results obtained by numerical analyses are not exact, the accuracy is sufficient for practical design applications, in particular when considering other uncertainties of the rock mass. Due to differences in the underlying material assumptions, different numerical methods have been developed for continuous and discontinuous problems, see Table 2.3 (Jing, 2003).

Table 2.3 Different numerical methods, after Jing (2003).

Continuous methods	Discontinuous methods
The finite difference method (FDM)	The discrete element method (DEM)
The finite element method (FEM)	The discrete fracture network method (DFN)
The boundary element method (BEM)	

A continuum approach is relevant for intact rock conditions as well as for cases when the discontinuities are so pervasive and closely spaced relative to the size of the problem domain that the rock mass can be represented as a continuum with equivalent rock mass properties, see Figure 2.9. This can be a rock mass property as well as a scale effect. If the rock mass contains either a few joints or a large number of closely spaced joints in several directions, the behaviour will be more or less continuous. If, for a given rock mass, the opening of interest is small or large (with the joint oriented in all directions) compared to the spacing of the joints the behaviour can also be expected to be continuous.

A discontinuum problem is, for example, when the rock mass of interest consists of a number of discrete, interacting blocks. The intact rock and the discontinuities are described separately; see Figure 2.9. In these models the rock mass movements are described with deformation of the intact rock, slips along joint surfaces, separation, and rotation.

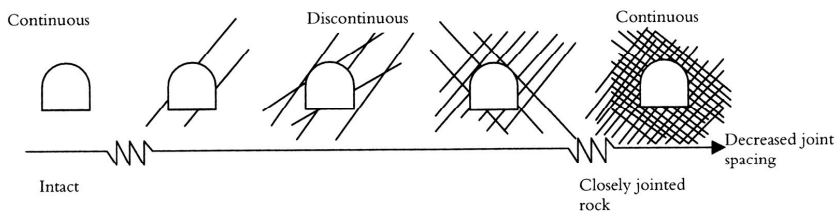


Figure 2.9 Examples of continuous and discontinuous rock masses (Edelbro, 2003).

In the continuum approach normally linear elastic behaviour is assumed for stress levels below strength or yield limit. The result of such analyses can be expressed in terms of stresses, infinitesimal strains and displacements. When the load on the rock exceeds the strength or yield limit, linear elastic behaviour will no longer give relevant stresses and deformations. Constitutive models simulating plastic behaviour can then be used. Because plastic deformations mean permanent displacement changes within the material, plastic strains cannot be defined uniquely in terms of the current state of stress. Plastic strain depends on the

loading history so the theory of plasticity must use an incremental loading approach in which incremental deformations are summed to obtain the total plastic deformation.

The continuum methods can also be divided into groups depending on the way the problem is solved. There are mainly two different approaches, the boundary element approach and the finite element/finite difference approach. In the boundary element method, all boundaries are discretised. The result is the exact solution on the boundary to the used discretisation of the problem. Finer elements will give a result which better represents the solution of the original problem. The boundary element method has limitations. The use of different material behaviour in different parts of a model is often not possible. Plastic models are not always available. For the group of methods based on finite element and finite difference formulations, the whole model is discretised, i.e., all material. The size of the elements with respect to the scale of the problem is crucial for the accuracy of the results. All kinds of constitutive models, such as elastic, plastic, isotropic and anisotropic, are generally available for these methods.

The numerical methods and programs used for the study of shallow seated tunnels must have the ability to consider the ground surface and to model the factors of interest. Continuous models will be used to study the behaviour of a closely jointed rock mass, the effect of weathering of the rock mass, and the damaged zone around the tunnel. The discontinuous models can be used in order to be able to study the effect of individual large- and small-scale discontinuities. Both types of models should also have the ability to model a varying topography, different virgin states of stress, different overburden, and loading applied to the ground surface. Since the stresses may exceed the strength in some cases the models should also be able to simulate non-elastic behaviour.

2.2.2 Stability analysis

Assessing failure mode

Modes of structurally controlled failure can be analysed by the means of the hemispherical projection technique. For a wedge to form in the roof or the walls of a tunnel, at least three joint planes must exist that separate the wedge from the rock mass. This will be visible on the stereonet by the great circles of three joint planes intersecting each other and forming a closed area in the stereo net.

The wedge analysis using hemispherical projection is a method that only considers if the kinematic conditions for a block/wedge are such that sliding can occur. It also considers if the sliding resistance is greater or less than the driving force, under the assumptions that the joint

strength is purely frictional. This methodology can, however, be very conservative, since a small contribution from the stresses in the vicinity of the opening to the normal stresses acting on a joint, may increase the stability considerably.

Block analysis

While hemispherical graphic projections may locate and to some extent judge whether the wedge is stable or not, there are also methods to calculate the safety factor against wedge failure. The factor of safety and an estimation of the weight of the formed wedges can be obtained through an analysis with, for example, the program UNWEDGE (Hoek et al., 1995). The calculation used to determine the wedges assumes that the discontinuities are ubiquitous, in other words that the wedges can occur anywhere in the rock mass. Furthermore, the program assumes that the joints, bedding planes and other structural features included in the analysis are planar and continuous. This means that the program will always detect the largest wedges, which can seem conservative since the size of the wedges will be limited by the persistence and spacing of the structural features. However, the program will allow wedges to be scaled down to more realistic sizes if desired. By typing in the density of the rock, the friction angle, and the cohesion of the joints, the safety factor against wedge failure for the different wedges is obtained.

Compressed arch action - Voussoir Beam Theory

Since the absolute stress magnitudes at shallow depth are generally low, the stability of the underground openings is governed by the possibility of blocks and wedges sliding or falling into the opening. The Voussoir beam theory or compressed arch theory is a method which considers the state of stress around the opening in the equilibrium analysis of blocks and wedges.

Compressed arch action

An arch is a construction which mainly transfer load as compressive force. The classical arch is a number of blocks arranged in such a way that the joints transfer only compressive forces (Stille et al., 2004).

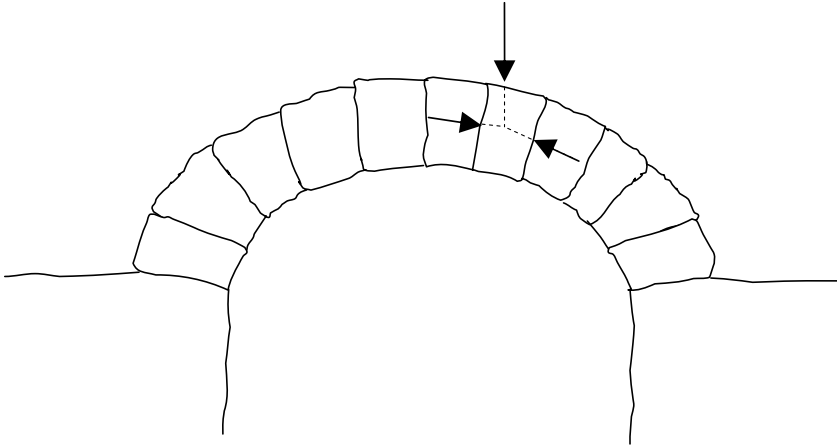


Figure 2.10 Transfer of load in an arch.

An arch can collapse in three ways

- sliding along joints,
- crushing of the joint surfaces or the block material, or
- rotation of blocks.

Sliding along a joint means that the shear stress exceeds the strength of the joint. Crushing or spalling occur when the compressive stress exceeds the compressive strength. Rotation of the blocks takes place if the load induces a bending moment causing a tensile stress in a joint with no tensile strength.

The compressed arch for a certain load $q(x)$, is obtained (Stille et al., 2004) by integration of

$$y'' = -\frac{q(x)}{H} \quad (2.3)$$

where H is the horizontal support reaction according to Figure 2.11.

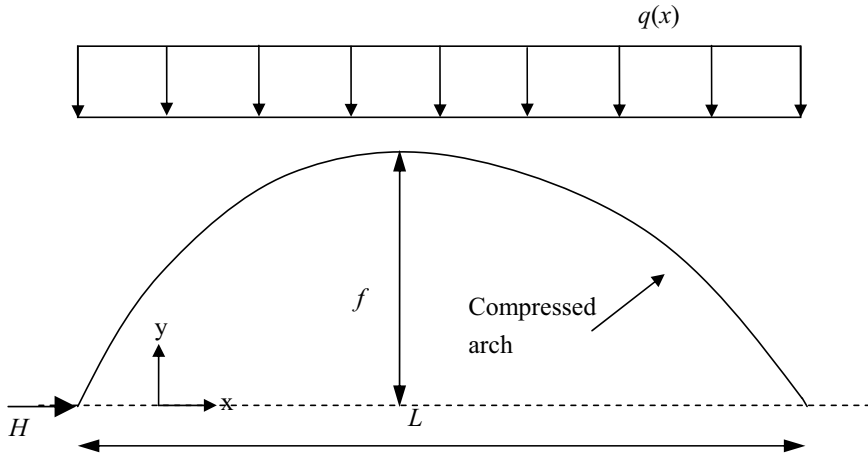


Figure 2.11 Compressed arch.

The expression for the compressed arch can be described as,

$$y = f \left[1 - \frac{(2x)^2}{L^2} \right] \quad (2.4)$$

and maximum load, q , which a compressed arch can carry, is determined by

$$q_{\max} = \frac{8Hf}{L^2} \quad (2.5)$$

which depends on the geometry of the arch (L and f) and the lateral pressure (horizontal support reaction, H).

Voussoir beam theory

The Voussoir beam theory also deals with the development of a compression arch. There are several versions of this model but we will refer here to the one presented by Diederichs (1999). The model considers deflection due to self weight, external loads such as load from the rock above, water pressure and support, and the deformability of the beam.

Rock masses characterized by parallel laminations are often encountered in underground excavations. Laminated rock can be a result of sedimentary layering, extensile jointing, and rock masses created through metamorphic or igneous flow processes or through stress

fracturing parallel to the excavation of massive ground. This structure can be the main factor controlling the stability of roofs of civil excavations or mines.

In most cases the rock mass is not only represented by the lamination partings but also by joint sets cutting through the laminations (Figure 2.12). These joint sets reduce the ability to sustain boundary parallel tensile stresses such as those assumed in conventional beam theory. However, if these joints cut through the laminations at steep angles or if reinforcement has been installed, one can assume that a compression arch can be generated within the beam which will transmit the beam loads to the abutments (Diederichs, 1999).

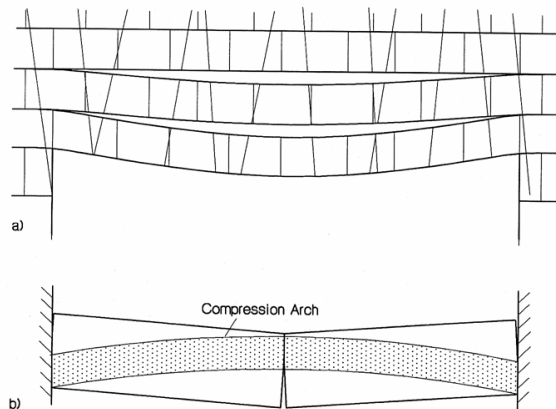


Figure 2.12 a) Jointed rock beam b) Voussoir beam analogue (Diederichs, 1999).

The primary modes of failure in the Voussoir beam model are buckling or snap-through failure, lateral compressive failure (crushing) at the midspan and abutments, abutment slip and diagonal fracturing, see Figure 2.13. Abutment slip or shear failure (Figure 2.13c) is observed when the ratio between span and thickness is low (i.e., thick beams), while crushing (Figure 2.13b) and snap-through (Figure 2.13a) are observed in thinner beams. Ran et al. (1994) showed that if the angle between the cross cutting joints and the normal to the lamination plane is less than 30 to 50 % of the effective friction angle of the joints then the application of the Voussoir beam theory is valid. If the angle between the cross cutting joints and the normal of the lamination plane is larger than 30 to 50 % of the effective friction, then slip along the cross cutting joints and premature shear failure of the beam is likely to occur.

Stimpson and Ahmed (1992) have shown in a physical model of thick laminations that external loading can produce diagonal tensile fracturing (Figure 2.13d) that propagates parallel to the compression arch, from the upper midspan to the lower abutments.

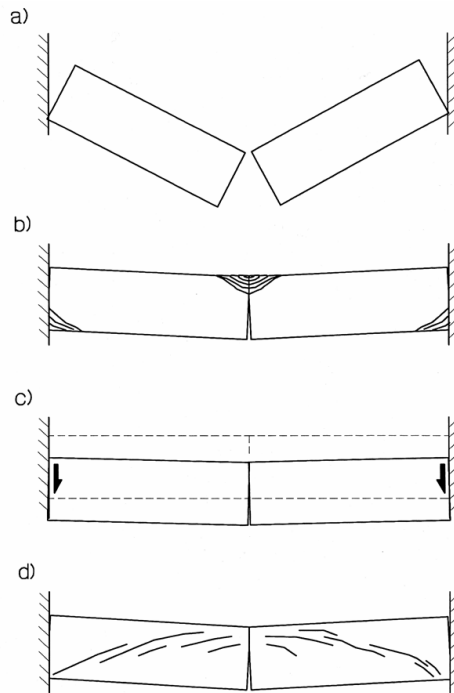


Figure 2.13 Failure modes of the Voussoir beam. a) snap-through, b) crushing at the midspan and abutments, c) abutment slip and d) diagonal fracturing (Diederichs, 1999).

2.2.3 Empirical design

Classification and characterisation

The rock mass is a complex composition of rock and discontinuities and it may be difficult to determine whether a certain rock mass is suitable for construction work or not. Analytical and numerical analyses of rock mechanical problems often needs simplifications or a large quantity of input that might be hard to determine.

Numerous classification/characterisation systems have been developed to judge the usefulness of the rock mass for different constructions. These systems combine the defined properties of the rock mass with practical experience from different kinds of constructions in rock.

In practice, the difference between the process of classification and characterisation of the rock mass is not that large. The difference is such that the rock mass characterisation describes the rock with emphasis on colour, shape, weight, properties etc, while rock mass classification is when one arranges and combines different features of a rock mass into different groups or classes following a specific system or principle (Edelbro, 2003). It is the descriptive terms that constitute the main difference between characterisation and classification. For detailed information, see for instance Palmström (1995).

Rock mass classification is today the most commonly used tool in preliminary design of rock excavations and in assessment of reinforcement. Rock mass classification can also be used for estimating deformation properties and strength of the rock mass, either directly (such as the Q -system) or indirectly (such as Hoek-Brown-RMR). Some of the classification systems have been modified to provide input data that describes the rock mass conditions in the Hoek-Brown and Mohr-Coulomb failure criteria.

RMR (Bieniawski 1974) and the Q -system (Barton et. al., 1974) are probably the most commonly used rock mass classification systems in Sweden today. Both were developed for designing tunnels and rock caverns, but their area of application has expanded to both mining applications and slopes. There are also systems, such as GSI (Hoek et al., 1995) and RMS (Stille et al. 1982). For more information see for example Edelbro et al. (2007).

The classification systems are made up of a number of basic parameters that are estimated in the field. These parameters are rated using tables. The parameters used for RMR and Q are presented in Table 2.4. In RMR , the ratings of the parameters are summed to obtain the RMR rating of the rock mass while the Q -system uses a multiplicative function

$$Q = \frac{RQD}{J_n} \frac{J_r}{J_a} \frac{J_w}{SRF} \quad (2.6)$$

Table 2.4 The basic parameters used for the *RMR* and *Q* systems.

<i>RMR</i>		<i>Q</i>	
1.	Uniaxial compressive strength of intact rock material	1.	<i>RQD</i> : Rock Quality Designation
2.	Rock quality designation (<i>RQD</i>)	2.	J_n : joint set number
3.	Ground water conditions	3.	J_r : joint roughness number
4.	Joint or discontinuity spacing	4.	J_a : joint alteration number
5.	Joint characteristics	5.	J_w : joint water and pressure reduction factor
		6.	<i>SRF</i> : stress reduction factor-rating for faulting, strength/stress ratios in hard massive rocks, and squeezing and swelling rock

The achieved classification value is then used to roughly determine the quality of the rock mass, see Table 2.5..

Table 2.5 Geomechanical classification (*RMR*) of rock masses (Bieniawski, 1974, Hoek and Brown, 1980) and *Q*-value and rock mass quality (Barton et al., 1974).

Sum of rating increments	Class	Description of rock mass	<i>Q</i> -value	Rock mass quality for tunnelling
81 - 100	I	Very good rock	0.001 - 0.01	Exceptionally poor
61 - 80	II	Good rock	0.01 - 0.1	Extremely poor
41 - 60	III	Fair rock	0.1 - 1.0	Very poor
21 - 40	IV	Poor rock	1 - 4	Poor
<20	V	Very poor rock	4 - 10	Fair
			10 - 40	Good
			40 - 100	Very good
			100 - 400	Extremely good
			> 400	Exceptionally good

The rock mass classification systems can also be used to estimate rock mass parameters for further analysis of constructions in rock. For example, the in situ deformation modulus of a rock mass is an important parameter in any form of numerical analysis. Bienawski (1976) and Serafim and Pereira (1983) studied case histories and both proposed a relationship for estimating the in situ deformation modulus, E_m , from RMR , see Table 2.6 (1) and (2), and Figure 2.14.

Barton et al. (1980), Barton et al. (1992) and Grimstad and Barton (1993) proposed a relationship between the Q -system and the deformation modulus, which found good agreement between measured displacements and predictions from numerical analyses, see Table 2.6 (3) and Figure 2.14.

Table 2.6 Relationships for estimation of the in situ deformation modulus from RMR and Q .

1	$E_m = 10^{\frac{(RMR-10)}{40}}$	Serafim and Pereira (1983)
2	$E_m = 2RMR - 100$	Bienawski (1978)
3	$E_m 25 \log_{10} Q$	Barton et al. (1980), Barton et al. (1992) and Grimstad and Barton (1993)

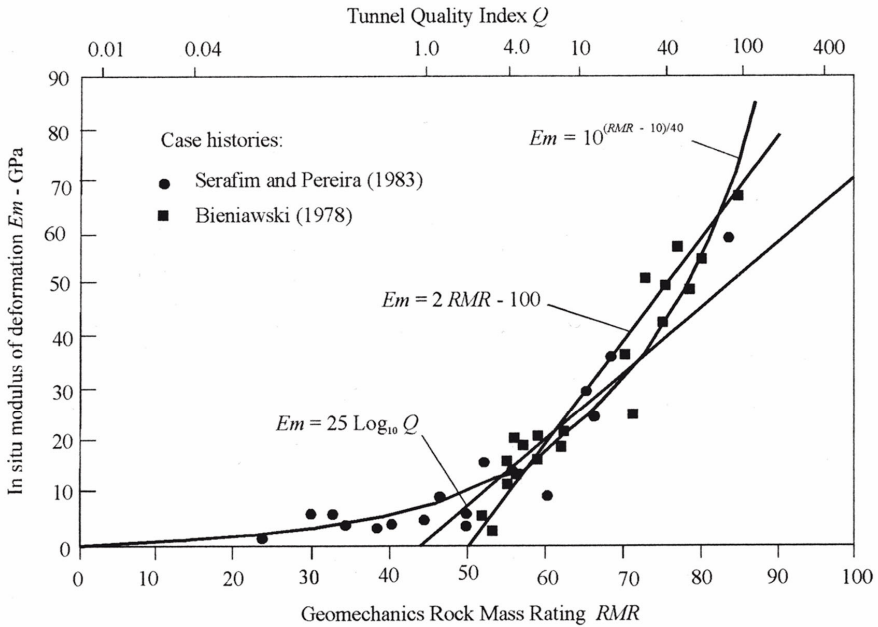


Figure 2.14 Relationships for estimation of the in situ deformation modulus from RMR and Q . (Hoek et al., 1995)

Rocscience Inc. has developed a program, RocLab (RocScience, 2006), for determining rock mass strength parameters based on the Hoek-Brown failure criterion in conjunction with GSI (Hoek et al. 2002). RocLab uses the Geological Strength Index (GSI), the unconfined compressive strength of intact rock, σ_{ci} , the intact rock parameter m_i and the disturbance factor D to determine the generalized Hoek-Brown strength parameters. In this report, this method was used to determine material parameters for the Mohr-Coulomb failure criterion.

Hoek et al., (1995) introduced the Geological Strength Index, as a complement to overcome the deficiencies in RMR for very poor quality rock masses. GSI estimates the reduction in rock mass strength for different geological conditions (Edelbro, 2004).

There are three ways of calculating the GSI :

1. By using the rock mass rating for good quality rock masses ($GSI > 25$)

For $RMR_{76}' > 18$

$$GSI = RMR_{76}' \quad (2.7)$$

For $RMR_{89}' > 23$

$$GSI = RMR_{89}' - 5 \quad (2.8)$$

For both versions, dry conditions should be assumed — i.e., assigning a rating of 10 in RMR_{76}' and a rating of 15 in RMR_{89}' for the groundwater. In addition, no adjustments for joint orientation (very favourable) should be made, since the water condition and joint orientation should be assessed during the rock mass analysis (Hoek et al., 1995). Since it is difficult to estimate RMR for very poor quality rock masses, Hoek et al., (1995) suggested that the Q -system (Barton et al., 1974) should be used for these circumstances, see below.

2. By using the Q -system

For all Q -values:

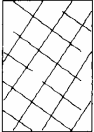
$$GSI = 9 \ln Q' + 44 \quad (2.9)$$

In doing this, both the joint water reduction factor (J_w) and the stress reduction factor (SRF) should be set to 1.

3. By using GSI -classification.

Hoek and Brown (1997) did not specifically recommend the use of the Q -system; rather they recommended using GSI -classification, see Table 2.7 (Hoek et al., 1995). The aim of the GSI system is to determine the properties of the undisturbed rock mass; otherwise, compensation must be made for the lower GSI -values obtained from such locations.

Table 2.7 Estimation of Geological Strength Index (GSI) (Hoek et al, 1997).

<p>GEOLOGICAL STRENGTH INDEX</p> <p>From the letter codes describing the structure and surface conditions of the rock mass (from Table 4), pick the appropriate box in this chart. Estimate the average value of the Geological Strength Index (GSI) from the contours. Do not attempt to be too precise. Quoting a range of GSI from 36 to 42 is more realistic than stating that GSI = 38.</p>		<p>SURFACE CONDITIONS</p> <p>VERY GOOD Very rough, fresh unweathered surfaces</p> <p>GOOD Rough, slightly weathered, iron stained surfaces</p> <p>FAIR Smooth, moderately weathered or altered surfaces</p> <p>POOR Slacksided, highly weathered surfaces with compact coatings or fillings of angular fragments</p> <p>VERY POOR Slacksided, highly weathered surfaces with soft clay coatings or fillings</p> <p>DECREASING SURFACE QUALITY ▾</p>				
<p>STRUCTURE</p>		<p>DECREASING INTERLOCKING OF ROCK PIECES ▾</p>				
 <p>BLOCKY - very well interlocked undisturbed rock mass consisting of cubical blocks formed by three orthogonal discontinuity sets</p>	80	70	60	50	40	
 <p>VERY BLOCKY - interlocked, partially disturbed rock mass with multifaceted angular blocks formed by four or more discontinuity sets</p>	60	50	40	30	20	
 <p>BLOCKY/DISTURBED- folded and/or faulted with angular blocks formed by many intersecting discontinuity sets</p>	50	40	30	20	10	
 <p>DISINTEGRATED - poorly interlocked, heavily broken rock mass with a mixture of angular and rounded rock pieces</p>	40	30	20	10	0	

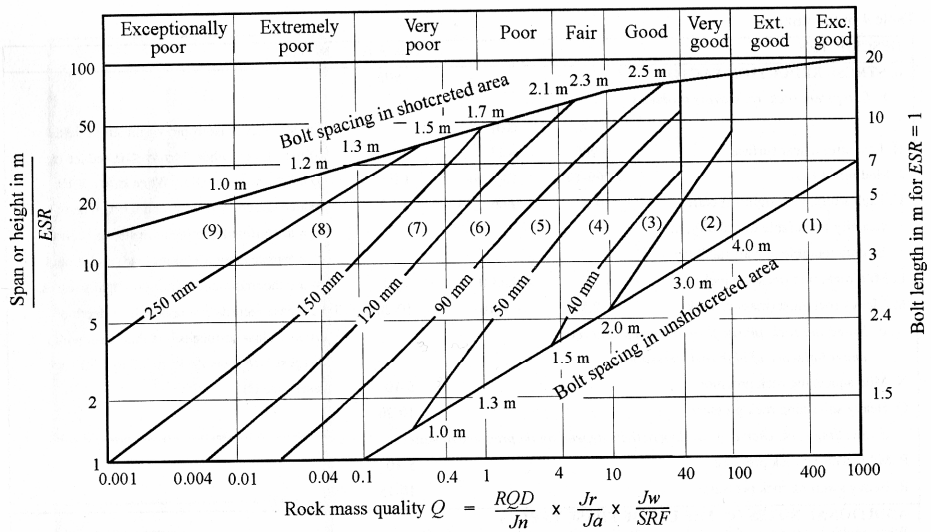
Guidelines for excavation and support have been developed for both *RMR* (see Bienawski, 1989) and the *Q*-system (see Grimstad and Barton, 1993). An example of how *RMR* is used to

estimate the needed support is presented in Table 2.8, where the excavation and support is presented for a 10 m span for different *RMR*-values.

Table 2.8 Guidelines for tunnelling and support of 10 m span following the RMR system (adapted from Bienawski, 1989)

Rock Mass Class	Excavation	Rock bolts (20 mm diameter, fully grouted)	Shotcrete	Steel sets
RMR: 81-100	Full face, 3 m advance	Generally no support required except spot bolting		
RMR: 61-80	Full face, 1-1.5 m advance. Complete support 20 m from face.	Locally, bolts in crown 3 m long, spaced 2.5 m with occasional wire mesh	50 mm in crown where required	None
RMR: 41-60	Top heading and bench, 1.5-3 m advance in top heading. Commence support after each blast. Complete support 10 m from face.	Systematic bolts, 4m long, spaced 1.5-2 m with occasional wire mesh.	50 mm in crown and 30 mm in sides.	None
RMR: 21-40	Top heading and bench, 1-1.5 m advance in top heading. Install support concurrently with excavation, 10m from face.	Systematic bolts 4-5 m long, spaced 1-1.5 m in crown and walls with wire mesh.	100-150 mm in crown and 100 mm in sides.	Light to medium ribs spaced 1.5 m where required.
RMR: <20	Multiple drifts 0.5-1.5 m advance in top heading. Install support concurrently with excavation. Shotcrete as soon as possible after blasting.	Systematic bolts 5-6 m long, spaced 1-1.5 m in crown and walls with wire mesh. Bolt invert.	150-200 mm in crown, 150 mm in sides and 50 mm on face.	Medium to heavy ribs spaced 0.75 m with steel lagging and forepoling if required. Close invert.

The Q-system uses a ratio between the tunnel span and the Excavation Support Ratio (ESR) which is a value related to the intended use of the excavation and ranges between 3 (temporary mine opening) and 0.8 (underground nuclear power stations etc.) and the Q-value to determine the support needed for the excavation, see Figure 2.15.



1. Unsupported

2. Spot bolting

3. Systematic bolting

4. Systematic bolting with 40-100mm
unreinforced shotcrete

5. Fibre reinforced shotcrete, 50-90mm, bolting

Reinforcement categories

6. Fibre reinforced shotcrete, 90-120mm, bolting

7. Fibre reinforced shotcrete, 120-150mm, bolting

8. Fibre reinforced shotcrete, >150mm, with
reinforced ribs of shotcrete, bolting

9. Cast concrete lining.

Figure 2.15 Support categories based on the Q-system (after Grimstad and Barton 1993).

3 CONCEPTUAL NUMERICAL ANALYSES

3.1 Introduction

To gain a better understanding of the performance of shallow seated underground constructions, conceptual numerical analyses were conducted. These analyses were carried out using the programs *FLAC*, *UDEC* and *Examine^{2D}*. *FLAC* (Fast Lagrangian Analysis of Continua) is a two-dimensional explicit finite difference program for engineering mechanics computation and *UDEC* (Universal Distinct Element Code) is a two-dimensional numerical program based on the distinct element method for discontinuum modelling. Both programs simulate both elastic and plastic behaviour of rock and soil. In *FLAC* the materials are represented by zones which form a grid that can be adjusted to fit the shape of the structure to be modelled. The elements behave according to a prescribed linear or nonlinear stress/strain law in response to the applied forces or boundary restraints. The material can yield and flow, and the grid is deformable (Itasca, 2005a). *FLAC* is used in this project when the rock mass is considered to be homogenous and isotropic.

UDEC simulates the response of discontinuous materials, such as jointed rock masses, subjected to either static or dynamic loading. The discontinuous materials are represented as a number of discrete blocks. The discontinuities are treated as boundary conditions between blocks. Individual blocks behave as either rigid or deformable. The deformable blocks are divided into a mesh of finite-difference zones, and each zone responds according to a prescribed linear or nonlinear stress-strain law (Itasca, 2005b). *UDEC* will be used in this project to study the impact on the stability given from large geological structures such as a large single joint transecting the overburden.

Examine^{2D} is a two-dimensional indirect boundary element and displacement discontinuity program for calculation of stresses and displacements around underground and surface excavations in rock (Rock Engineering Group, 1996). Since the material cannot yield in *Examine^{2D}*, this program has only been used in the development of a satisfying *FLAC* model.

The impact of the different factors is analyzed using a conceptual model where the behaviour of the tunnel is studied. This involves a series of numerical simulations in which each parameter is varied. The design of the models and the used input data for all analyses has aimed at as much as possible resemble real case parameters and the design of a shallow tunnel. However, it is important to remember that the results should only be seen as trends showing the impact of different parameters.

3.2 Conceptual model factors

There are a large number of factors that influence the stability of a tunnel at shallow depth. Stability problems occur when the stress exceeds the strength of the rock mass (both in compression and tension) and/or fallouts and sliding along geological structures occur. When the stability of a shallow tunnel is considered, the factors that control the stability can be divided into five groups of factors, namely the strength of the rock mass, tunnel size and location of the tunnel in the rock mass, surface loads, geological structures and the state of stress, Figure 3.1.

Weathering and blast damage decrease the strength of the rock mass and are therefore important factors. Tunnel size and shape is of course of importance, but can seldom be altered. At shallow depth a small tunnel with an arched roof is preferable. The tunnel location is also an obvious factor to consider.

Since shallow tunnels are more frequent in urban areas, loading from buildings and bridges on the surface is common. This affects the tunnel in many ways. Firstly, the weight of the structure on the surface will affect the tunnel stability negatively. There is also a risk that subsidence due to tunnelling will jeopardize the stability of the structure of the surface.

Geological structures such as faults, crushed zones and joints are a part of the rock mass. These are of great importance, especially at shallow depth, when the in situ stresses are relatively low. This means that the state of stress also is a factor to consider. It will affect both failure controlled by geological structures to some degree, as well as stress induced failure.

The factors discussed above are visualized in Figure 3.2.

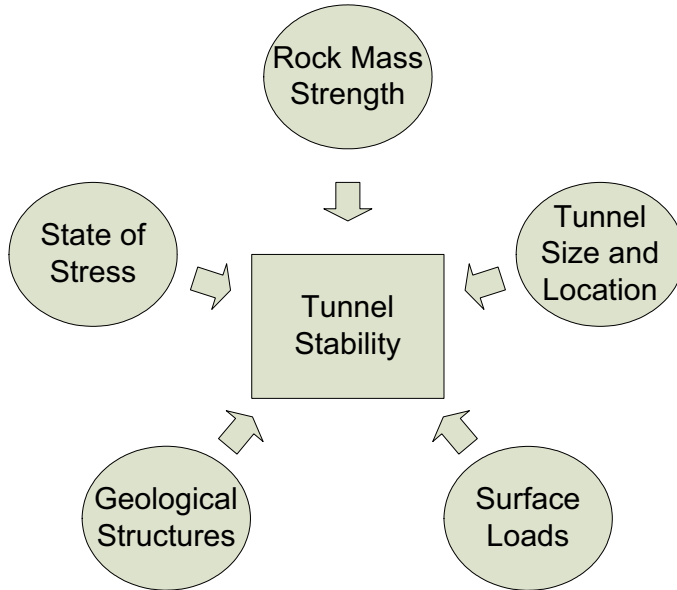


Figure 3.1 Groups of factors that influence the tunnel stability.

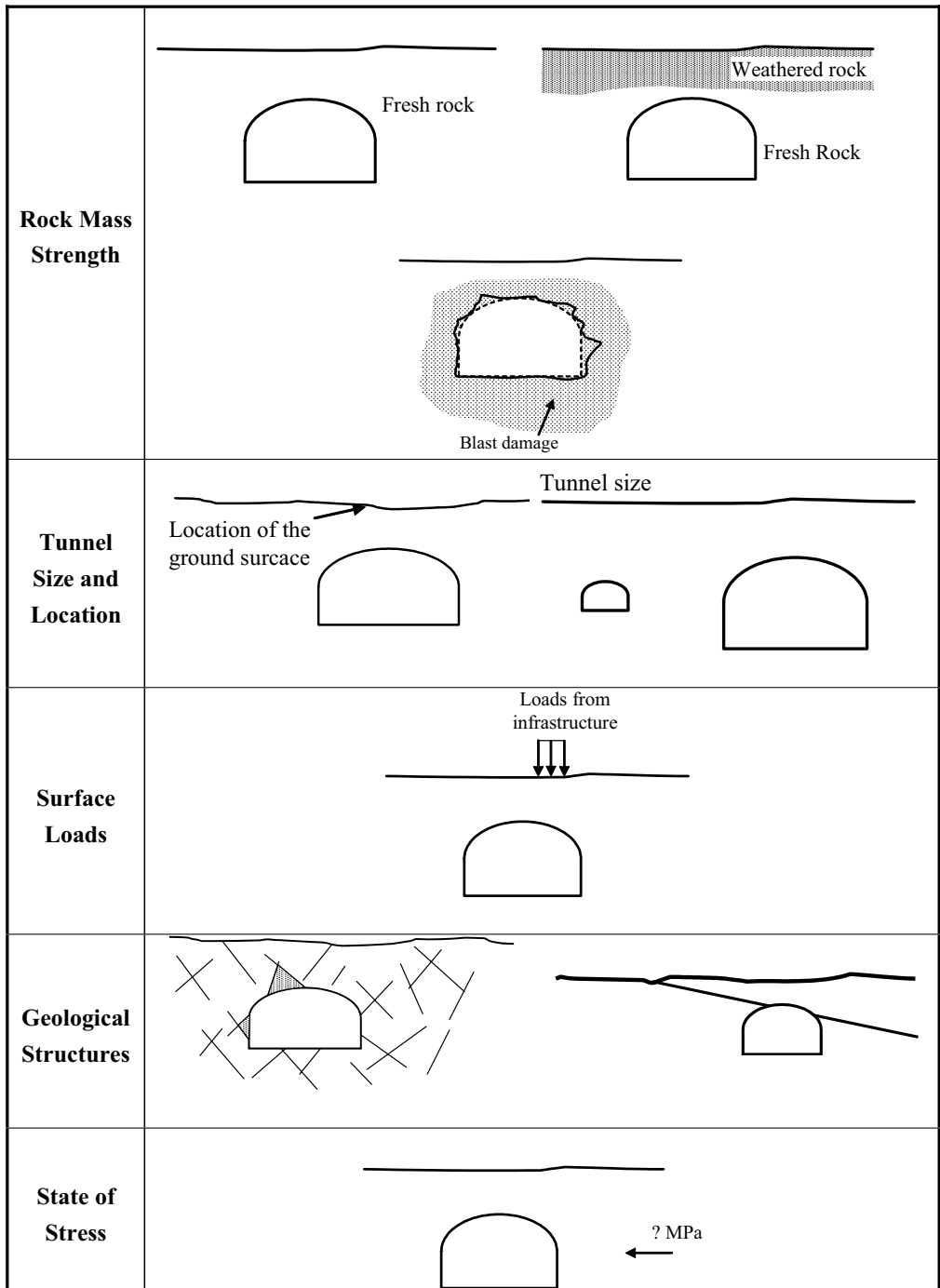


Figure 3.2 Examples of factors that influence the behaviour and stability of shallow tunnels.

In this work conceptual models have been used to study the effect of different factors on the stability and behaviour of a tunnel. A base case was established. The different factors were varied to study the impact of the rock mass parameters on the behaviour and stability of the tunnel. The factors have been varied in such a way to resemble the uncertainty and scatter of measurements and estimations of such parameters in real preliminary tunnel investigations. This was done with respect to the precision and uncertainty of methods used to estimate/calculate the parameters. The parameters that are studied here are the following:

- Virgin stresses
- Intact uniaxial compressive strength
- *GSI*-value
- Rock mass tensile strength
- Overburden
- Young's modulus
- Cohesion/Friction of the rock mass
- Large geological structures
- Excavation damaged zone
- Weathering of the ground surface

Small scale geological structures such as joints that cut through the rock mass, forming wedges and weaknesses have not been studied in this work even though it is considered an important factor. The reason for this is that there are an infinite number of variations of joint lengths, orientations and positions that can occur in a rock mass.

Loads from the ground surface have also been excluded even though it is an important factor. The loads are site specific, and differ greatly from site to site. It was decided to exclude this factor from the conceptual analysis. However, in the case study, Arlandabanan, loads on the rock surface will be present.

3.3 Input data – Typical Swedish rock mass conditions

The input data in this work has been chosen to resemble a typical Swedish rock mass. Obviously there are no typical rock masses, since they differ greatly from site to site, but the chosen data are considered representative of a hard Swedish rock mass that is not exceptionally competent or exceptionally poor.

In the first part of the work conducted for this thesis a preliminary set of data was used. Later a new set of parameters have been used. This was done from a conclusion that the earlier base case somewhat overestimated the rock mass strength. This does not mean that the values used earlier were unrealistic, but that some of the data had to be slightly changed, otherwise more or less linear elastic conditions were obtained. The parameters that have been used in the majority of this work are called the main data set. Both sets can be seen in Table 3.1. The values that are marked in red are the same for both sets and the purple indicates where they are interacting.

The intervals of the parameters have been chosen in reference meetings for this project, and they were chosen to resemble possible variations Swedish rock masses. The variation of the virgin state of stress has been done by using a number of stress versus depth expressions presented in the literature.

Table 3.1 Model data for the preliminary data set and the main data set.

Storhet	Preliminary data set			Main data set		
$RMR (GSI)$		60		48	60	72
ν		0.25			0.25	
σ_{ci} [MPa]	$0.5 \sigma_{ci}$	250	$1.5 \sigma_{ci}$	140	180	220
m_i		33			33	
σ_{H} [MPa]	$1.5 \sigma_v$	$2.8 + 0.04z$	$2.5 \sigma_v$	$2.8 + 0.04z$	$6.7 + 0.0444z$	$10.4 + 0.0446z$
σ_v [MPa]		$2.2 + 0.024z$		$2.2 + 0.024z$	$0.8 + 0.0329z$	$5 + 0.0286z$

Two types of cross-sections have been used in the analyses, the Banverket maximum single track tunnel (cross-section A) and the standard double track tunnel (cross-section B). Cross-section A was used in the first part, and is used in this report only to analyze the effect of size of the model and zones and the geometry of the floor. Since it is more likely that stability problems will occur in openings with a larger span, the double track cross-section was chosen for all further analyses. The double track cross-section is the Banverket 2002 standard double track cross-section, with an extra 0.25 m around the theoretical cross-section which is considered to be closer to the real cross-section after excavation.

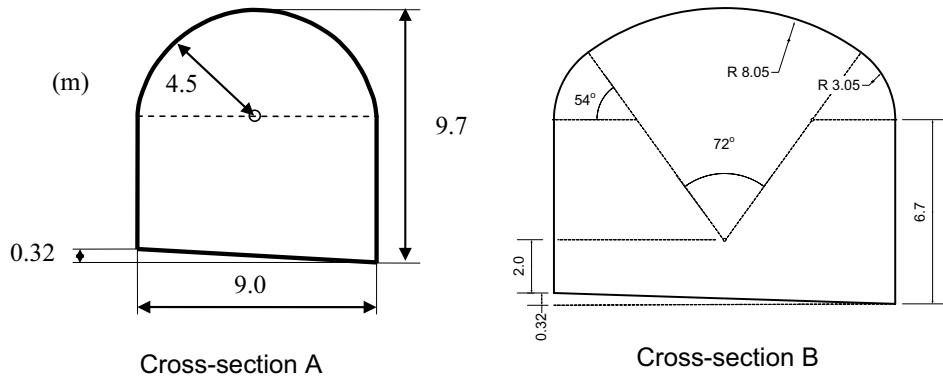


Figure 3.3 Cross-sections used in this work, after Banverket (2002).

3.4 Model development

A finer grid gives more accurate results but too many zones give long calculation times. To achieve accurate results and acceptable computational time, the model consists of an inner grid with finer zones and an outer grid with coarser zones, see Figure 3.4. The ratio of the zone length of the outer and the inner grids was set to 4, since this will give a smooth transition of displacements across the boundaries between the grids according to Itasca (2005a). A sensitivity analysis was conducted to determine how large the zone sizes should be, if the size of the finer grid was significant for the results of the model, and how large the outer model boundaries should be to avoid boundary effects. The cross-section that was used in these analyses is A from Figure 3.3. A circular cross-section was also analyzed in order to compare the model results to an analytical solution.

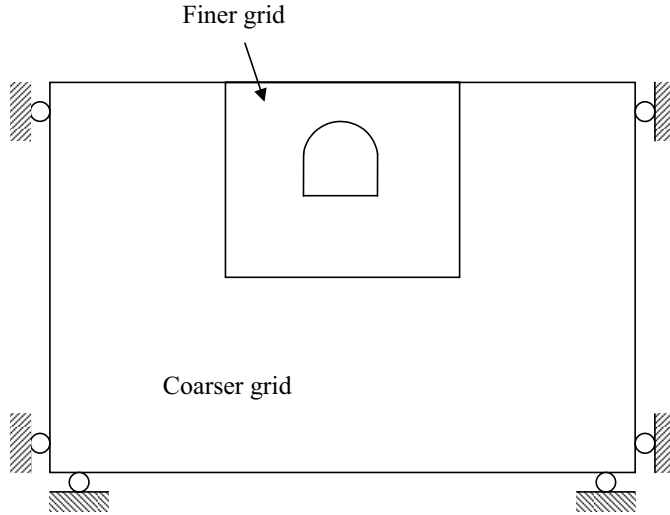


Figure 3.4 Simplified model setup for the analyses made in *FLAC*.

According to the standard cross-section there should be a ditch on one side where the wall meets the floor, however this is not done when the tunnel is excavated due to technical reasons. Instead an inclined floor is used, see Figure 3.3.

A model was also constructed in the program *Examine^{2D}* in order to compare the results from the *FLAC* model with results from another program. The *Examine^{2D}* model used the same cross-section as the model in *FLAC*.

3.4.1 Model setup and input data

An overburden of 5 m was used for all models in this preliminary study. The model was fixed in the y -direction at the bottom and in the x -direction at the vertical boundaries. The virgin state of stress was defined by Table 2.1 ((3) after Stephansson, 1993). The material properties of the rock mass were chosen to resemble a normal Swedish rock mass, with a *RMR*-value of 60, from which Young's modulus was calculated, according to Serafim and Pereira (1983), to 17.8 GPa and a Poisson's ratio of 0.25 was assumed. From a defined base case, variation of the three factors was studied by comparing the base case with two other models according to Figure 3.5, Table 3.2 and Table 3.3.

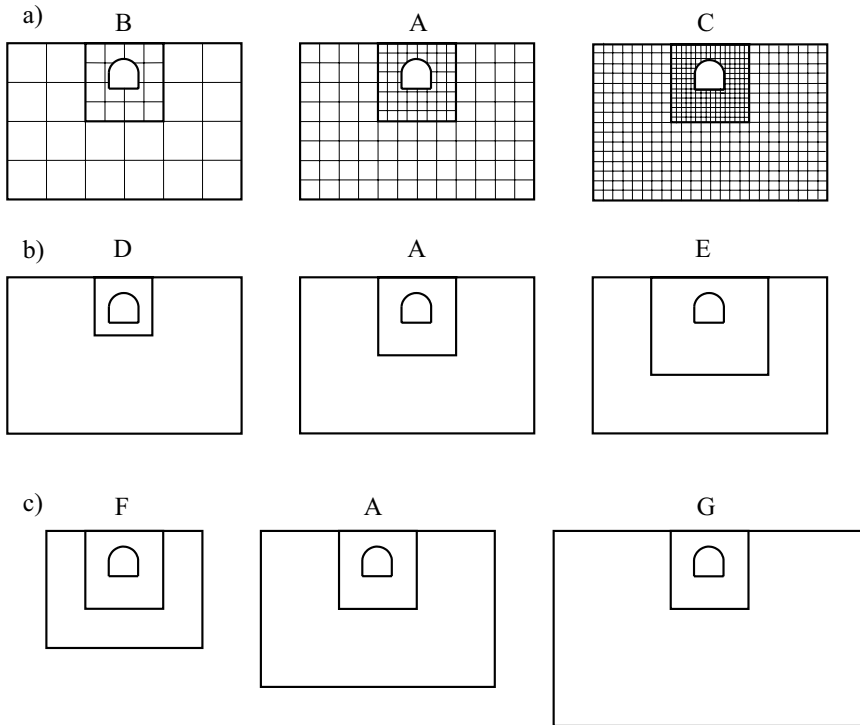


Figure 3.5 The different factors studied in the analysis, a) zone size, b) the size of the inner grid and c) model size.

Table 3.2 Models used in the sensitivity analysis.

Model	Model size Width x Height [m x m]	Inner grid		Outer grid
		Width x Height [m x m]	Zone size (Width x height) [m x m]	Zone size (Width x height) [m x m]
A: Base case	70 x 50	27 x 25	0.25 x 0.25	0.5 x 0.5
B: Fine grid			0.125 x 0.125	0.25 x 0.25
C: Coarse grid			0.5 x 0.5	1 x 1
D: Small inner grid	50 x 40	18 x 20	0.25 x 0.25	0.5 x 0.5
E: Large inner grid		45 x 34		
F: Small model		27 x 25		
G: Large model	100 x 70			

Table 3.3 Input data for the models.

Parameter	Value
E_m	17.8 GPa
ν	0.25
σ_v	$\rho g z$
σ_H	$2.8 + 0.04z$
σ_h	$2.2 + 0.024z$

The input data used for the *Examine*^{2D} model is according to Table 3.3. The boundary element size used in this model was 0.071 m.

The results show that the greatest differences among the models occur for zone size and model size. Very small differences could be observed for different sizes of the inner grid, see Table 3.4. It could also be observed that a model with smaller zones gives a smoother curve over the arch shaped roof, see Figure 3.6b. The results show that different zone sizes and different model sizes are the most important factors to consider and that the model size seems to give the greatest difference. Therefore, model B: Fine grid and model G: Large model, should be combined, if possible.

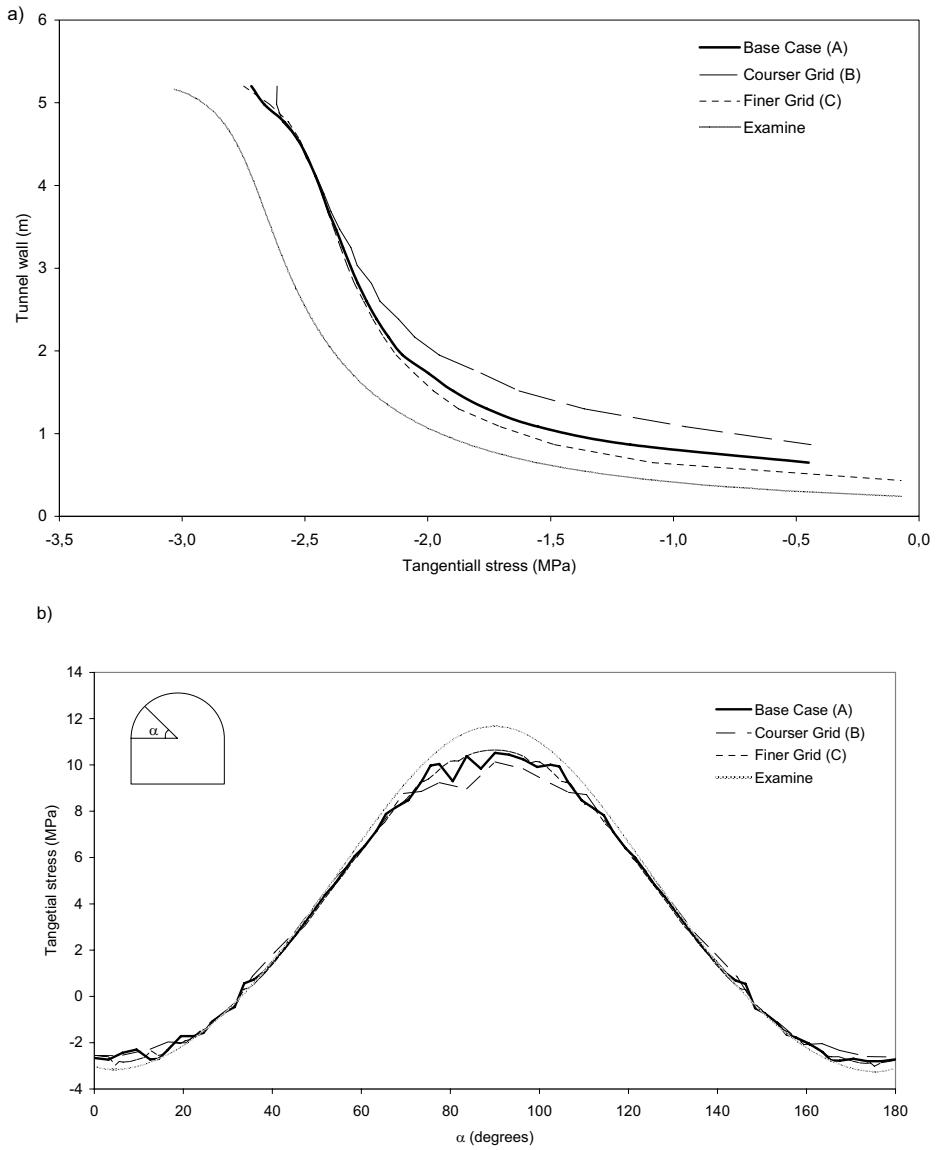


Figure 3.6 The tangential stress on the boundary of the a) tunnel wall and b) roof for the cases with different zone sizes.

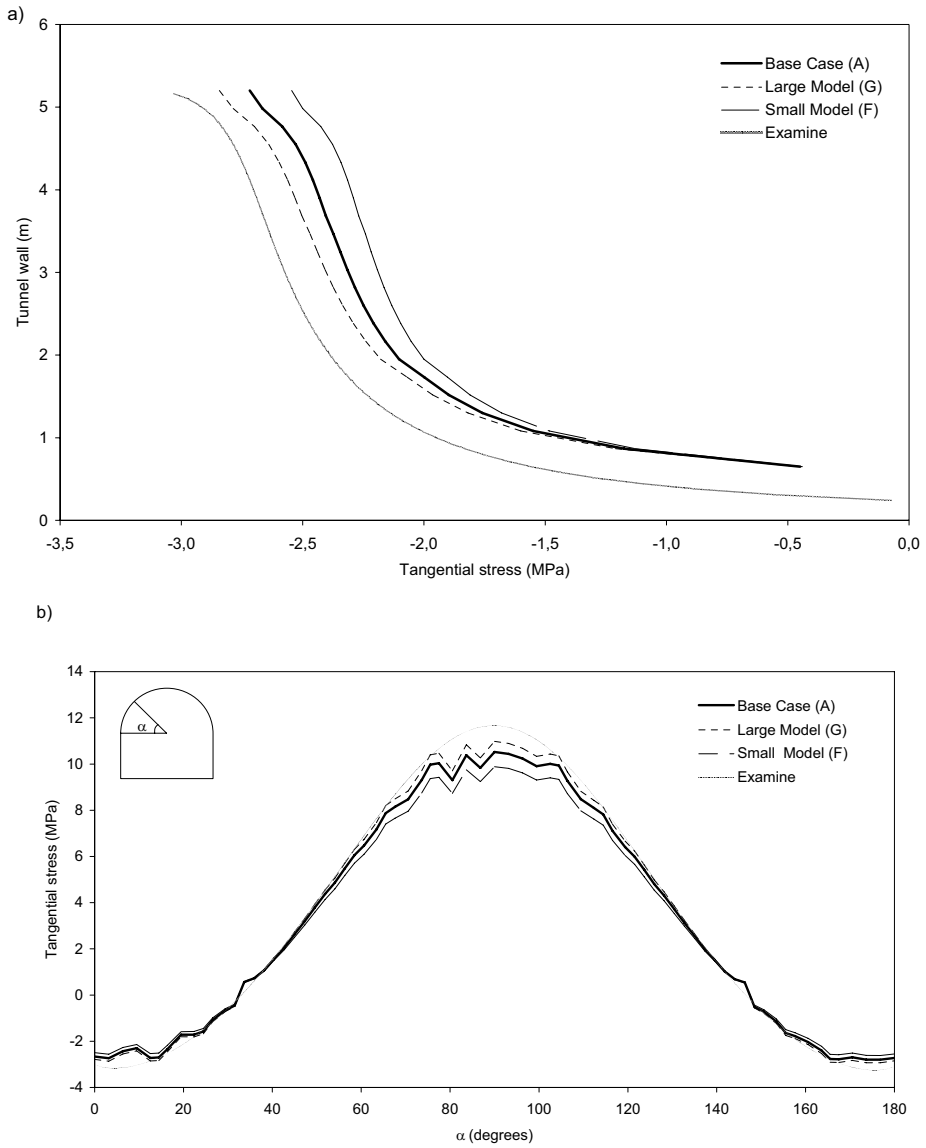


Figure 3.7. The tangential stress on the boundary of the a) tunnel wall and b) roof for the cases with different model sizes.

Table 3.4 The results from the sensitivity analysis.

Zone size	B: Coarse	A: Base case	C: Fine
Vertical displacement of ground surface (mm)	0.429	0.438	0.439
Vertical displacement of tunnel roof (mm)	0.508	0.517	0.519
Tangential stress in tunnel roof (MPa)	10.47	10.90	11.03
Tangential stress in tunnel wall (MPa)	-2.84	-2.88	-2.89
Horizontal displacement of tunnel wall (mm)	-0.551	-0.557	-0.559
Inner grid size	D: Small	A: Base case	E: Large
Vertical displacement of ground surface (mm)	0.437	0.438	0.438
Vertical displacement of tunnel roof (mm)	0.0517	0.0517	0.0517
Tangential stress in tunnel roof (MPa)	10.90	10.90	10.90
Tangential stress in tunnel wall (MPa)	-2.88	-2.88	-2.88
Horizontal displacement of tunnel wall (mm)	-0.557	-0.557	-0.557
Model Size	F: Small	A: Base case	G: Large
Vertical displacement of ground surface (mm)	0.454	0.438	0.411
Vertical displacement of tunnel roof (mm)	0.525	0.517	0.497
Tangential stress in tunnel roof (MPa)	10.22	10.90	11.39
Tangential stress in tunnel wall (MPa)	-2.75	-2.88	-2.98
Horizontal displacement of tunnel wall (mm)	-0.516	-0.557	-0.579

3.4.2 Comparison of analytical and numerical solution

Tests were also performed to compare a *FLAC* model and an *Examine^{2D}* model with an analytical solution from Mindlin (1939). To be able to do this, some new input data had to be used. A circular cross-section had to be used in this model, along with constant horizontal stresses and no vertical stresses, see Table 3.5. The model size and grid size for the *FLAC* model in this study were the same as for the base case, A, in the earlier studies.

Table 3.5 Input data for the models that were compared to an analytical solution.

Parameter	Value
E_m	17.8 GPa
ν	0.25
σ_v	0 MPa
σ_H	3.2 MPa

The results showed that the analytical solution and the *Examine*^{2D} model are identical, while the *FLAC* model shows some discrepancy. One explanation for the discrepancy can be that some zones are distorted in an unfavourable way when the grid is adjusted to fit a circular excavation.

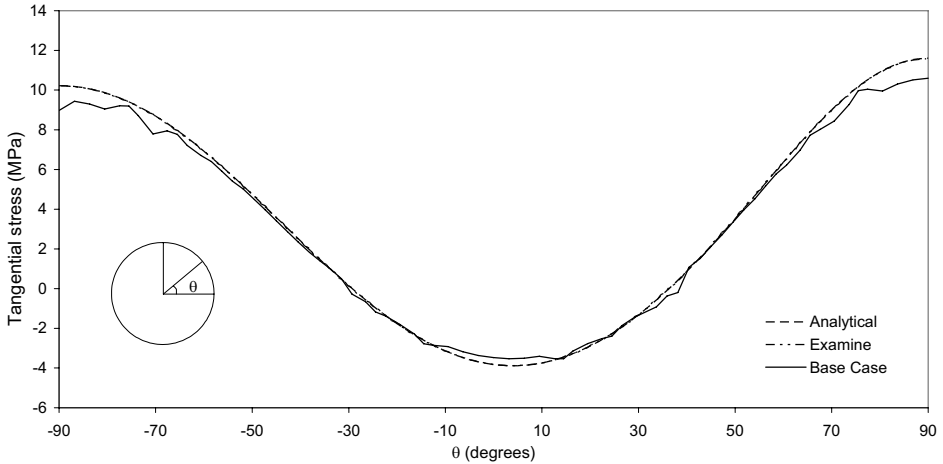


Figure 3.8 Comparison of the tangential stress distribution around a circular tunnel calculated by an analytical solution, *Examine*^{2D} and *FLAC*.

3.4.3 Effect of floor inclination

It is shown in the sensitivity analysis that a larger model gives more accurate results, see Figure 3.6, while a finer grid gives smoother results, see Figure 3.7. Since the computer capacity limits the number of total zones, symmetry with respect to the y-axis has to be assumed for the model. However, the cross-sections according to Banverket (2002) have an inclined floor. To be able to use symmetry the cross-section has to be somewhat altered, from the inclined floor to a horizontal floor, see Figure 3.9. The behaviour of the original and the symmetric model was therefore compared. The model size and grid size for the *FLAC* model in this test were the same as the base case, A, in the earlier tests. The model setup and the input data can be seen in Table 3.6 and Figure 3.10.

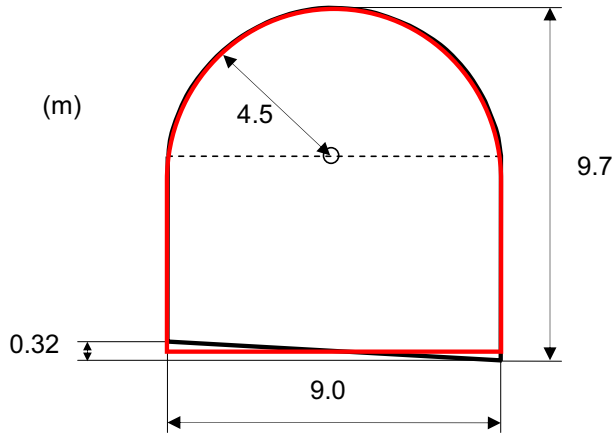


Figure 3.9 Alternative cross-section of a Banverket (2002) single track tunnel.

Table 3.6 Parameters used in symmetry analysis.

Parameter	Value
E_m	17.8 GPa
σ_v	$\rho g z$
σ_H	$2.8 + 0.0399z$
σ_h	$2.2 + 0.0286z$
ρ	2700 kg/m^3

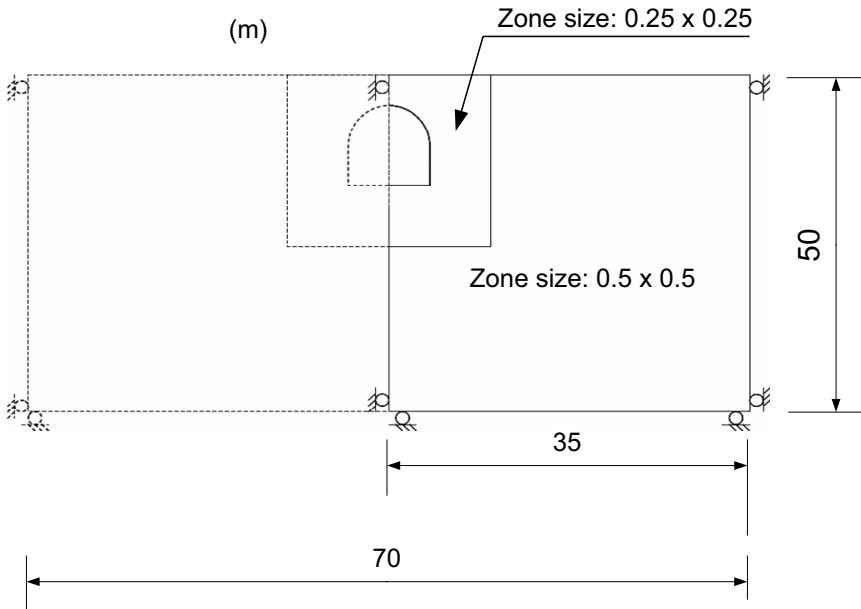


Figure 3.10 Model dimensions used in symmetry analysis.

When examining the roofs of the two different cross-sections, no significant differences can be detected, while small differences can be seen in the lower abutments, see Figure 3.11. Since the floor and lower abutments are not of great importance for the stability of a tunnel, this difference is considered acceptable and a cross-section with a horizontal floor will be used in all further analyses.

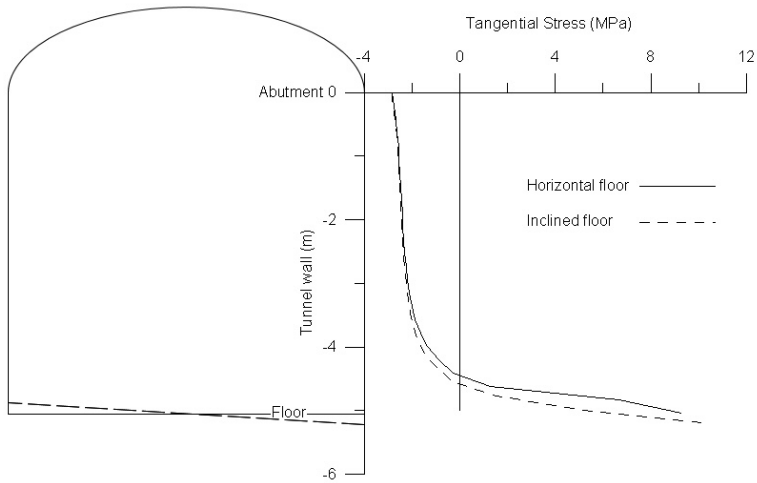


Figure 3.11 The tangential stress in the walls and lower abutments for the two different cross-sections.

3.5 Parameter study

3.5.1 Model setup and input data

From previous analyses the model was set up. It is shown in Chapter 3.4 that the zone size and the model size were of importance to get a reliable model. It was also shown that it is possible to assume vertical symmetry. With this in mind, and with the availability of a computer with more capacity, the model was set up as in Figure 3.12, with a model width of 70 m (when symmetry is assumed) and a height of 70 m. Furthermore, the finer inner grid size is three times the tunnel radius with a zone size of 0.1 x 0.1 m while the coarser grid zone size is 0.2 x 0.2 m.

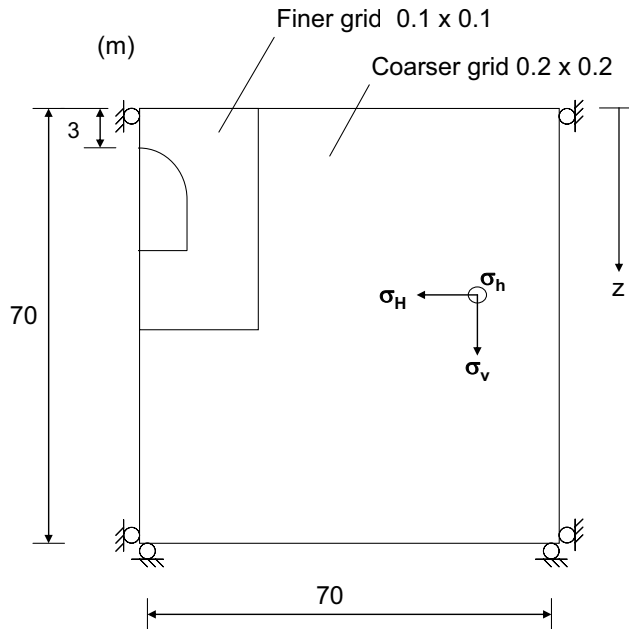


Figure 3.12 Model size, zone size and stress directions for the continuum model

However, when the case of discontinuities was analyzed, a symmetric model could not be used. For these models, *UDEC* 4.0 (Itasca, 2005b) was used. The model setup can be seen in Figure 3.13. This model has the same model size, 140 x 70 m as well as the same cross-section (Figure 3.3b) as the *FLAC* model. The maximum edge length near the tunnel was 0.5 m, and then increased in two steps, to 1.0 m and 1.5 m, as seen in Figure 3.13. Some extra cracks were used to obtain an even grid. These cracks were given high strength parameters to inhibit any slip on these “fictitious” discontinuities. Otherwise, the discontinuum model uses the same strength data, except for additional data for the discontinuity. A variation of discontinuity parameters, as well as a variation of dip angles, α , were used in the discontinuum analysis. The discontinuity, marked in blue in Figure 3.13, was oriented so that it intersected the tunnel in the roof centre point for all dip angles.

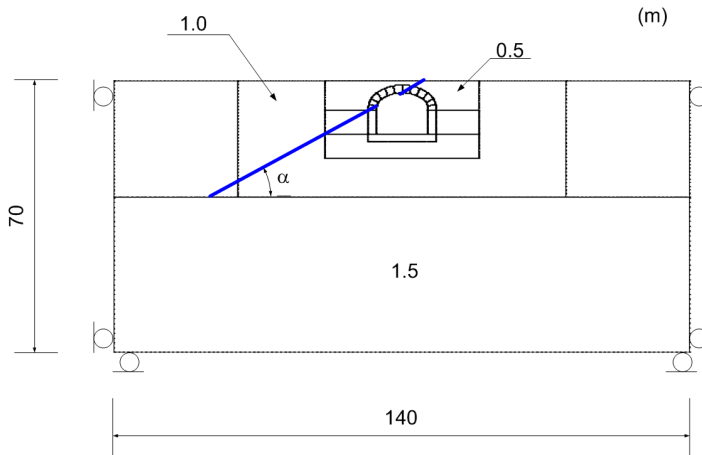


Figure 3.13 Model size and maximum edge length of the discontinuum model.

The cross-section used is the Banverket (2002) normal double track cross-section as described in Figure 3.3, but with a horizontal floor, see Figure 3.14.

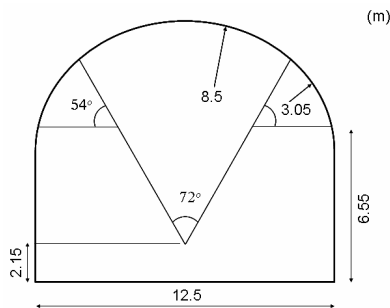


Figure 3.14 The cross-section used in the parameter study.

The input data for the base case was chosen to correspond to normal hard bedrock in Sweden. As described earlier, the program *RocLab* (RocScience, 2006) can be used to estimate rock mass parameters according to the generalized Hoek and Brown failure criterion, (Hoek et al. 2002). The elasto-plastic material properties are determined through fitting a Mohr-Coulomb failure envelope to the Hoek-Brown criterion, using the programme *RocLab*, see Figure 3.15. The Hoek-Brown criterion is based on the intact compressive strength, σ_{ci} , the intact rock parameter, m_i , the geological strength index, GSI , and the disturbance factor, D , along with a failure envelope range, σ_{3max} . The σ_{3max} -value is determined by examining a σ_3 plot of an elastic model. A maximum value of σ_3 from the area of a tunnel width around the tunnel was chosen from the base case, see Figure 3.16 (the stress concentrations in the corners were not considered). This gave $\sigma_{3max} = 2.5$ MPa.

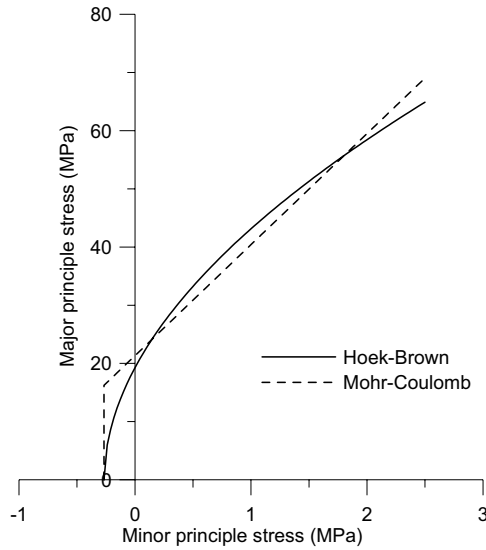


Figure 3.15 Hoek-Brown criterion with a Mohr-Coulomb fit.

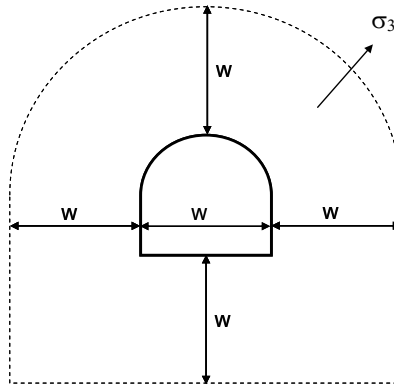


Figure 3.16 Area from where σ_3 was chosen.

A *GSI*-value of 60 corresponds to a blocky to intact rock mass, with good to fair surface conditions. The intact uniaxial compressive strength was chosen to 180 MPa, which is approximately that of a gabbro or gneiss. A disturbance factor of 0, corresponds to high quality controlled blasting (which can be assumed for very shallow tunnels), and a m_i factor of 33, which is normal for a granite or a gneiss was chosen. The density of the rock mass was assumed to be 2700 kg/m³ and the overburden 3 m. The parameters are listed in Table 3.7.

Table 3.7 Input data for the base case in the parameter study.

Parameter	Value
GSI	60
σ_v	ρgz
σ_H	$6.7 + 0.0399z$
σ_h	$0.8 + 0.0329z$
ρ	2700 kg/m^3
σ_c	180 MPa
Overburden	3 m
m_i	33
D	0
σ_{3max}	2.5 MPa
c	2.4 MPa
ϕ	64°
σ_t	-0.27 MPa

It should be emphasized that the water pressure has been considered negligible and not been used in this work. Furthermore, a solve command was used to automatically terminate the model when equilibrium has reached, which was considered to occur at an out-of-balance force limit, $f=0.5$.

3.5.2 Parameter variation

For the conceptual analyses, the sensitivity to variations in the following parameters was studied:

1. Virgin state of stress.

The significance of the state of stress was examined by using the different stress relations presented in Table 2.1. The direction of the stresses can be seen in Figure 3.12. A fourth model, where σ_H and σ_h changed places, i.e., the horizontal stresses were rotated 90° from the base case, so that the major horizontal stress was parallel to the tunnel axis and the minor horizontal stress was perpendicular to the tunnel axis.

2. Rock mass strength.

The variation of the rock mass strength was studied by changing the rock mass

strength in the whole model. The impact of uniaxial compressive strength as well as the *GSI*-value were examined, which are input parameters in *RocLab* to obtain the rock mass parameters cohesion, friction angle, tensile strength and Young's modulus. The impact of these rock mass parameters was studied as well. The uniaxial compressive strength and the *GSI*-value intervals were chosen to resemble "typical" Swedish rock masses.

Even though cohesion, friction angle, tensile strength and Young's modulus all are functions of *GSI* and the uniaxial compressive strength (in *RocLab*), it is still interesting to conduct a study of the influence of a variations of each of these parameters. When the Mohr-Coulomb failure criterion is used in *FLAC*, the residual tensile strength, $\sigma_{m,res}$, is zero. One extra model with a residual tensile strength just below σ_m was analyzed.

To study how the cohesion and friction angle of the rock mass affected the stability of the tunnel, the cohesion was reduced while the friction angle was increased so that the rock mass would still have the same strength. In the other case the cohesion was increased while the friction angle was reduced. In this way, one can observe if the cohesion or the friction angle are more significant for the stability of a shallow tunnel.

3. Overburden.

Analyses with different overburden thicknesses, with a maximum of 5 m, were conducted to find out how important the overburden is for the stability.

4. Weathered and damaged rock.

Two cases of weathered rock masses and one case of an excavation damaged zone (*EDZ*) were analyzed to investigate the impact they have on the tunnel stability. The weathered rock has a reduction of 50 % in both strength and stiffness. Two different depths were also used. The damaged rock was simulated using a disturbance factor equivalent for poor quality blasting and a zone size corresponding to Malmgren (2005).

5. Discontinuities.

The impact that a discontinuity, cutting through the tunnel roof, has on the stability and behaviour of a tunnel was tested. Two different kinds of discontinuities, one considered as soft (data from Fredriksson, 2006) and one considered as relatively

stiff (data from Malmgren, 2005) were used, The dip angle of the stiff discontinuity was varied.

Parameters 1 to 4 above were analysed using *FLAC* 5.0. The input data for these models are listed in Table 3.8. Factor 5, discontinuities, was analyzed with the discontinuum program, *UDEC* 4.0. The input data for these models are listed in Table 3.9.

Table 3.8 Input data for the models ran in *FLAC*

Parameter Model	Virgin state of stress MPa	σ_{ci} MPa	<i>GSI</i>	σ_{im} MPa	Over- burden, <i>m</i>	<i>E</i> , GPa	Cohesion MPa
							Friction °
1 Basecase	$\sigma_H = 6.7 + 0.0444z$ $\sigma_h = 0.8 + 0.0329z$	180	60	From Roclab 0.267	3	From Roclab 17.8	From Roclab 2.4
							From RocLab 64
2	$\sigma_H = 10.4 + 0.0446z$ $\sigma_h = 5 + 0.0286z$	180	60	0.267	3	17.8	2.4
							64
3	$\sigma_H = 2.8 + 0.0399z$ $\sigma_h = 2.2 + 0.0024z$	180	60	0.267	3	17.8	2.4
							64
4	$\sigma_h = 0.8 + 0.0329z^*$ $\sigma_H = 6.7 + 0.0444z^*$	180	60	0.267	3	17.8	2.4
							64
5	$\sigma_H = 6.7 + 0.0444z$ $\sigma_h = 0.8 + 0.0329z$	140	60	0.208	3	17.8	2.1
							63
6	$\sigma_H = 6.7 + 0.0444z$ $\sigma_h = 0.8 + 0.0329z$	220	60	0.267	3	17.8	2.7
							65
7	$\sigma_H = 6.7 + 0.0444z$ $\sigma_h = 0.8 + 0.0329z$	180	48	0.108	3	8.9	1.8
							62
8	$\sigma_H = 6.7 + 0.0444z$ $\sigma_h = 0.8 + 0.0329z$	180	72	0.661	3	35.4	3.8
							66
9	$\sigma_H = 6.7 + 0.0444z$ $\sigma_h = 0.8 + 0.0329z$	180	60	0	3	17.8	2.4
							64
10	$\sigma_H = 6.7 + 0.0444z$ $\sigma_h = 0.8 + 0.0329z$	180	60	2*0.267	3	17.8	2.4
							64
11	$\sigma_H = 6.7 + 0.0444z$ $\sigma_h = 0.8 + 0.0329z$	180	60	$\sigma_{m,res} =$ 0.26 MPa**	3	17.8	2.4
							64
12	$\sigma_H = 6.7 + 0.0444z$ $\sigma_h = 0.8 + 0.0329z$	180	60	0.267	2	17.8	2.4
							64
13	$\sigma_H = 6.7 + 0.0444z$ $\sigma_h = 0.8 + 0.0329z$	180	60	0.267	5	17.8	2.4
							64
14	$\sigma_H = 6.7 + 0.0444z$ $\sigma_h = 0.8 + 0.0329z$	180	60	0.267	3	14.2	2.4
							64
15	$\sigma_H = 6.7 + 0.0444z$ $\sigma_h = 0.8 + 0.0329z$	180	60	0.267	3	21.4	2.4
							64

Table 3.8 (continued.)

16	$\sigma_H = 6.7 + 0.0444z$ $\sigma_h = 0.8 + 0.0329z$	180	60	0.267	3	17.8	1.9
							70
17	$\sigma_H = 6.7 + 0.0444z$ $\sigma_h = 0.8 + 0.0329z$	180	60	0.267	3	17.8	2.9
							59
18	$\sigma_H = 6.7 + 0.0444z$ $\sigma_h = 0.8 + 0.0329z$	90***	60***	0.134***	Weathered thickness 3 m	8.9***	1.75**
							60**
19	$\sigma_H = 6.7 + 0.0444z$ $\sigma_h = 0.8 + 0.0329z$	90***	60***	0.134***	Weathered thickness 5 m	8.9***	1.75***
							60***
20	$\sigma_H = 6.7 + 0.0444z$ $\sigma_h = 0.8 + 0.0329z$	180****	60****	0.149****	EDZ thickness 0.5 m	11.6****	1.7****
							60****
<p>*σ_H is parallel to the tunnel axis, σ_h is perpendicular to the tunnel axis. **σ_{tm} is the same as for the base case, i.e. 0.267 MPa. ***These are the parameters for the weathered rock mass. The fresh rock mass has the same input data as the base case, model 1. The overburdens of the models are 3 m. ****These are the parameters for the EDZ zone. The fresh rock mass has the same input data as the base case, model 1. The overburden of the model is 3 m.</p>							

Table 3.9 Properties of discontinuities used in the analysis.

Parameter	Unit	Stiff*	Soft**
Friction angle	[°]	35	25
Cohesion	MPa	0	0.05
Tensile strength	MPa	0	0
Normal stiffness	GPa/m	110	0.2
Shear stiffness	GPa/m	9	8
Discontinuity angle	[°]	15	
		30	30
		60	
* Malmgren (2005)			
** Fredriksson (2006)			

3.5.3 Instability indicators

The aim of this project was to investigate the importance of a number of factors on the stability and performance of shallow excavations in hard rock. Although this has proven to be more difficult than first expected, some instability indicators were chosen in order to determine the sensitivity to variations in the examined parameters. Because different programs were used for the continuum and discontinuum models, slightly different instability

indicators were used. The instability indicators for continuum models are (i) tangential stress around the tunnel boundary, (ii) deformation of the tunnel boundary, (iii) deformation of the ground surface, (iv) area of plasticity, and (v) extent of a complete tensile stress state (all principal stresses are tensile in an elastic model).

For the discontinuum models, (I) deformation of the ground surface, (II) the zone of plasticity, (III) roof stability (velocity vectors), and (IV) opening in and/or slip in the discontinuity, were the primary indicators of instability. A short explanation of all indicators follows below.

(i) Tangential stress around the tunnel boundary

One of the greatest risks of shallow tunnelling is considered to be fallouts of wedge formations due to low confining stresses. Low tangential stresses (risk of opening of pre-existing joints or tensile failure) as well as very high stresses (risk of compressive failure) are therefore a threat to the stability of the tunnel. The tangential stress has been examined at the boundary and 0.5 m from the boundary.

(ii) Deformations of the tunnel boundary

Deformations of the tunnel boundary are an important quantity to examine. Too large deformations might be an indication of instability. Furthermore, large deformations may affect rock reinforcement and installations such as electricity, water and ventilation.

(iii) Deformations of the ground surface

Subsidence or heaving of the ground surface is mostly important when infrastructure or buildings are located above the tunnel. It is therefore important to control the deformations when tunnelling in, for example urban areas.

(iv) Area of plasticity

An important parameter for the stability and the rock support of a tunnel is the zone of plasticity. In *FLAC*, such a zone indicates that plastic flow is occurring and may provide a pattern that tells if a mechanism has developed. It was observed that the zone of plasticity was dependent on when the model is terminated since the state hovered between “yield in tension” and “yield in past”. The area in which the tensile strength has been changed from peak to residual illustrates areas where tensile failure has occurred. The areas in the model where

“yield in past” is indicated and the tensile strength is still equal to the peak value represents areas where shear failure has occurred.

By comparing the model state plot and the tensile strength plot, the area that has yielded in tension can be identified in the zone labelled “yield in past” see Figure 3.17. This does also mean that if the peak tensile strength is indicated in the area labelled “yield in past”, this portion has yielded in shear.

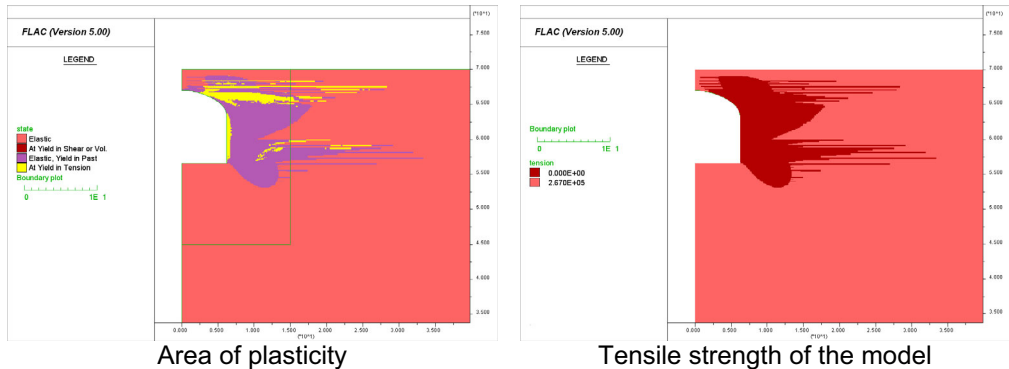


Figure 3.17 Comparison of area of plasticity and tensile strength.

(v) Extent of tensile stresses

Many stability problems at shallow depth are a result of low compressive or tensile stresses. When all principal stresses are tensile in an elastic model, this can be considered as a potential risk of failure. It is therefore something that needs to be examined.

(I) Deformation of the ground surface

This is basically the same as (iii) subsidence of the ground surface.

(II) Area of plasticity

This is basically the same as (iv) area of plasticity.

(III) Roof stability (velocity vectors)

Some of the discontinuum models could not be run to equilibrium without having a part of the roof deforming unrealistically and had to therefore be stopped prematurely. Examination of the velocity vectors of the models assisted in the detection of unstable areas.

(IV) Opening of and/or slip in the discontinuity

The stability of a discontinuity is basically defined by the occurrence of slip and/or opening. Discontinuities with zero normal stress are defined as open in *UDEC* and discontinuities at shear limit are considered to be in state of slip.

3.5.4 Results – Continuum models

(i) Tangential stress around the tunnel boundary

Figure 3.18, Figure 3.19 and Figure 3.20 show that the tangential stress at the tunnel boundary is tensile or zero at the wall and the abutment, while it is compressive in the roof. At a distance of 0.5 m from the boundary, the behaviour seems to be similar, with the difference that the compressive stresses start a few metres closer to the abutment.

Figure 3.18 shows that the cases with lower horizontal virgin stress perpendicular to the tunnel axis show smoother curves and lower values than the cases with higher horizontal stresses. Furthermore, figure 3.18 shows higher values for σ_{ci} and *GSI*, since greater strength can carry greater stresses.

In Figure 3.19, it is shown that with a greater overburden the compressive tangential stresses start closer to the abutment of the tunnel and vice versa. In the cases of weathering and *EDZ* (Figure 3.20), the rock mass strength and the stiffness (*E*) have been reduced, which gives lower stresses in the tunnel roof. It is also seen that the tangential stress is only weakly dependent on the variation of cohesion, Young's modulus and the tensile strength.

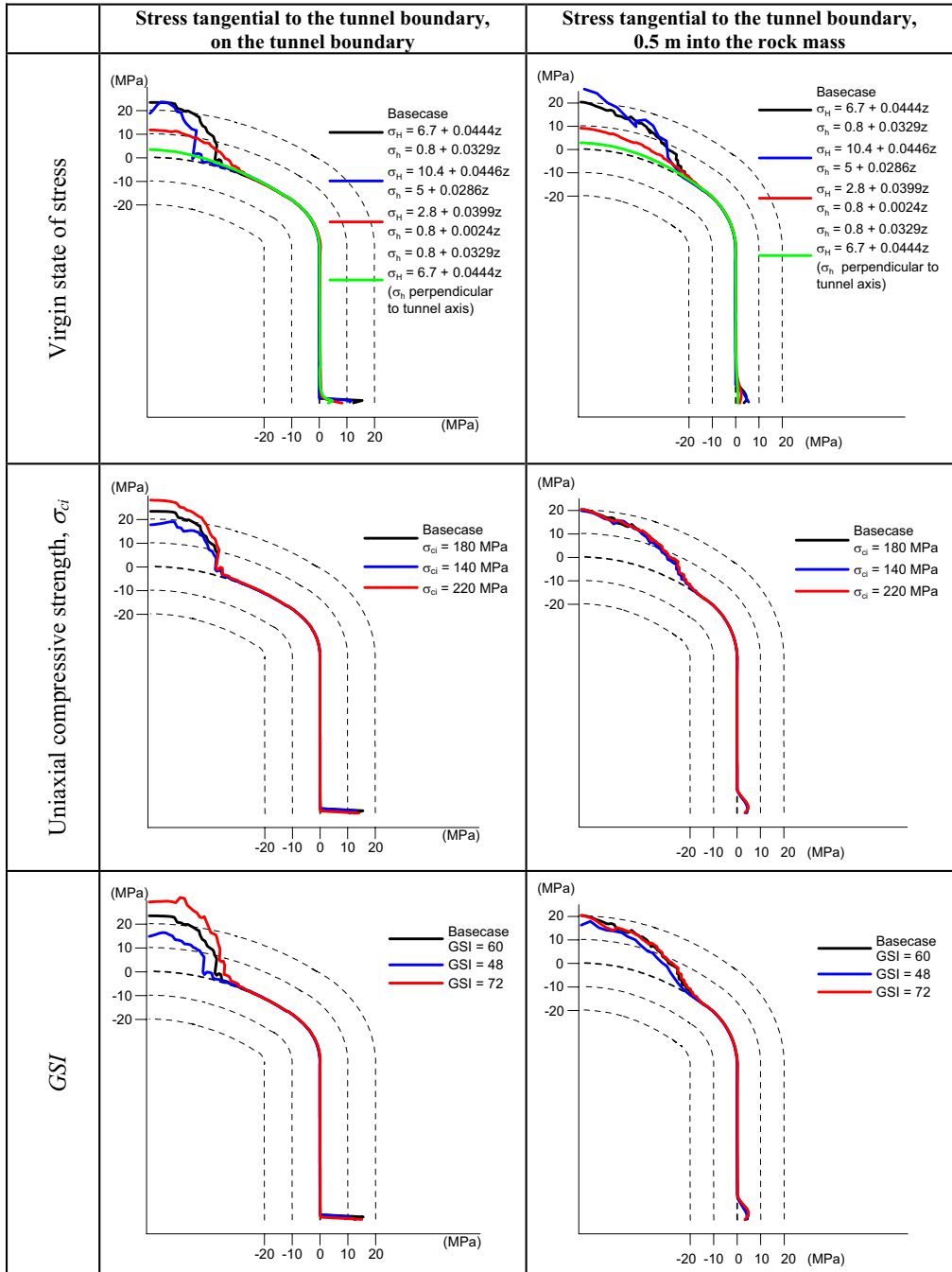


Figure 3.18 The tangential stress and its variation due to variations in virgin state of stress, uniaxial compressive strength and *GSI*.

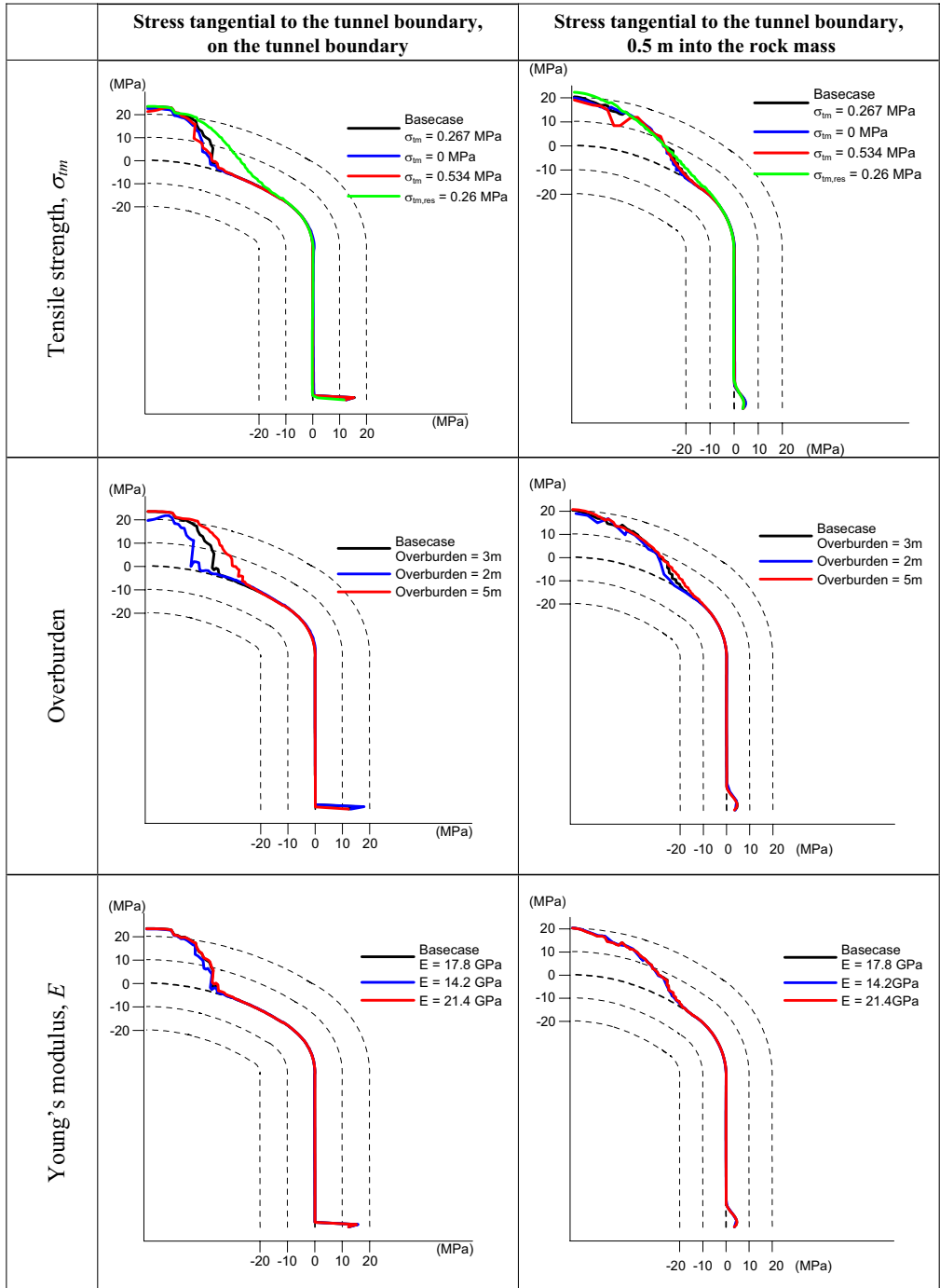


Figure 3.19 The tangential stress and its variation due to variations in tensile strength, overburden and Young's modulus.

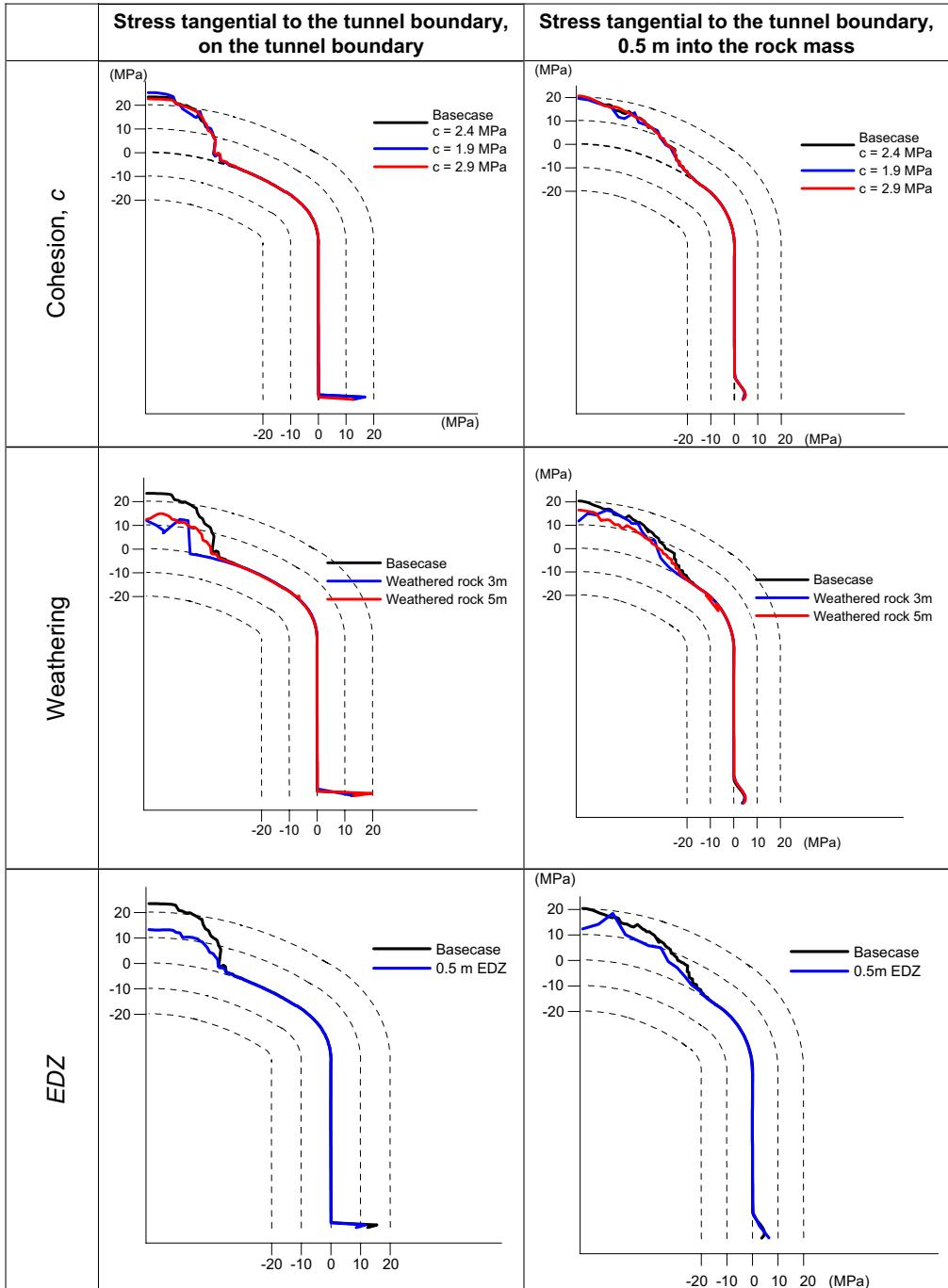


Figure 3.20 The tangential stress and its variation due to variations in cohesion, weathering and *EDZ*.

(ii) Deformation of the tunnel boundary

The impact of the variation of rock mass properties on the deformation of the tunnel boundary is presented in Figure 3.21 and Figure 3.22. A similar pattern of the deformation can be seen for all factors, except the case where the residual tensile strength is not set to zero. The tunnel wall and the abutment converge while the roof heaves. Variation of the virgin state of stress gave the largest differences in deformation. With low stresses, the deformations are very small, while greater stresses show larger deformations, see Figure 3.21. Other factors that seem to have impact on the deformations are *GSI* and the overburden. The variation of weathering (Figure 3.22) might seem strange, but the reason for this behaviour is that there is a separation between the weathered rock mass and the fresh rock, as seen in Figure 3.23, because the overburden and the depth of the weathered rock mass are the same.

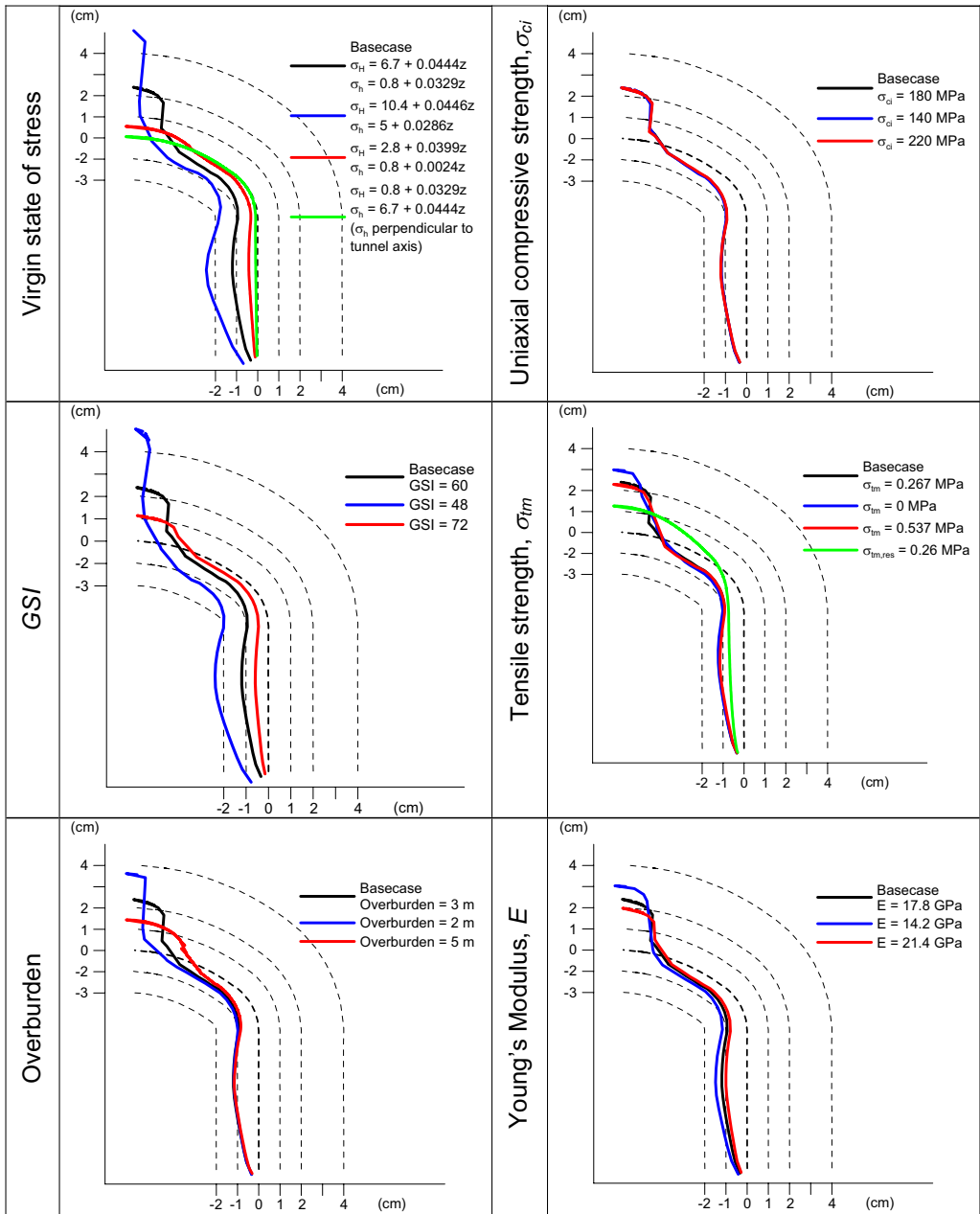


Figure 3.21 The sensitivity of variations in virgin state of stress, intact uniaxial compressive strength, GSI , tensile strength, overburden and Young's modulus on deformation on the tunnel boundary.

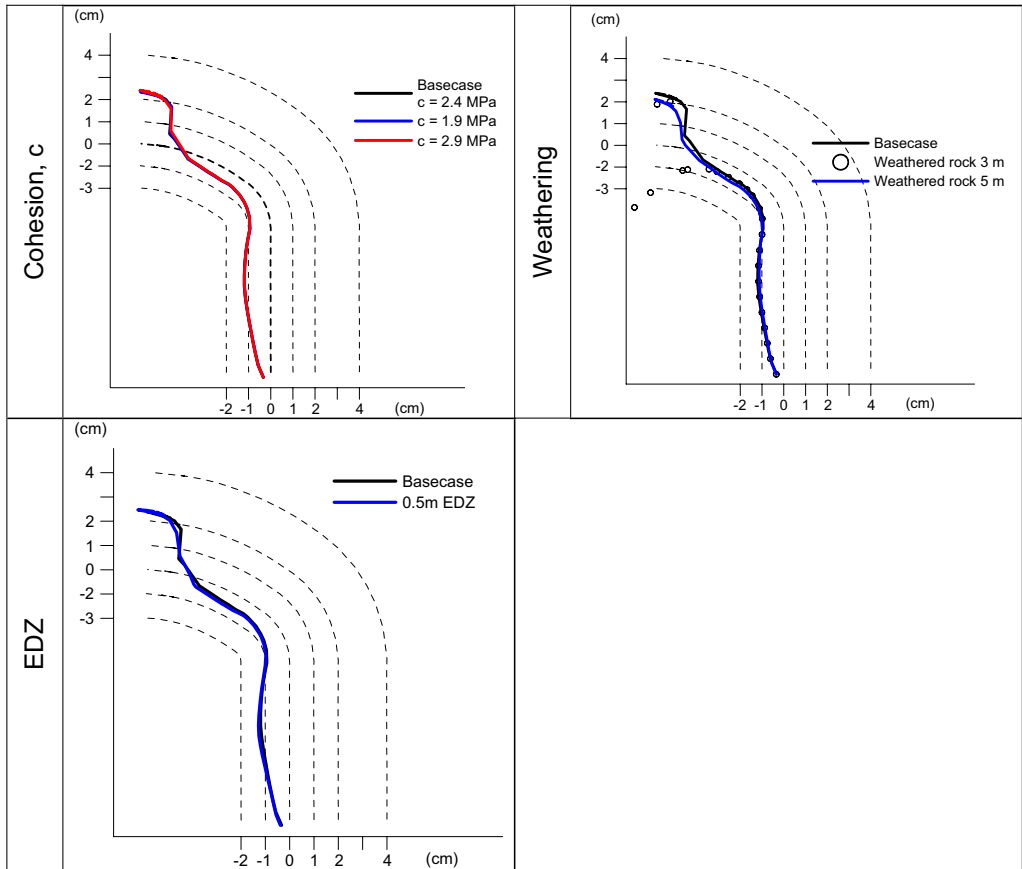


Figure 3.22 The sensitivity of variations in cohesion, weathering and *EDZ* on deformation on the tunnel boundary.

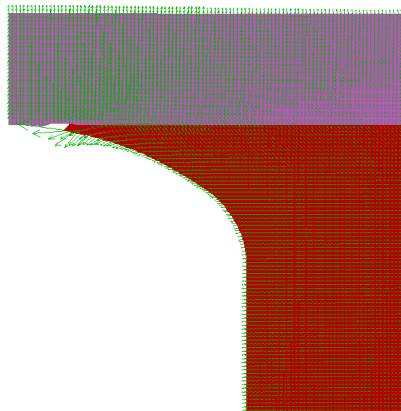


Figure 3.23 Separation between the weathered rock mass and the fresh rock.

(iii) Deformation of the ground surface

The results of the analysis are visualized in Figure 3.24. For all cases the ground surface is heaving between 0.1 mm (very low horizontal stresses) and about 5 mm (for high horizontal stresses and low GSI value). Besides GSI and virgin stresses, variations of Young's modulus and overburden results in a ground deformation that deviates significantly from that of the base case.

There is a negligible difference in ground surface deformation if σ_{tm} is 0.27 MPa or 0.53 MPa, while there is a noticeable difference if σ_{tm} is 0 MPa. The cases when $\sigma_{tm} = 0.27$ MPa with a residual $\sigma_{tm,res}$ of 0.26 MPa shows considerably less heaving than the case with a greater peak value.

The variations of the intact uniaxial compressive strength, weathering of the overburden and the cohesion have no affect on the behaviour of the overburden.

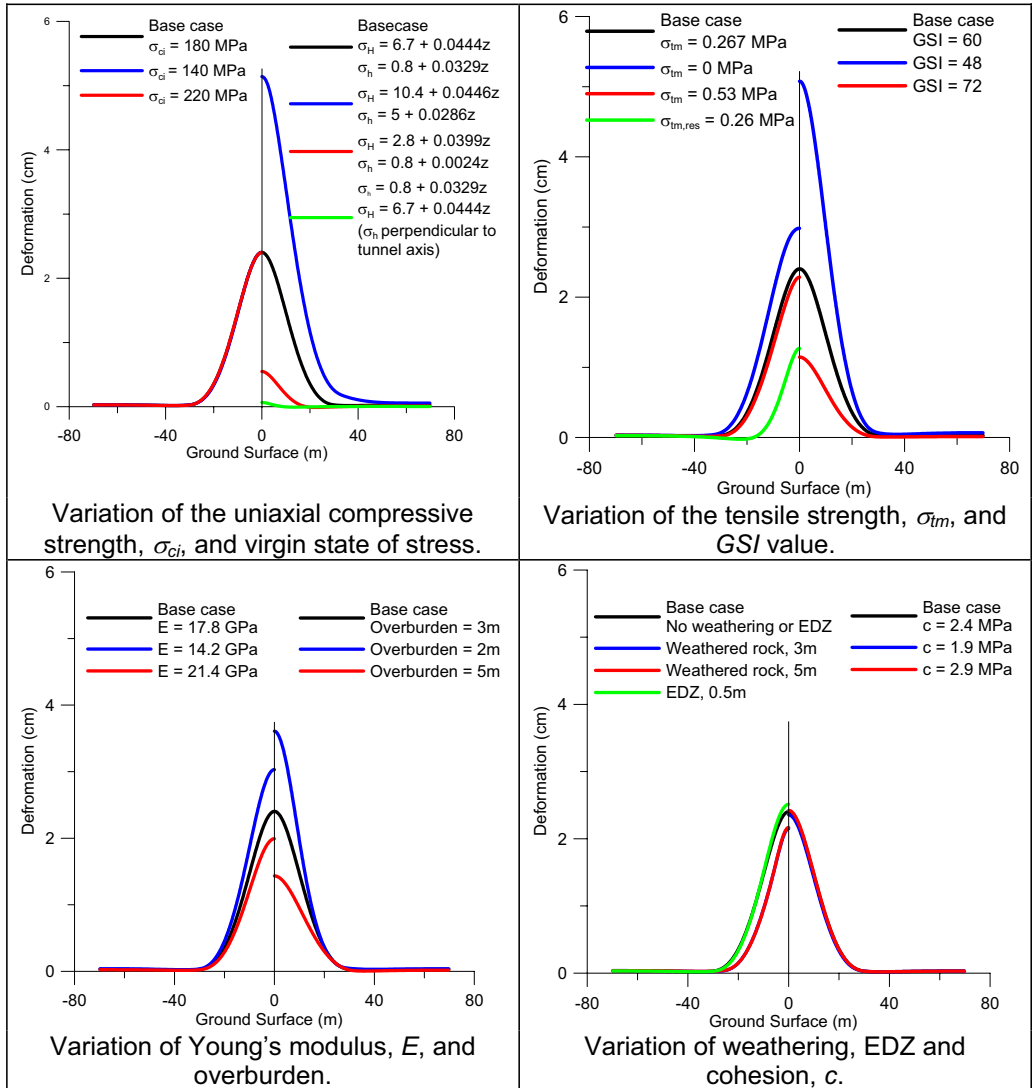


Figure 3.24 The sensitivity of variations in rock mass parameters on ground surface deformation.

(iv) Area of plasticity

The results from the study of the impact of variations of the rock mass properties on the area of plasticity are presented in Figure 3.25 - Figure 3.33. A similar pattern of zones which have experienced yielding can be seen for all factors. There is an area, primarily in the tunnel wall and the abutment where tensile failure has occurred. Almost all plastic flow is due to tensile stresses. A very small area where the rock is at yield in shear next to the tunnel roof centre can also be detected in most cases.

The different virgin states of stress analyzed in this study show the greatest differences in the area of plasticity (Figure 3.25). Low stresses give a small area, while the case with the highest stresses show a large area of plasticity that reaches the ground surface. Comparison of the area of plasticity plot with the plot of the tensile strength in the case of high stress, shows that yield in shear can be detected in the middle of the tunnel roof and at the ground surface over the abutment of the tunnel.

Furthermore, the area of plasticity is strongly dependent on both the *GSI*-value (Figure 3.27) and tensile strength (Figure 3.28). In the case of a low *GSI*-value, the area of plasticity reaches ground surface, and some shear failure can be observed above the tunnel centre and above the abutment at ground level. Only a small difference in area of plasticity can be observed when σ_{tm} is 0.267 MPa and 0.537 MPa. $\sigma_{tm, res} = 0.26$ MPa shows similar size of the area of plasticity, but a smoother pattern. The model with $\sigma_{tm} = 0$ MPa, on the other hand, shows a great difference in the area of plasticity compared to the base case. The area of plasticity is larger, and extends over a large portion of the ground surface, see Figure 3.28. Since σ_{tm} is equal to $\sigma_{t, res}$ for this case, tensile failure cannot be detected in the tensile strength plot in Figure 3.28.

The variation of the overburden shows that it is a significant factor for the area of plasticity, where it is larger and closer to the ground surface when the tunnel is shallower (Figure 3.29). Variations in Young's modulus (Figure 3.30), cohesion (Figure 3.31), weathering (Figure 3.32) and *EDZ* (Figure 3.33) seem to have a small effect on the area of plasticity. However, the case of the *EDZ* shows more shear failure, under the tunnel floor and in the middle of the tunnel roof, than the base case.

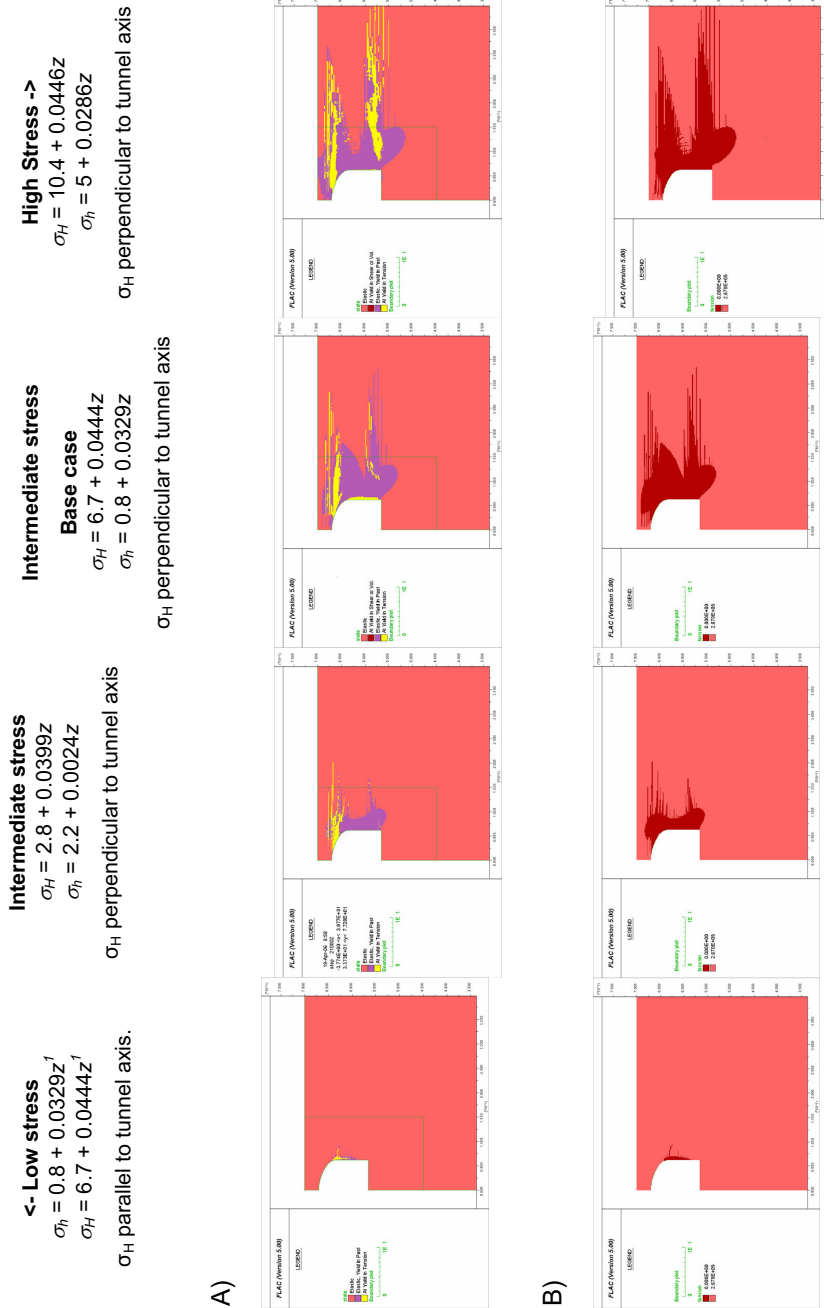


Figure 3.25 The sensitivity of variations of the primary state of stress in area of plasticity (A) and tensile strength (B).

High compressive strength
 $\sigma_{ci} = 220 \text{ MPa}$

Intermediate compressive strength
Basecase
 $\sigma_{ci} = 180 \text{ MPa}$

Low compressive strength ->
 $\sigma_{ci} = 140 \text{ MPa}$

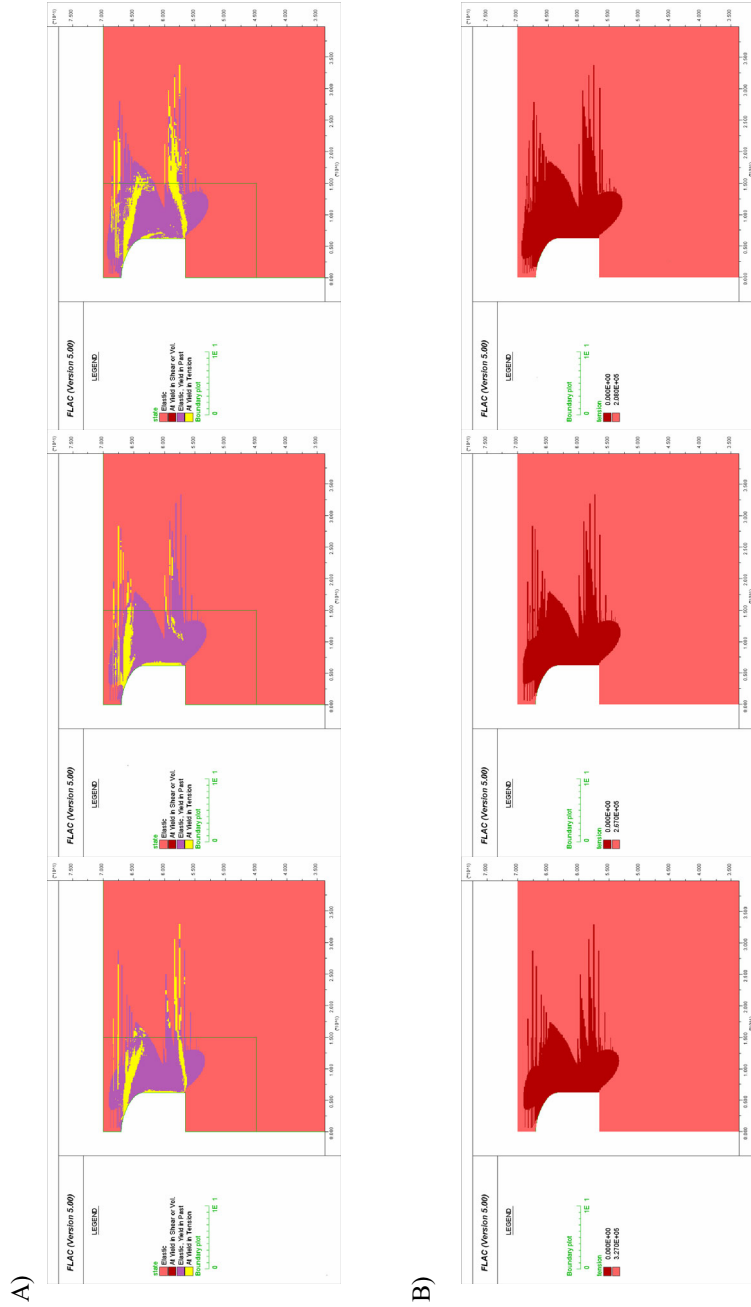


Figure 3.26 The sensitivity of variations of the compressive strength, σ_{cs} in area of plasticity (A) and tensile strength (B).

<- High *GSI*-value
GSI = 72
 Intermediate *GSI*-value
 Basecase
GSI = 60
 Low *GSI*-value ->
GSI = 48

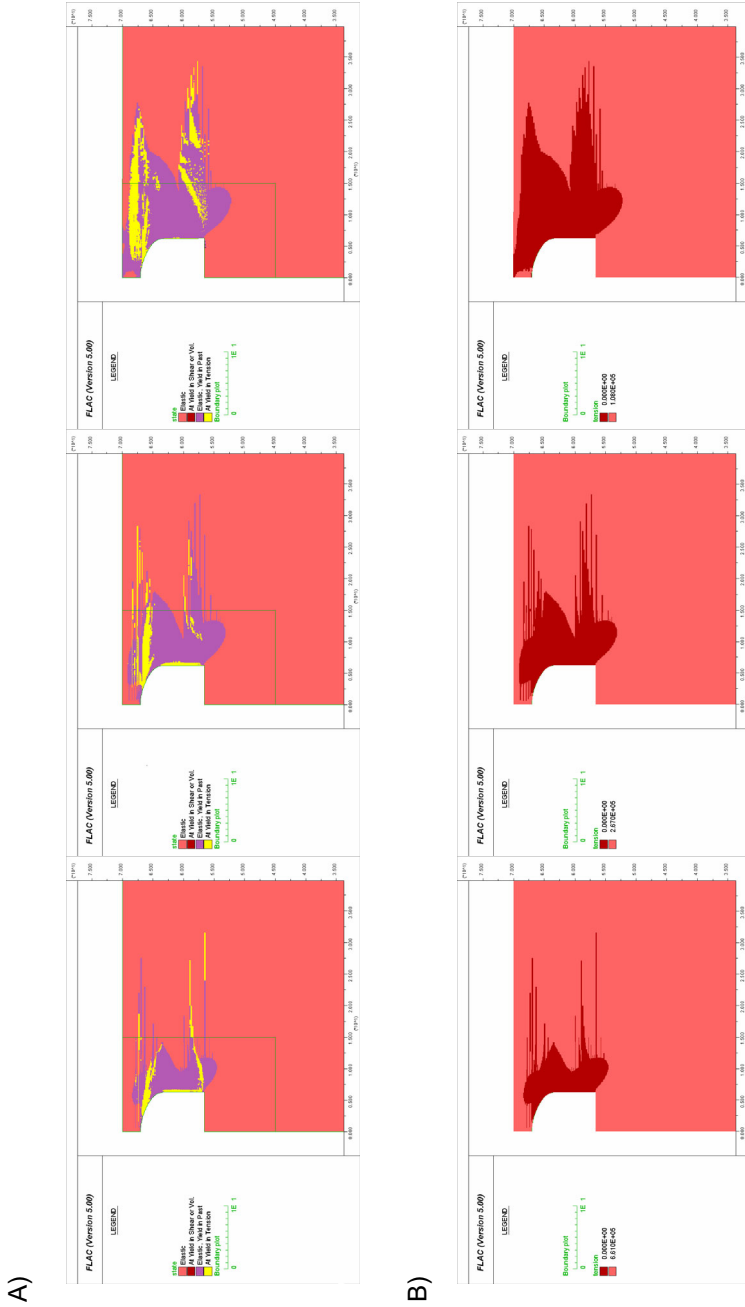


Figure 3.27 The sensitivity of variations of the *GSI*-value on area of plasticity (A) and tensile strength (B).

Low tensile strength ->

$$\sigma_{tm} = 0 \text{ MPa}$$

$$\sigma_{tm, res} = 0 \text{ MPa}$$

Intermediate tensile strength

Basecase

$$\sigma_{tm} = 0.267 \text{ MPa}$$

$$\sigma_{tm, res} = 0 \text{ MPa}$$

Residual tensile strength

$$\sigma_{tm} = 0.267 \text{ MPa}$$

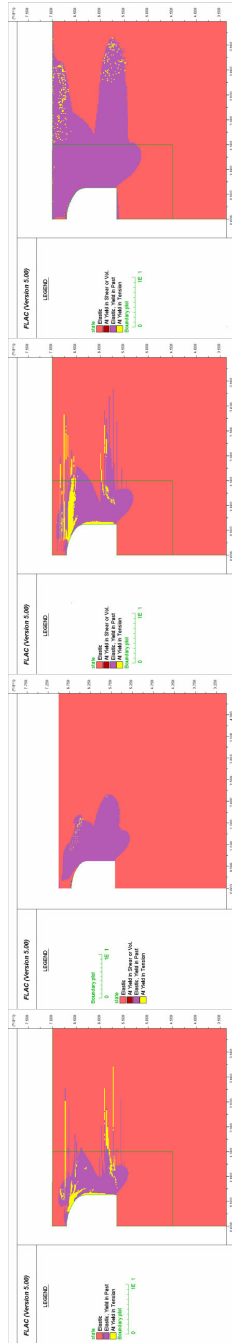
$$\sigma_{tm, res} = 0.26 \text{ MPa}$$

<- High tensile strength

$$\sigma_{tm} = 0.534 \text{ MPa}$$

$$\sigma_{tm, res} = 0 \text{ MPa}$$

A)



B)

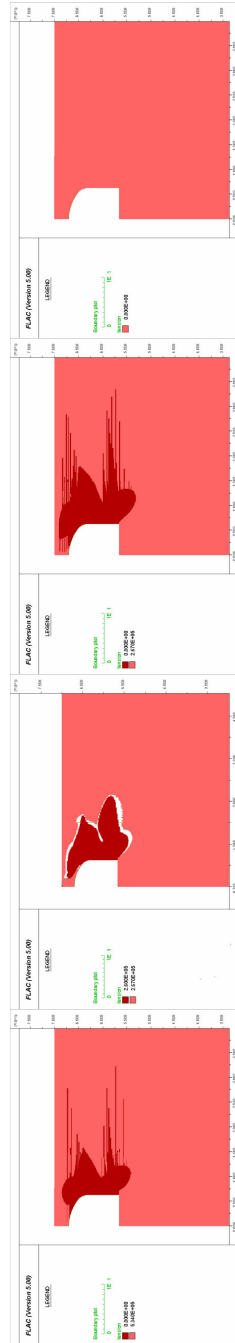
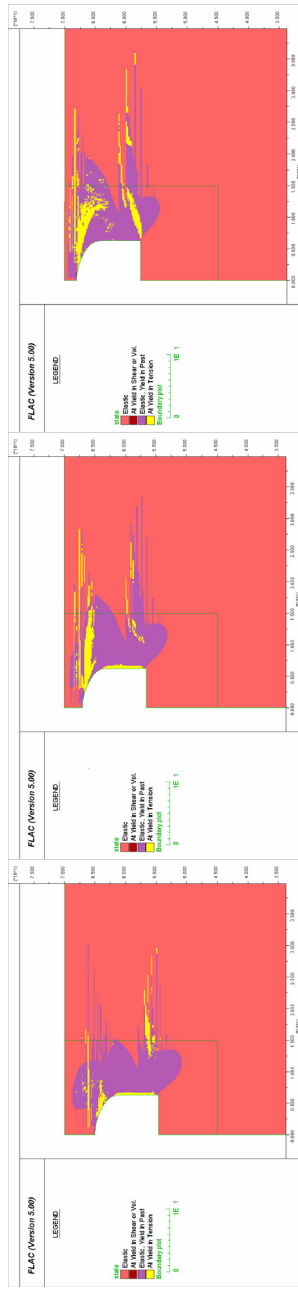


Figure 3.28 The sensitivity of variations of the tensile strength, σ_{tm} , on area of plasticity (A) and tensile strength (B).

<- More overburden 5 m
 Intermediate overburden Basecase 3 m
 Less overburden -> 2 m

A)



B)

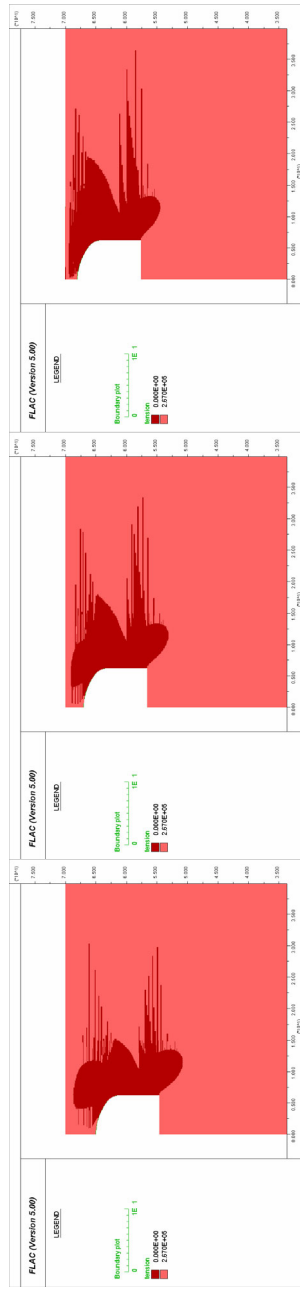


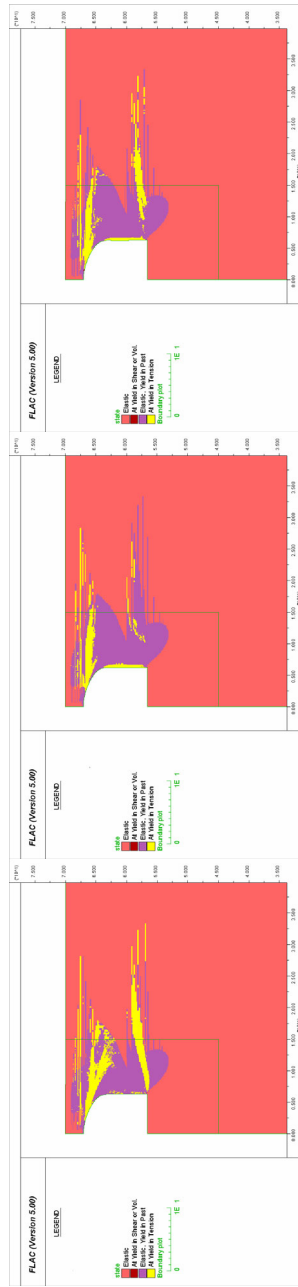
Figure 3.29 The sensitivity of variations of the overburden thickness on area of plasticity (A) and tensile strength (B).

<- High stiffness
 $E = 21.4\text{GPa}$

Intermediate stiffness
Basecase
 $E = 17.8\text{GPa}$

Low stiffness->
 $E = 14.2\text{GPa}$

A)



B)

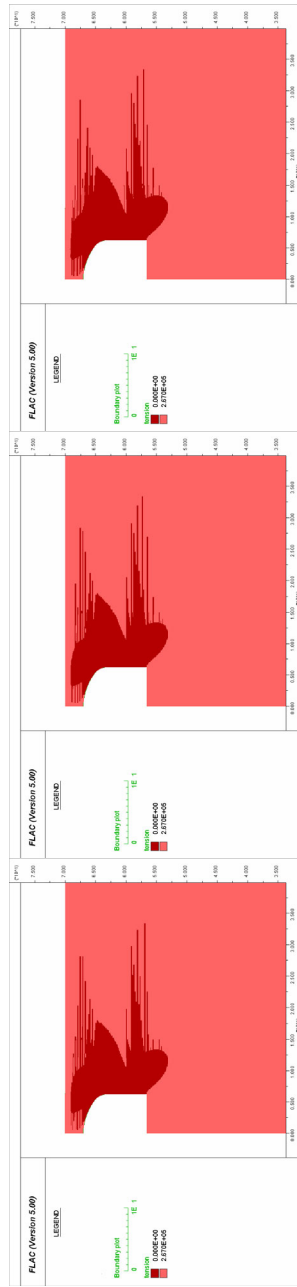
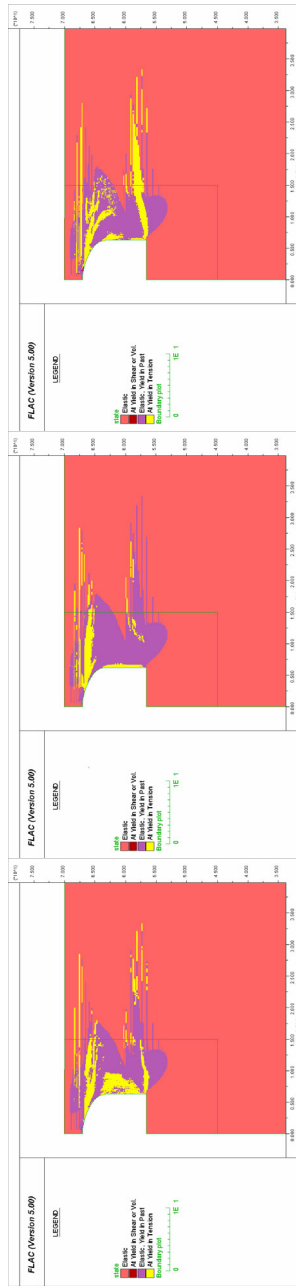


Figure 3.30 The sensitivity of variations of Young's modulus, E , on area of plasticity (A) and tensile strength (B).

<- High cohesion
 $c = 2.9 \text{ MPa}$
 Intermediate cohesion
 Basecase
 $c = 2.4 \text{ MPa}$
 Low cohesion ->
 $c = 1.9 \text{ MPa}$

A)



B)

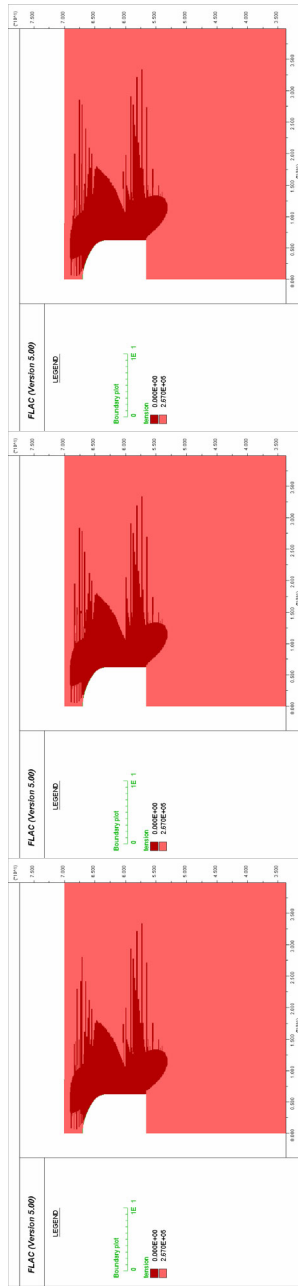


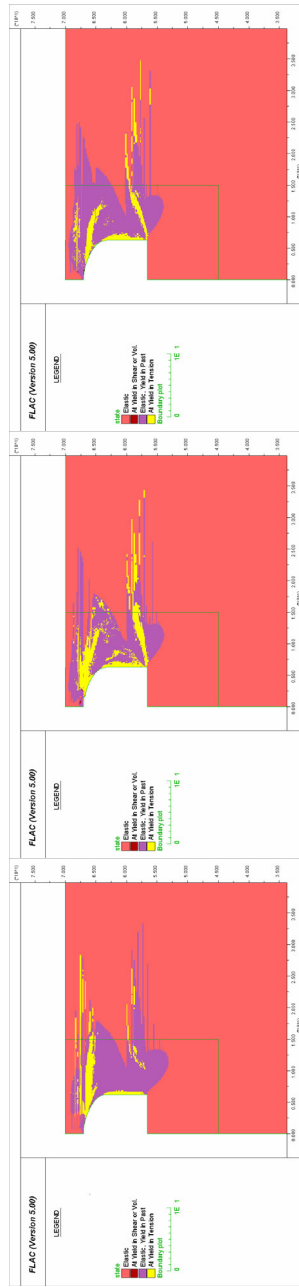
Figure 3.31 The sensitivity of variations of the cohesion, c , on area of plasticity (A) and tensile strength (B).

5 m of weathered rock

3 m of weathered rock

<- No weathering
Basecase

A)



B)

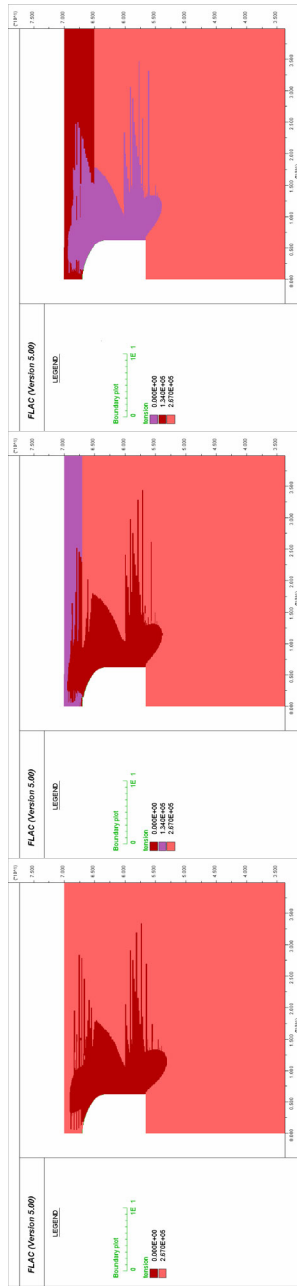


Figure 3.32 The sensitivity of variation of weathering on area of plasticity (A) and tensile strength (B).

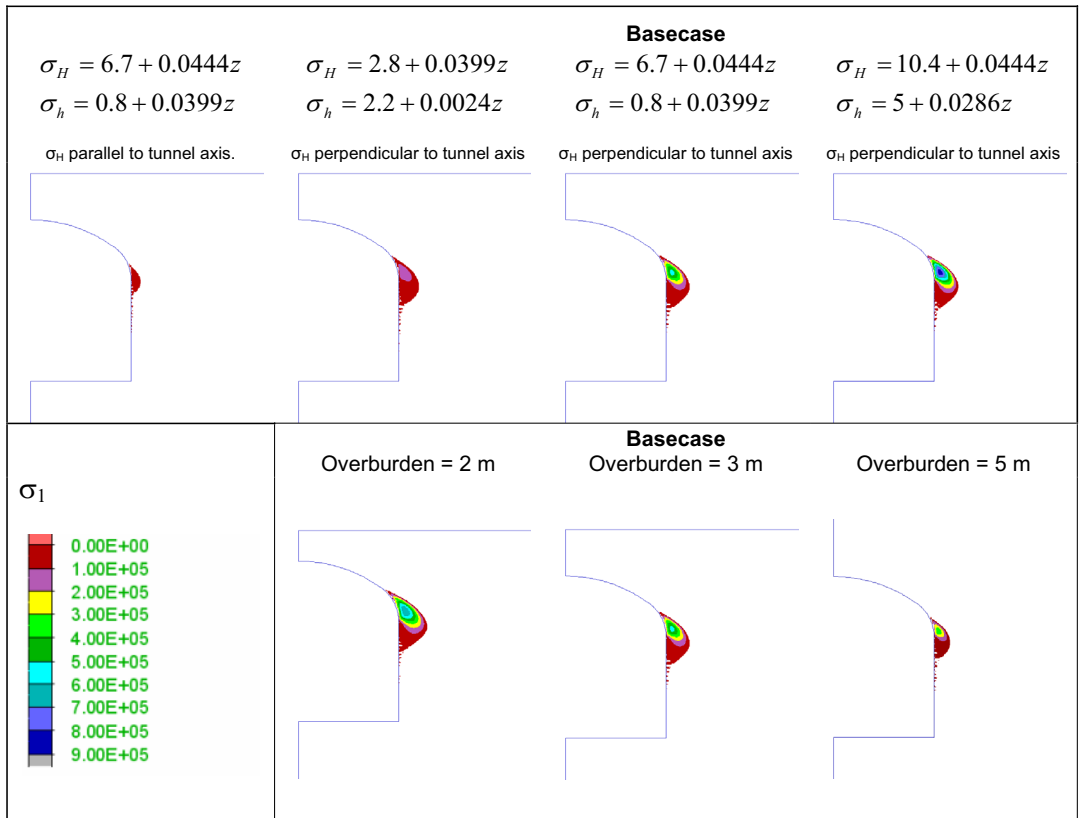


Figure 3.34 The sensitivity to variations of elastic rock mass parameters on the extent of tensile stresses. In *FLAC*, tensile stresses are positive and compressive stresses negative, hence a positive scale for tensile stresses.

3.5.5 Results – Discontinuum models

(I) Deformation of the ground level

The sensitivity of variation of discontinuity parameters on the deformation of the ground surface is presented in Figure 3.35. The deformation depends on the angle of the discontinuity. Although the behaviour is similar with the discontinuity angles of 15° and 30° , the amplitude differs. The deformation of the ground surface in the case with $\alpha = 60^\circ$ is very similar to the response of the base case without a discontinuity. The subsidence/heaving of the cases with a stiff discontinuity and the soft discontinuity are similar in both behaviour and amplitude.

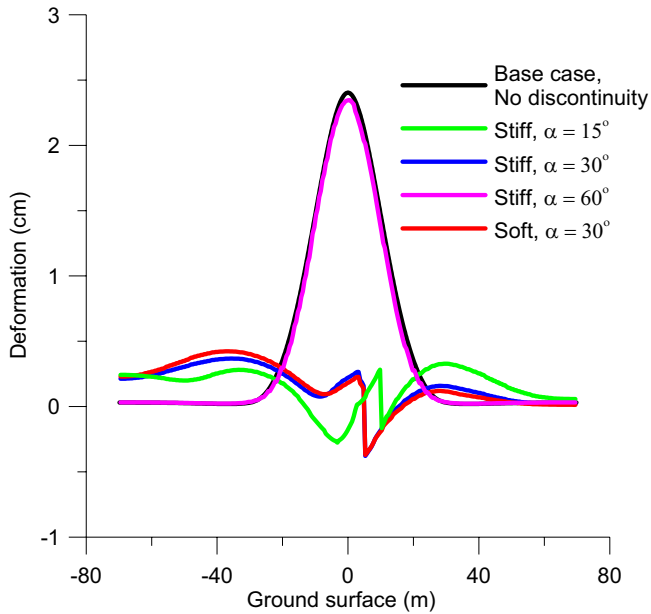


Figure 3.35 The subsidence (negative values) and/or heaving (positive values) of the ground surface for the different cases of discontinuity.

(II) Area of plasticity

Figure 3.36 show that a discontinuity does affect the area of plasticity. Furthermore it shows that the area of plasticity is more developed for a low angle (α), and the area where yield has occurred decreases when the angle gets steeper. No significant difference can be observed between a stiff and a soft discontinuity.

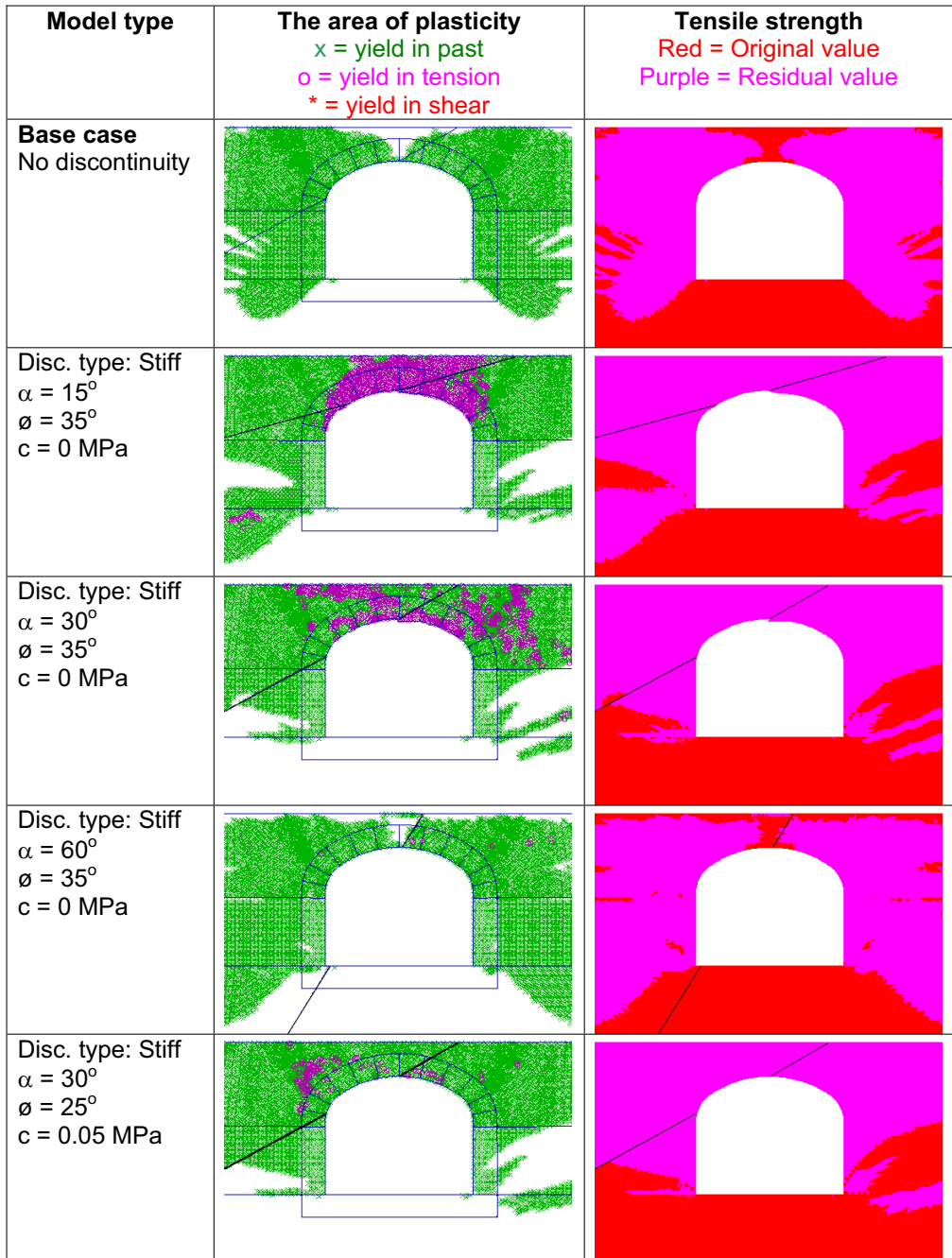


Figure 3.36 The sensitivity of varying discontinuity parameters on the area of plasticity and the tensile strength.

(III) Opening of and/or slip in the discontinuity

The analysis of the sensitivity of discontinuity parameters on the opening of and slip in the discontinuity is presented in Figure 3.37. It shows that discontinuities with small dip angles tend to open and the risk of slip increases. This is due to the fact that the major principal stress in the overburden is horizontal. The normal stress of the discontinuity will decrease with a decreasing dip angle. No significant difference can be seen between the soft and the stiff discontinuities.

(IV) Roof stability (velocity vectors)

The sensitivity to variation in discontinuity parameters on the roof stability, i.e. velocity vectors is presented in Figure 3.38. It is shown that steeper discontinuities results in more stable conditions. Moreover it is shown that the stiff discontinuity is less stable than the soft discontinuity. This can be explained with the low normal forces present in the discontinuity. This means that friction is less important than cohesion for the stability when the normal stresses are relatively small.

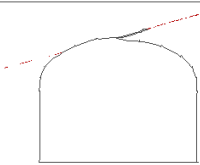
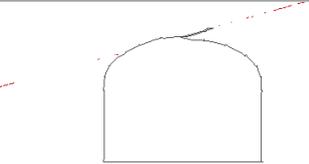
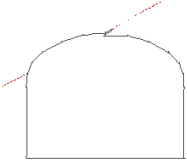
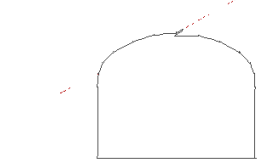
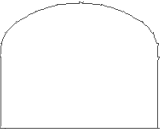
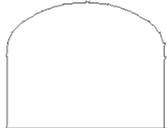
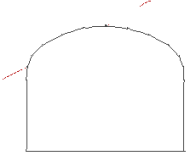
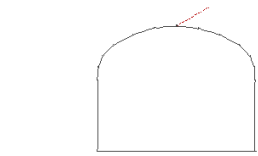
Model type	Open Joints with zero normal force or stress	Slip Joints at shear limit
Base case No discontinuity	No discontinuity	No discontinuity
Disc. type: Stiff $\alpha = 15^\circ$ $\phi = 35^\circ$ $c = 0$ MPa		
Disc. type: Stiff $\alpha = 30^\circ$ $\phi = 35^\circ$ $c = 0$ MPa		
Disc. type: Stiff $\alpha = 60^\circ$ $\phi = 35^\circ$ $c = 0$ MPa		
Disc. type: Stiff $\alpha = 30^\circ$ $\phi = 25^\circ$ $c = 0.05$ MPa		

Figure 3.37 The sensitivity to variations in discontinuity parameters in opening and slip in discontinuities.

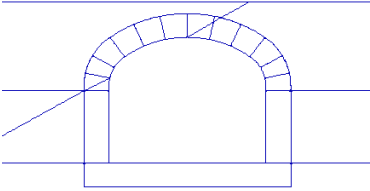
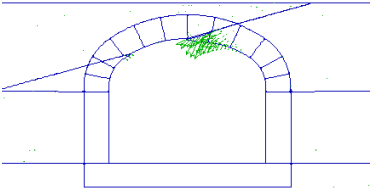
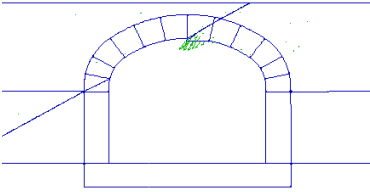
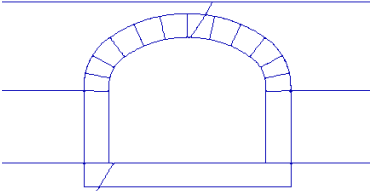
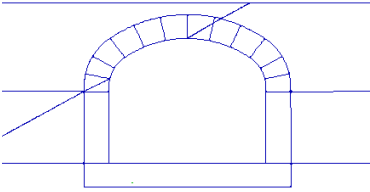
Model type	Roof stability Velocity vectors
Base case No discontinuity	
Disc. type: Stiff $\alpha = 15^\circ$ $\phi = 35^\circ$ $c = 0 \text{ MPa}$	
Disc. type: Stiff $\alpha = 30^\circ$ $\phi = 35^\circ$ $c = 0 \text{ MPa}$	
Disc. type: Stiff $\alpha = 60^\circ$ $\phi = 35^\circ$ $c = 0 \text{ MPa}$	
Disc. type: Stiff $\alpha = 30^\circ$ $\phi = 25^\circ$ $c = 0.05 \text{ MPa}$	

Figure 3.38 The sensitivity to variations of discontinuity parameters on roof stability

4 IDENTIFICATION OF IMPORTANT FACTORS

The main objective of this project was to identify the factors that are most important for the stability and behaviour of shallow constructions in hard rock. The parameter values chosen for the base case, were chosen to represent typical Swedish rock conditions. In order to study how uncertainties in the input parameters affect the behaviour of shallow underground constructions, intervals for all parameters (representing a factor) were chosen, see Chapter 3.5.

The conceptual analysis showed that the most important factor was the presence of discontinuities. This was actually the only time that instability problems could be confirmed in the conceptual analyses. Furthermore, the most important parameter of the discontinuity was the dip angle. A steep angle is more favourable than a shallow angle. Equally important is to know the location of the tunnel in relation to discontinuities and the ground surface. A larger overburden is preferable, if there is a possibility to choose.

The sensitivity of the tangential stress in the walls, abutments and roof of the tunnel and at the ground surface and the deformation of the ground surface and the tunnel boundary to variations in the rock mass parameters are presented in Figure 4.1, Figure 4.2 and Figure 4.3, where they are presented relative the base case. The value of the base case is 100 %. The figures show that the tangential stress and the deformations are highly sensitive to variations in the virgin state of stress and *GSI*. Other factors that give significant deviations in tangential stresses and deformations are the size of the overburden and the tensile strength. However, the only parameter that definitely indicated stability problems was the presence of discontinuities. When the discontinuity parameters were examined, the discontinuity angle was the most important factor for the stability. Furthermore, it showed that with low normal stresses on the discontinuity, cohesion contributes more than friction to the stability.

The failures that have occurred in the conceptual analyses have mainly been tensile, which means that the tensile strength is an important factor. However, the analyses show that the main issue is not to know whether the peak tensile strength is 0.26 MPa or 0.52 MPa. It is more important to know the post failure properties of the tensile strength, i.e. the residual tensile strength. Variations of the residual tensile strength were shown to have much more impact on the instability indicators than the peak strength.

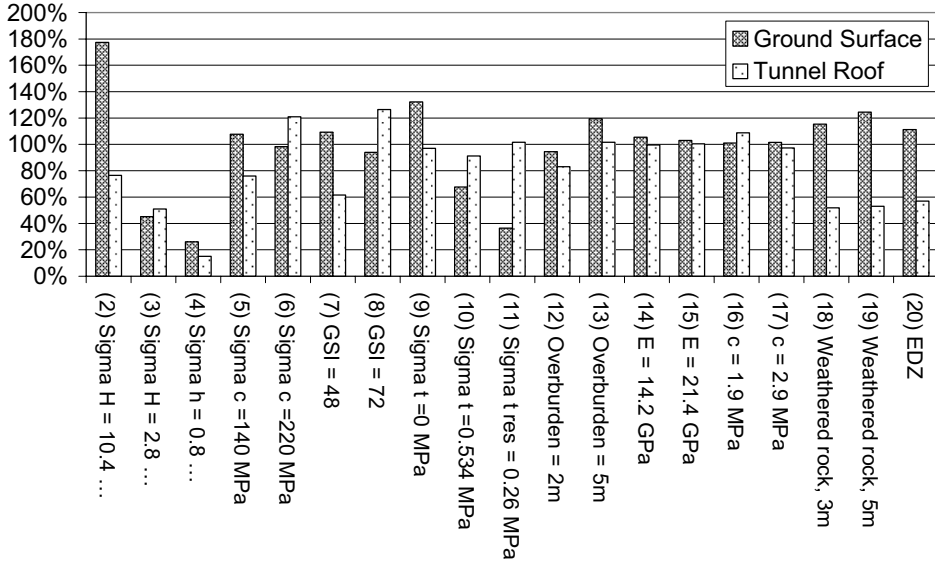


Figure 4.1 Tangential stress in the tunnel roof and on ground surface, relative the base case. The value of the base case represents 100%.

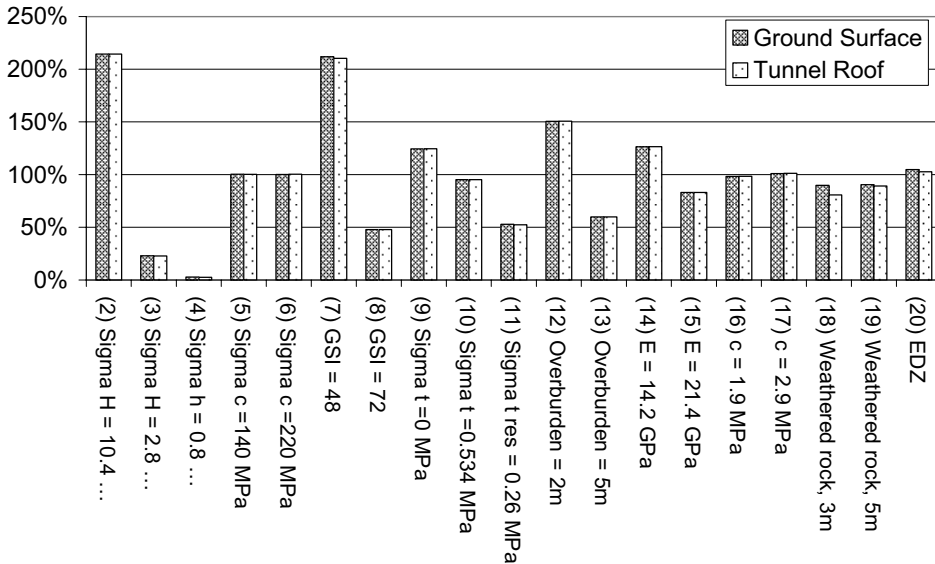


Figure 4.2 Heaving of the ground surface. Vertical deformation measured in the centre of the tunnel roof boundary and on ground surface. The value of the base case represents 100%.

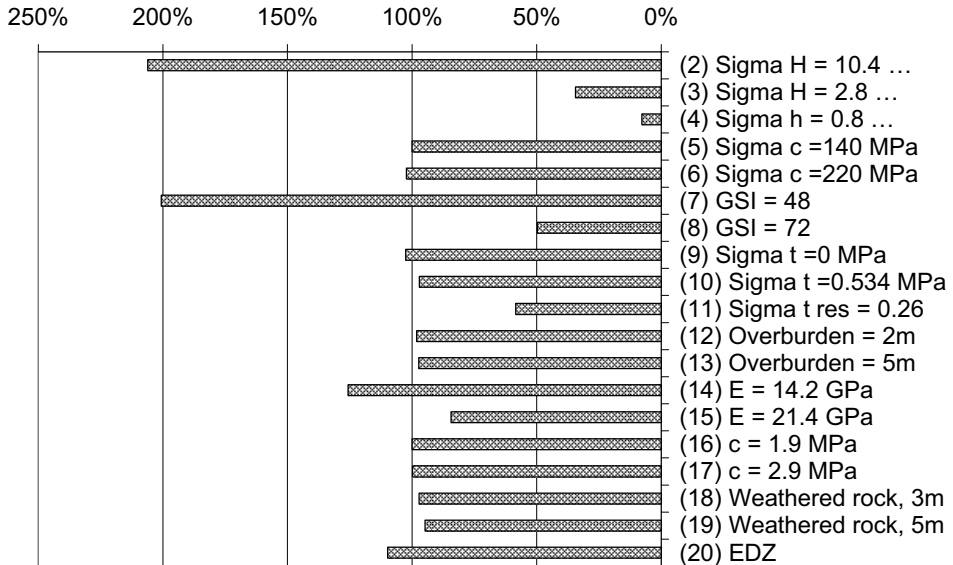


Figure 4.3 Deformation in the tunnel wall relative to the base case. The value of the base case represents 100%.

The sensitivity to variations in the state of stress was large for all instability indicators. This causes a dilemma. Stress measurements conducted at shallow depths are often considered as unreliable since the stresses at shallow depth are more sensitive to disturbances affecting the magnitude and direction and at the same time have a lower magnitude than stresses at greater depth. This means that the standard deviation of the measurements may be of the same magnitude as the stress. This fact has resulted in few stress measurements at shallow depth, and when the stress is measured, it is not considered to be reliable. Berg (2005), however, suggests an easy, fast and cheap stress measurement method where the closure of a slit made by a saw cut is measured. The theory of elasticity can be used to evaluate the state of stress. Saw cuts in different directions may give information about the stress orientation. The studies made by Berg (2005) show that the stresses at the rock surface are good indicators of the stress situation at shallow depth.

The conceptual analyses show that all instability indicators are sensitive to variations in GSI , which makes GSI a very important factor for the analysis of stability and behaviour. The GSI -value was varied 12 points. Edelbro (2004) showed that many of the classification systems are very subjective, and GSI can easily be varied more than 12 points on the same rock mass, due to subjective interpretations.

Moreover it is of interest to know whether the rock mass or regions of the rock mass have been subjected to weathering or other strength reducing mechanisms. If areas of the roof and abutments lose 50 % of strength and stiffness, the rock mass will lose its ability to carry stresses. This can lead to distressed areas and fallouts of wedge formations.

A general overview of how sensitive the instability indicators are to variations of the different parameters is presented in Table 4.1. The sensitivity to the variation of a specific parameter on the stability indicators was divided into three categories, high, medium and low. The intervals of the categories for tangential stress, σ_{θ} , in the tunnel walls, abutments and roof as well as deformation of the tunnel boundary and the ground surface are presented in Table 4.2. The sensitivity is estimated by comparing the results obtained for the maximum and minimum values of the varied parameters with the results from the base case.

Area of plasticity and extent of tensile stresses could not be valued in the same way. For these indicators, the ratings have been set by a subjective estimation.

Table 4.1 The impact that the rock parameters have on the instability indicators.

	σ_{tan} , tunnel boundary	Deformation of tunnel boundary	Subsidence / heaving	Area of Plasticity	Extent of tensile stresses
Virgin state of stress	High	High	High	High	High
σ_{ci}	Medium	Low	Low	Low	-
<i>GSI</i>	High	High	High	High	-
σ_t	High	Medium	High	High	-
Over burden	High	High	High	Medium	Medium
<i>E</i>	Low	Medium	Medium	Low	-
<i>c/φ</i>	Low	Low	Low	Low	-
Weathering	High	Medium	Low	Low	-
<i>EDZ</i>	High	Low	Low	Low	-
Discontinuities	High	High	High	High	-

Table 4.2 Rating intervals for Table 4.1.

	σ_{tan} on tunnel boundary (MPa)	Deformation of tunnel boundary (cm)	Deformation of ground surface (cm)
High	> 10	> 1	> 1
Medium	> 5	> 0.5	> 0.5
Low	< 5	< 0.5	< 0.5

Deformations on the tunnel boundary and ground surface are very important, although in this work, the deformations cannot be directly translated into how they affect the stability of the tunnel. If the deformation is 200 % larger than for the base case, it does not necessarily mean that it is 2 times as unstable as the base case. This is still interesting information since it affects reinforcement, media (water, electricity, ventilation etc.) and buildings and structures located above the tunnel.

The tangential stress around the tunnel acts to hold blocks and wedges in place. Very low compressive or tensile stresses increase the risk of fallouts and progressive failure, while too high stresses can lead to compressive failure. It was shown in Chapter 3 that the tangential stresses are low in the walls and abutments of the tunnel. This increases the risk of fallouts defined by pre-existing structures, but the risk cannot be quantified in this work.

5 CASE STUDY – ARLANDABANAN

5.1 Introduction

To be able to study if the conceptual models are compatible to a case study, and to gain further knowledge of stability of shallow tunnels, a real case was analysed. A tunnel section of Shuttle station 2 in Arlandabanan, a railroad tunnel under Arlanda airport was chosen.

The Arlandabanan tunnel project was unique in Sweden especially since the design work was done simultaneously with the rock excavation, so-called “active design”. For every blast, geological mapping was carried out by the shift working geologist. Weekly follow-ups were performed where the deformations and drilling rates were measured and joint mapping was conducted. These follow-ups were then used along with weekly visits at the excavation site to determine the amount of reinforcement that was needed (Chang and Hellstadius, 1998).

Shuttle station 2 is 155 m long and has a span of 23 m. The overburden varies between 8 and 13 m. Terminal 5 is founded on the rock surface above the station. The rock mass consists of mica schist and mica gneiss. The structures of the rock mass have a general strike of 10 to 20° to the tunnel axis and a dip of approximately 70°, see Figure 5.1. Two larger structures have been encountered, a weaker zone consisting of a pegmatite dyke, and a clay gouge, Chang et al. (1998). They can be seen in Figure 5.2.

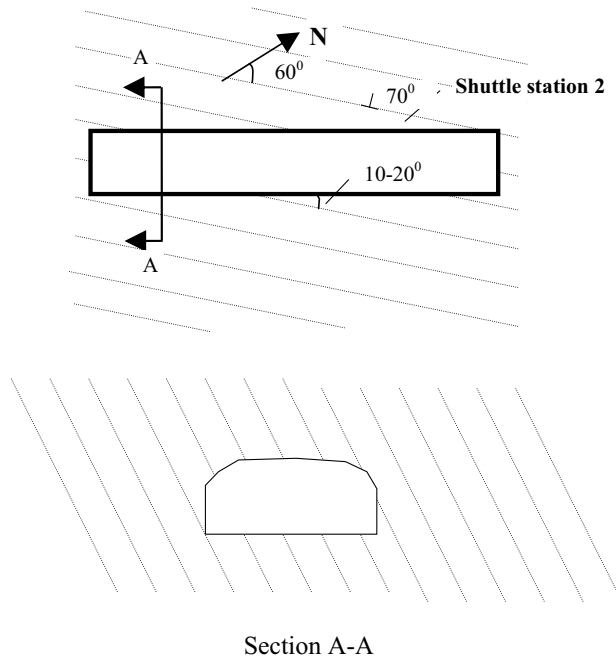


Figure 5.1 The position of the station in relation to the strike and dip of the mica schist, Chang et al. (1998).

The cross-section used for this case is 39/317, because both extensometer and convergence measurements have been conducted in this cross-section. Also, there are three foundation loads from Terminal 5 located in this cross-section. The location of extensometers, convergence pins and surface loads is shown in Figure 5.2.

The tunnel is excavated with two smaller pilot tunnels, labelled U2 and N2 in Figure 5.2, followed by pillar removal. However, in section 39/317, a small part of the pillar was left for an elevator shaft (excavated after the pilot tunnels). The shaft will not be taken into consideration in this work. This will probably result in larger deformations in the numerical analysis than the real case. The excavation of the pilot tunnels are referred to as excavation stage 1, or stage 1. The removal of the pillar is referred to as stage 2 of the excavation.

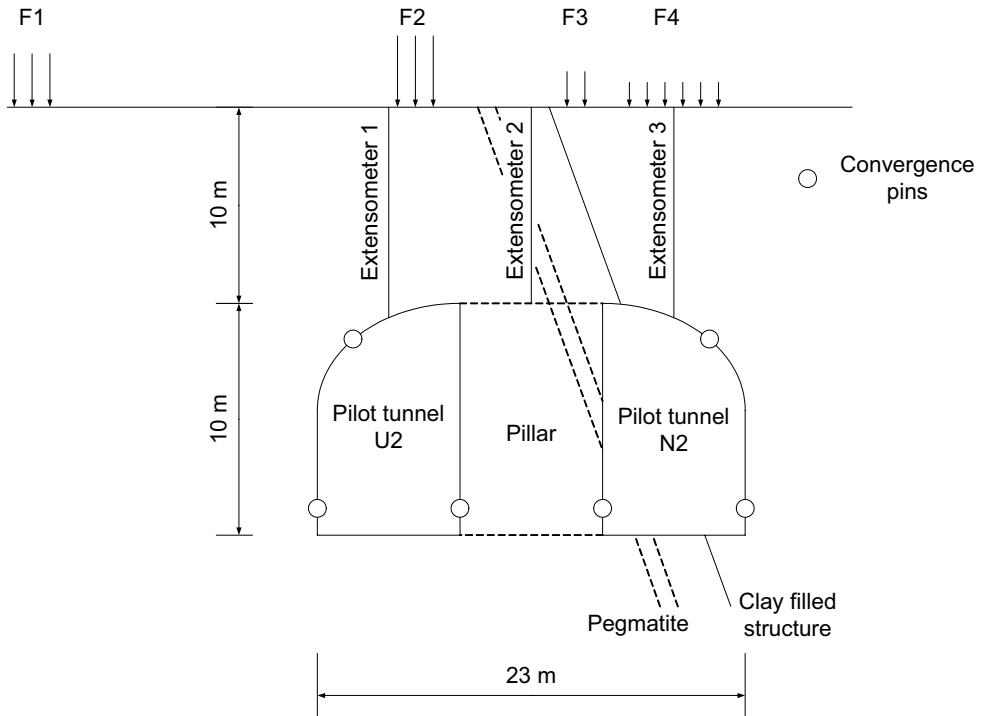


Figure 5.2 Schematic sketch for the excavation of Shuttle station 2.

5.2 Model setup and input data

FLAC 5.0 was used to model Shuttle station 2. In this case, no symmetry could be used due to the geological conditions (anisotropy and large structures) and surface loads. The effect of the pegmatite dyke was considered negligible and the clay filled structure and the mica schist would serve as weaknesses. Since the cross-section of Shuttle station 2 is wider than the cross-section in the conceptual analysis, the model size had to be somewhat altered. The width of the model of Shuttle station 2 was set to 210 m, and the height to 80 m, see Figure 5.3, to avoid boundary effects. The inner, finer grid size was set to at least one tunnel diameter in each direction, i.e. 70 m wide and 30 m high. Since this model is much larger than previous models, the zone size could not be kept the same. The finer grid size in this model is 0.25 x 0.25 m and the coarser grid 0.5 x 0.5 m. An interface was used in *FLAC* to simulate the clay filled structure, while the structure of the mica schist was simulated with ubiquitous joints.

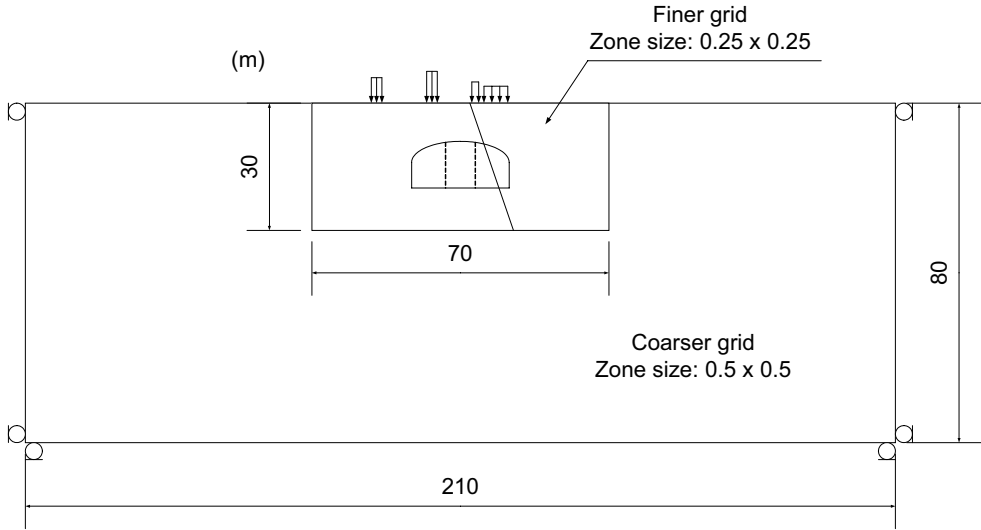


Figure 5.3 Model and grid size for the Shuttle station 2 analysis.

The virgin state of stress at Shuttle station 2 was estimated from rock stress measurements conducted by Bergsten et al. (1995) close to Shuttle station 2, see Figure 5.4. The measurements were interpreted and gave the following stress relations,

$$\sigma_H = \frac{z}{5.27} \quad [\text{MPa}] \quad (5.1)$$

$$\sigma_h = \frac{z}{10.0} \quad [\text{MPa}] \quad (5.2)$$

$$\sigma_v = \rho g z \quad [\text{MPa}] \quad (5.3)$$

where z is the depth, ρ is the density of the material, g is the gravitational force, σ_H is the major horizontal stress, σ_h is the minor horizontal stress and σ_v is the vertical stress. In Figure 5.4 it can be seen that the direction of σ_H is around 120 to 150° from north, which makes σ_H perpendicular to the tunnel axis.

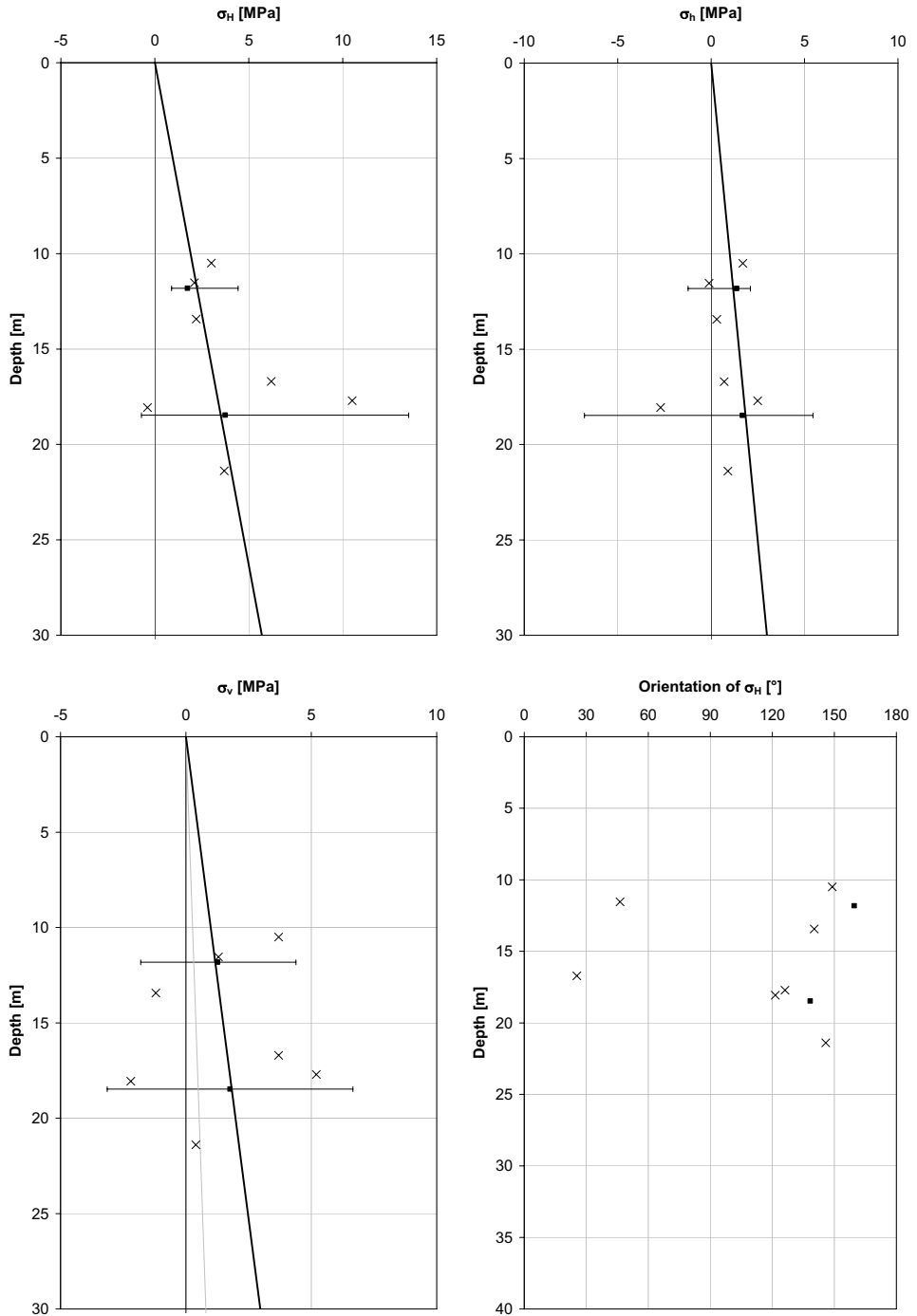


Figure 5.4 Stress measurements conducted close to Shuttle station 2, modified from Bergsten et al., (1995).

The strength of the rock mass at Shuttle station 2 was determined from mapping protocols. The Q-system was used to classify the rock mass of the station. The Q -value was converted to a GSI -value according to Equation (2.9), suggested by Hoek et al., (1995).

The result of the classification of the station is presented in Figure 5.5. The cross-section examined in this work is at co-ordinate 39317. The GSI -value chosen for this analysis was 58, illustrated by the dashed line in Figure 5.5, and the straight vertical line represents the cross-section.

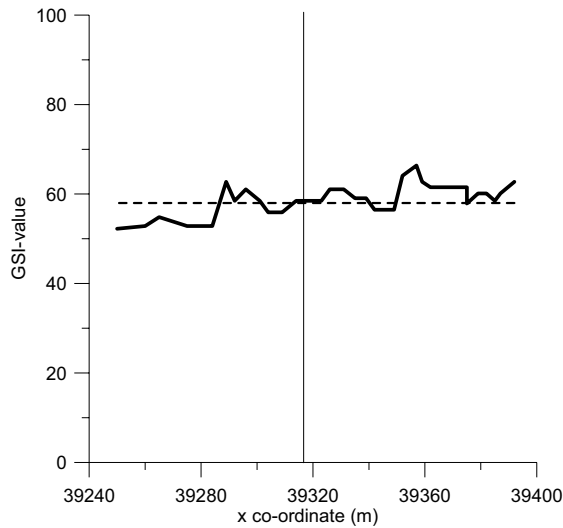


Figure 5.5 GSI -values for the x-coordinates of Shuttle station 2.

The intact uniaxial compressive strength was estimated using the values of the R -scale (Brown, 1981). In the area of the cross-section 39/317, the R -values were $R3$ and $R4$. $R3$ has a uniaxial compressive strength span of 25-50 MPa and $R4$, 50-75 MPa. According to *RocLab*, both groups could include schist. The uniaxial compressive strength for the base case, or Case 1 was assumed to be 75 MPa, and another case (Case 2) was examined with an uniaxial strength of 50 MPa, see Table 5.2.

There are three foundations that transfers load to the rock surface. A fourth, more widely distributed load is located approximately 20 m away from the investigated cross-section, see Figure 5.2 and Figure 5.6. These foundations transfers permanent loads of 7150 kN (F1), 11000kN (F2), 1300 kN (F3) and 10000 kN (F4). The load that the foundation transfers to the rock surface has in this two-dimensional model been simulated as a distributed load in the

cross-section with an infinite extension length in the tunnel direction. The foundation loads have in this study been divided with the area of the foundation to get the load per meter tunnel, see Table 5.1. Six different cases have been analysed, see Figure 5.7.

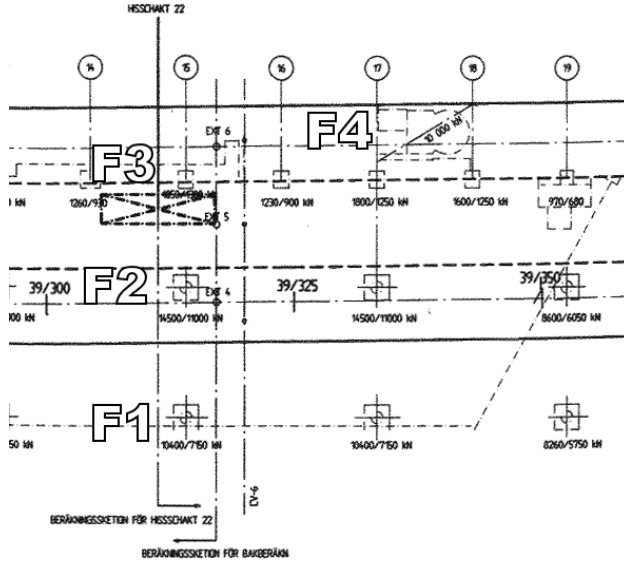


Figure 5.6 Location of surface loads

Table 5.1 Surface loads.

	Load	Area	Effective load
F1	7150 kN	2.5 x 2.5 m ²	1.14 MPa
F2	1100 kN	2.5 x 2.5 m ²	1.76 MPa
F3	1300 kN	2.5 x 2.5 m ²	0.58 MPa
F4	10000kN	5.5 x 9.2 m ²	0.20 MPa

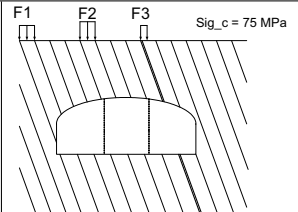
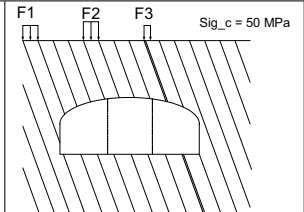
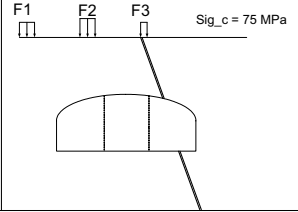
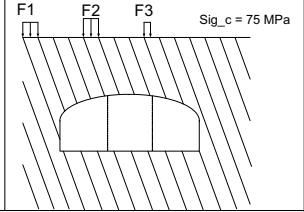
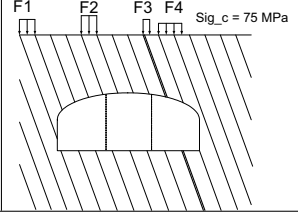
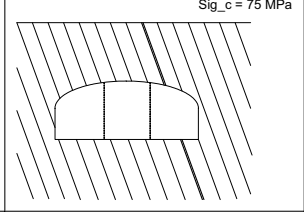
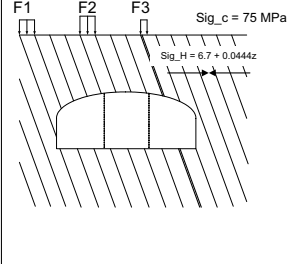
<p>Case 1</p> <p>Considers the mica schist orientation, clay filled structure and loads 1 - 3</p>		<p>Case 2</p> <p>Same as case 1, but with lower σ_{ci}.</p>	
<p>Case 3</p> <p>Same as case 1, except no consideration to mica schist orientation.</p>		<p>Case 4</p> <p>Same as case 1, except no consideration to clay filled structure.</p>	
<p>Case 5</p> <p>Same as case 1, except load F4 is considered.</p>		<p>Case 6</p> <p>Same as case 1, except no surface loads.</p>	
<p>Case 7</p> <p>Same as case 1, except virgin state of stress same as base case in conceptual analysis.</p>			

Figure 5.7 Description of the different cases of Shuttle station 2.

Table 5.2 Data used for the analysis of Shuttle station 2, cases 1 to 7.

		Case 1	Case 2	Case 3	Case 4	Case 5	Case 6	Case 7
Rock mass	σ_{ci} (MPa)	75	50	75	75	75	75	75
	GSI	58	58	58	58	58	58	58
	E (GPa)	17.6	17.6	17.6	17.6	17.6	17.6	17.6
	c (MPa)	1.1	0.8	1.1	1.1	1.1	1.1	1.1
	ϕ ($^{\circ}$)	55	52.5	55	55	55	55	55
	σ_r (MPa)	0.32	0.21	0.32	0.32	0.32	0.32	0.32
Clay filled structure	c (MPa)	0.05	0.05	0.05	-	0.05	0.05	0.05
	ϕ ($^{\circ}$)	25	25	25	-	25	25	25
	σ_r (MPa)	0	0	0	-	0	0	0
Ubiquitous Joints	c (MPa)	0.3	0.3	-	0.3	0.3	0.3	0.3
	ϕ ($^{\circ}$)	40	40	-	40	40	40	40
	σ_r (MPa)	0	0	-	0	0	0	0
Surface loads	$F1$ (MPa)	1.14	1.14	1.14	1.14	1.14	-	1.14
	$F2$ (MPa)	1.76	1.76	1.76	1.76	1.76	-	1.76
	$F3$ (MPa)	0.58	0.58	0.58	0.58	0.58	-	0.58
	$F4$ (MPa)	-	-	-	-	0.20	-	-
Virgin state of stress	σ_H	$z/5.27$	$z/5.27$	$z/5.27$	$z/5.27$	$z/5.27$	$z/5.27$	$6.7+0.044z$
	σ_h	$z/10.0$	$z/10.0$	$z/10.0$	$z/10.0$	$z/10.0$	$z/10.0$	$0.8+0.033z$
	σ_v	ρgz						

5.3 Focus areas of the analysis

Since Arlandabanan and Shuttle station 2 already are excavated and fully operational, it is known that Shuttle station 2 is stable. It is also known that no major instability problems occurred during the excavation of this tunnel. To be able to study the difference in stability and behaviour of the different cases defined above, and to be able to compare data from measurements conducted during the construction of the station, four different indicators were studied. They are (i) tangential stress around the tunnel boundary, (ii) deformation of the tunnel boundary, (iii) the area of plasticity and (iv) extensometer measurements. All analyses have been divided into stage 1 (the two pilot tunnels), and stage 2 (removal of the pillar). Short explanations of the analyses follow below.

The analysis of deformations of the tunnel boundary (ii) includes a comparison with the convergence measurements conducted when excavating the station. The same applies for extensometer measurements, where the extensometer measurements are compared to the expansion of the overburden.

(i) Tangential stress around the tunnel boundary

The tangential stress around the tunnel boundary is an important factor for the stability of wedges. Low compressive or tensile tangential stress increases the risk of opening of pre-existing joints and tensile failure, while high compressive stresses can lead to compressive failure. The tangential stress was determined in 6 different points in each pilot tunnel and in 9 boundary points in the fully excavated station.

(ii) Deformation of the tunnel boundary

The deformation of the tunnel boundary can be an indicator of instability, but might also affect rock reinforcement and installations such as electricity, water and ventilation. The deformations of the models are compared with the results from convergence measurements conducted during the excavation of the tunnel.

(iii) Deformation of the ground surface

During the construction of the Arlandabanan, the deformation of the ground surface was a main concern. Terminal 5 has its foundations on the rock surface above Shuttle station 2. Not only does the foundations distribute load on the rock mass, but the deformation of the ground surface must also be controlled to avoid damage to the terminal.

(iv) Extensometer measurements

The expansion and/or contraction of the overburden were measured with three sets of extensometer measurements. The expansion and/or contraction over the overburden is highly connected to the subsidence or heaving of the ground surface, but not necessarily equivalent. The vertical displacement of the overburden was measured for the different cases, and compared to the measurements conducted when excavating the station.

5.4 Results

It should be noted that in Case 2 (the uniaxial compressive strength, σ_{cis} , was 50 MPa instead of 75 MPa) the model was unable to reach equilibrium in Stage 2 of the analysis (removal of the pillar). The tunnel suffers chimney caving between load F2 and the clay filled structure, see Figure 5.8. Therefore Case 2 will not be present in the presentation of results for Stage 2. However, The results for Stage 1 will be presented since the model was able to reach equilibrium in this part of the analysis.

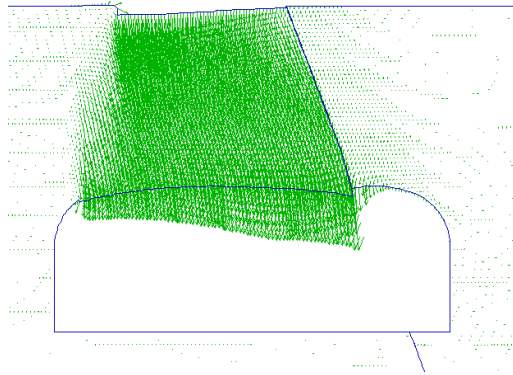


Figure 5.8 The displacement directions for case 2, where chimney caving occurs when pillar is removed.

5.4.1 Tangential stress around the tunnel boundary

Stage 1

Generally the tangential stress is low, yet compressive. Higher values are generally obtained at measurement points 3 (~ 6-8 MPa) and 10 (~ 4-8 MPa), see Figure 5.9, Figure 5.10 and Figure 5.11. Case 3 (does not include the orientation of the mica schist) and case 4 (does not include the clay filled structure) show similar behavior of the tangential stress with very low stresses in the tunnel wall of tunnel N2 while the abutment of tunnel N2 has higher stresses than the other cases.

Case 6 (no surface loads) has generally lower tangential stresses around the tunnel boundary, especially in the pillar which seems destressed. Case 7 (higher virgin state of stress) does also show a destressed pillar, but with high stresses at measurement point 3 and 10.

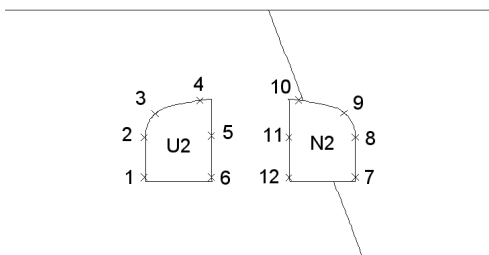
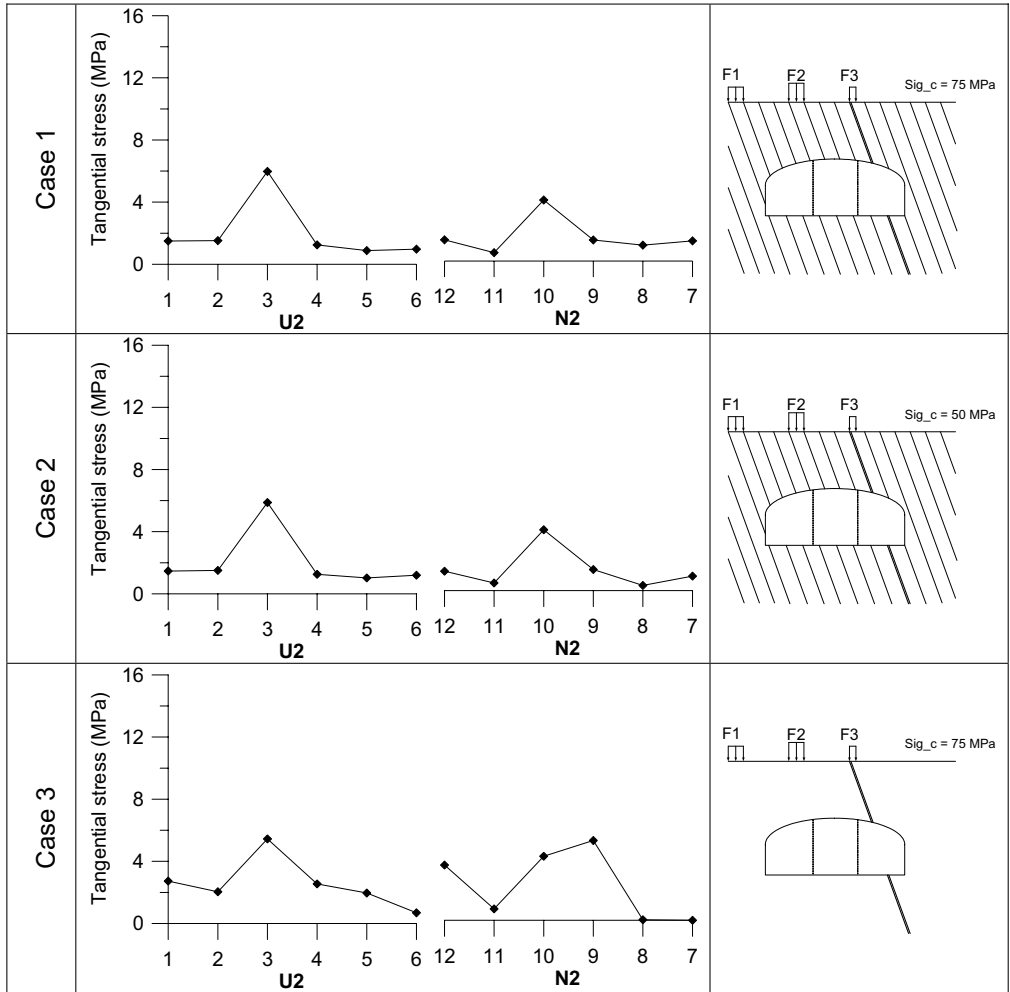


Figure 5.9 Tangential stress around the pilot tunnels U2 and N2 for cases 1, 2 and 3.

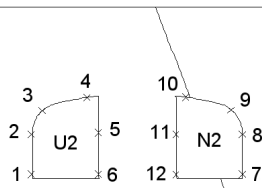
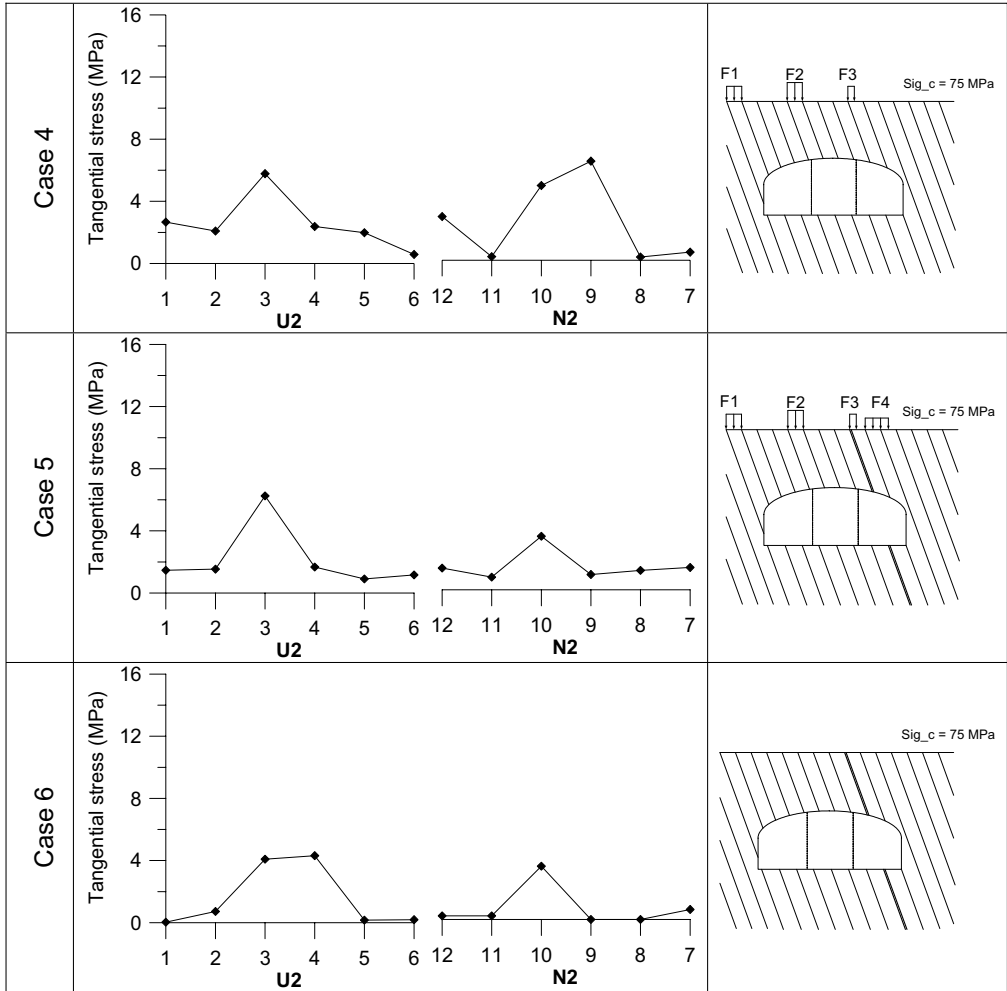


Figure 5.10 Tangential stress around the pilot tunnels U2 and N2 for cases 4, 5 and 6.

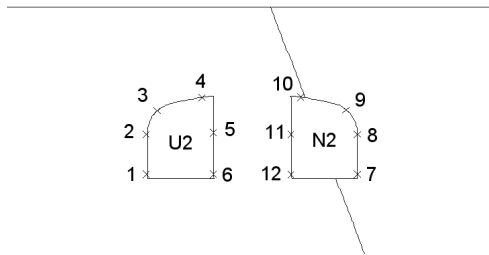
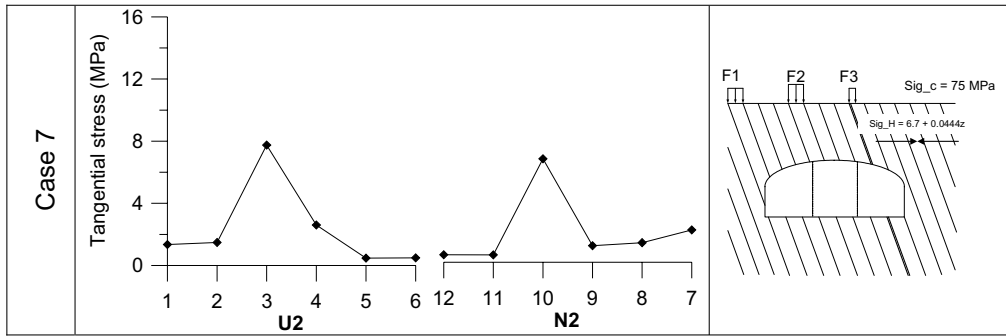


Figure 5.11 Tangential stress around the pilot tunnels U2 and N2 for case 7.

Stage 2

The results from the pillar extraction show that the stresses increase in magnitude compared Stage 1 of the excavation, but the stresses can still be considered as fairly low. However, at measurement point 3, which is located at the left abutment of the tunnel, the tangential stress is higher than the other measurement points, while the tangential stress in measurement point 4, on the left side of the tunnel roof, is considerably than in the others points. This applies for all cases except case 6 (no surface loads) and case 7 (higher virgin state of stress). In case 6, the tangential stress is more evenly distributed over the tunnel boundary. However, the tangential stress at the right abutment and wall of case 6 is lower than in the other points. Case 7 show high tangential stress over the tunnel roof. The results of this analysis are presented in Figure 5.12 and Figure 5.13.

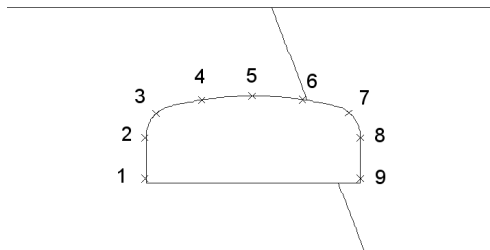
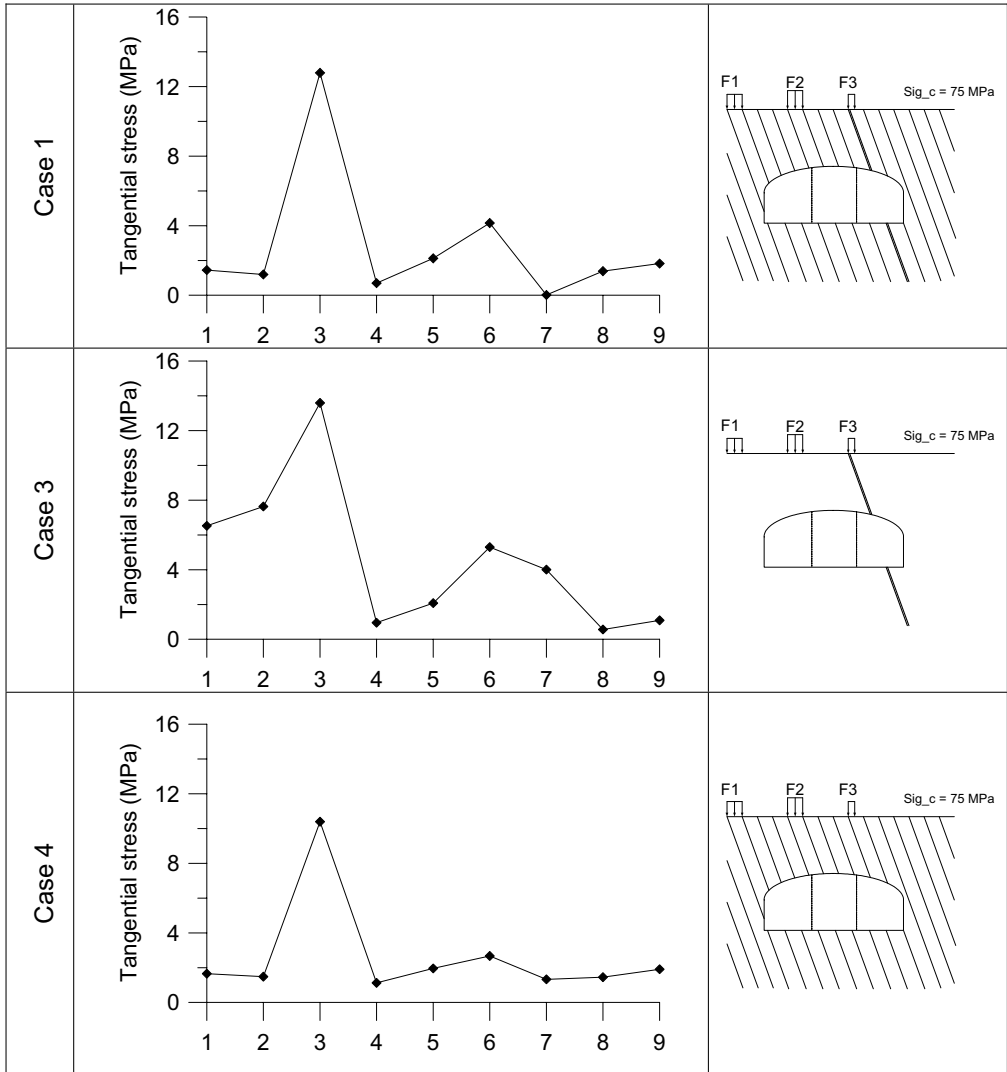


Figure 5.12 Tangential stress around the tunnel after stage 2, for cases 1, 3 and 4.

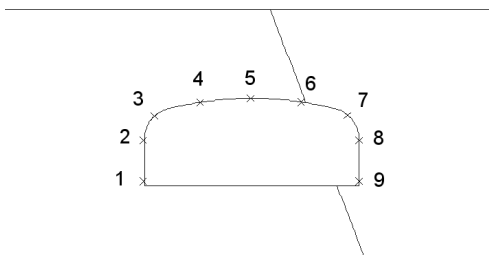
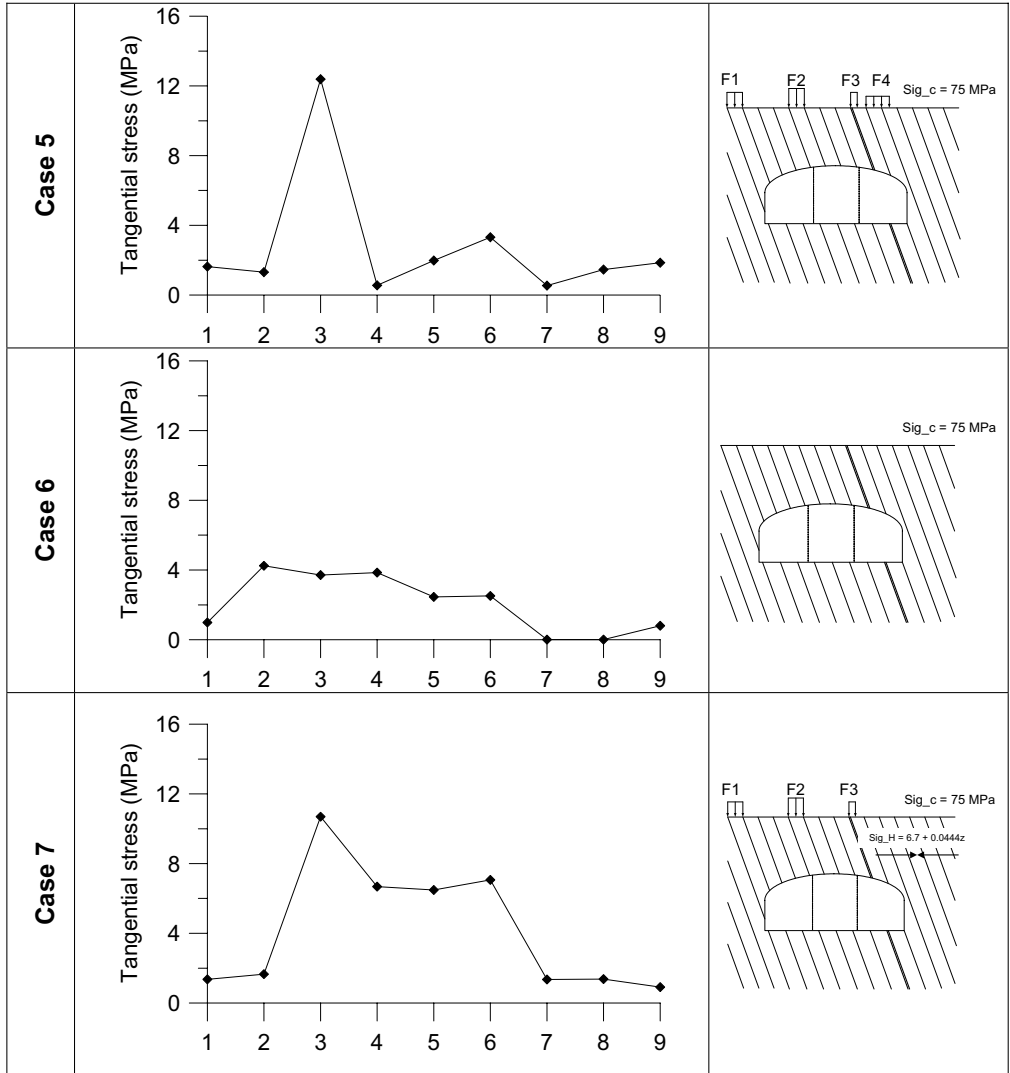


Figure 5.13 Tangential stress around the tunnel after stage 2, for cases 5, 6 and 7.

5.4.2 Deformation of the tunnel boundary

Stage 1

The results from the analyses of the deformation of the tunnel boundary of stage 1 are presented in Figure 5.14 and Table 5.3. The deformations from the numerical analyses are multiplied with a factor of 300 to become visible in Figure 5.14 while the measured convergences are only showing the general direction of the deformations. Cases 1 to 6 show that the tunnel walls deform inwards and limited, if any, deformation is seen in the pillar. The tunnel roof is deforming inward in all cases except case 6, where no consideration is taken to surface loads. A shear displacement can be seen in the clay filled structure for all cases except case 4, where the structure is not present. Case 7 (higher virgin state of stress) show greater deformation than the other cases. The multiplication factor had to be reduced to 200 to get an understandable image of the deformation in Figure 5.14. It can also be seen that some heaving of the floor of tunnel N2 (right) occur.

The convergence measurements at Shuttle station 2, show that most of the deformation is in the horizontal plane. The walls converge, while the pillar contracts.

A comparison of the tunnel measurements and the calculated displacements for the numerical analyses, show that the measurement points in the tunnel walls (1 and 4) show good agreement. The measurement point in the abutments (2 and 3) show good agreement in the x-direction, while the deformations in the y-directions are contradictory. The measured displacements in the pillar and the calculated displacements have moved in opposite directions.

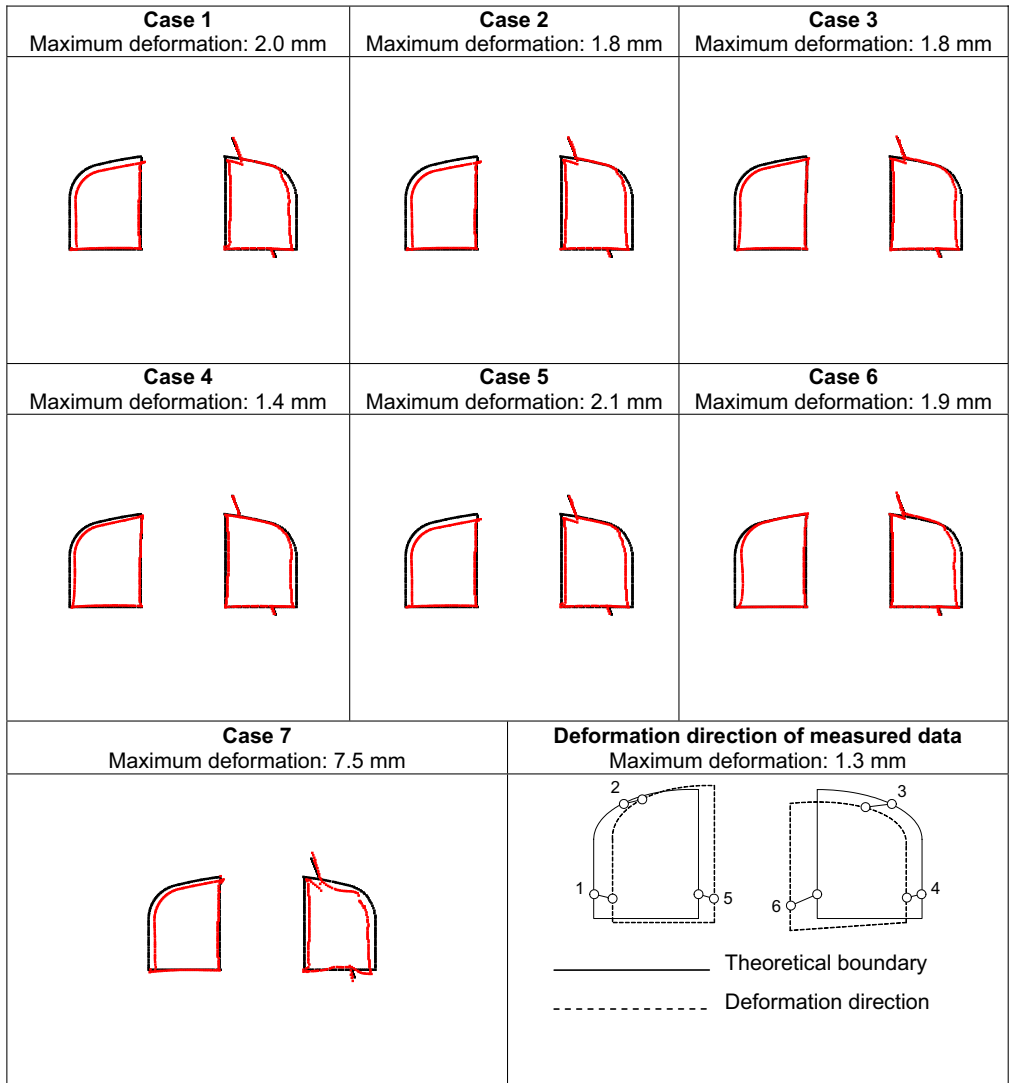
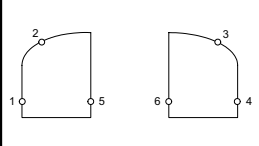


Figure 5.14 Deformation of the tunnel boundaries for Stage 1 calculated for cases 1 to 7 and deformations from convergence measurements of the pilot tunnels. The deformations from numerical analyses are multiplied with a factor of 300 for all cases except case 7, which is multiplied with 200. The measured convergences only show general direction.

Table 5.3 Results from convergence measurements and values calculated for the different cases for stage 1.

		Measured values (mm)	Case 1 (mm)	Case 2 (mm)	Case 3 (mm)	Case 4 (mm)	Case 5 (mm)	Case 6 (mm)	Case 7 (mm)
1	xdisp	0,9	1,8	1,8	1,2	1,2	1,8	1,9	6,9
	ydisp	-0,2	-0,5	-0,5	-0,4	-0,4	-0,4	-0,0	-0,7
2	xdisp	0,9	1,5	1,5	1,2	1,2	1,4	1,3	7,5
	ydisp	0,3	-1,8	-1,8	-1,1	-1,1	-1,7	0,2	-1,7
3	xdisp	-1,3	-0,3	-0,5	-1,0	-1,0	-0,3	-1,3	-4,3
	ydisp	-0,1	0,0	0,2	0,4	0,4	-0,4	0,6	-2,1
4	xdisp	-0,7	-1,8	-1,8	-1,6	-1,6	-1,8	-1,7	-6,0
	ydisp	-0,2	-0,2	-0,1	-0,1	-0,1	-0,2	-0,4	-2,4
5	xdisp	0,8	-0,5	-0,5	-0,4	-0,4	-0,5	-0,5	-0,7
	ydisp	-0,2	0,2	0,2	0,0	0,0	0,2	-0,1	-0,4
6	xdisp	-1,3	1,1	1,2	0,5	0,5	1,1	0,7	5,0
	ydisp	-0,6	-0,9	-0,9	-0,5	-0,5	-1,3	0,1	-3,9

Stage 2

The results from the pillar extraction (stage 2) are shown in Figure 5.15 and Table 5.4. The deformations calculated in the numerical analyses shown in Figure 5.15 are multiplied with a factor of 150, to become visible, while the measured convergences of Shuttle station 2 only show the general direction of the deformations.

Cases 1 to 7 show that the tunnel roof moves downwards. Case 1, 3 and 5 show similar behavior with a maximum total deformation at the clay filled structure of 23 to 26 mm. Cases 4 (does not include the clay filled structure) and 6 (no surface loads) show considerably less deformation of the tunnel boundary. Case 7 (higher virgin state of stress) shows more deformation of the tunnel walls, and heaving of the tunnel floor. It can also be seen that the effect of the clay filled structure is reduced, when the stresses are higher.

Convergence measurements of the tunnel show subsidence of the left part of the tunnel (measurement points 1 and 2) while the middle and right part (measurement points 3, 4 and 5) of the tunnel heaves. The numerical analyses and the measured values show better agreement in the left side of the tunnel than at the right side.

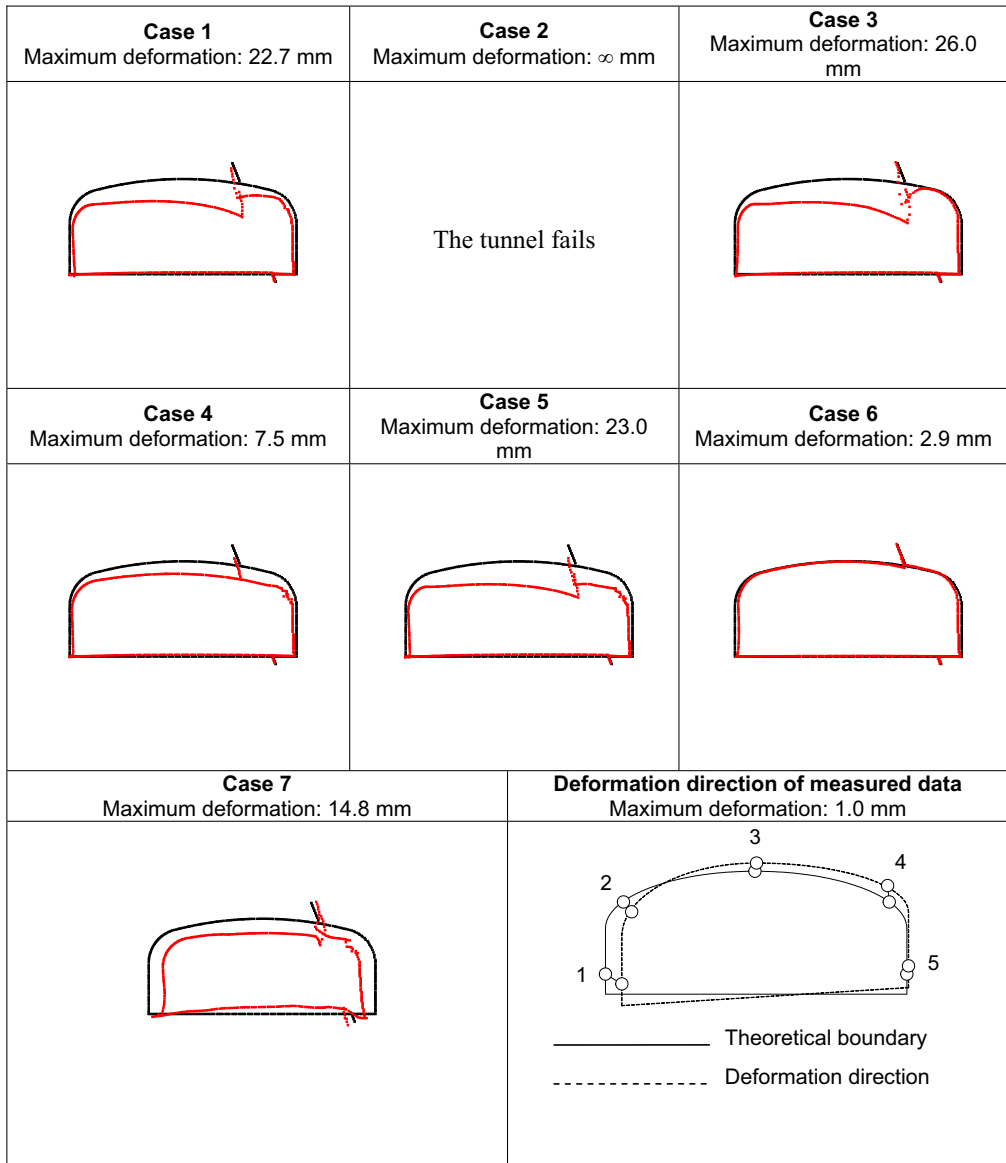
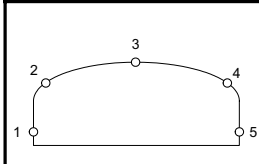


Figure 5.15 Deformation of the tunnel boundaries for Stage 2 calculated for cases 1, 3, 4, 5, 6 and 7 and deformations from convergence measurements of the pilot tunnels. The deformations from numerical analyses are multiplied with a factor of 150. The measured convergences only show general direction.

Table 5.4 Results from convergence measurements and values calculated for the different cases for stage 2.

		Measured values (mm)	Case 1 (mm)	Case 3 (mm)	Case 4 (mm)	Case 5 (mm)	Case 6 (mm)	Case 7 (mm)
1	xdisp	1,0	2,0	1,0	1,5	1,7	1,86	7,9
	ydisp	-0,6	-1,4	-1,7	-0,9	-1,2	0,01	-1,7
2	xdisp	0,5	2,0	1,8	1,0	1,4	1,35	8,9
	ydisp	-0,6	-8,7	-8,5	-5,0	-8,8	0,04	-5,2
3	xdisp	0,1	3,2	3,2	1,3	2,4	0,30	7,3
	ydisp	0,5	-16,3	-17,6	-8,6	-16,5	-0,23	-9,8
4	xdisp	-0,1	-1,0	-1,6	1,2	-0,2	-1,33	-6,0
	ydisp	1,0	-3,5	0,1	-8,4	-8,8	0,55	-5,0
5	xdisp	0,1	-2,0	-1,9	-1,7	-1,9	-1,73	-7,8
	ydisp	0,5	-0,3	-0,1	0,1	-0,2	-0,33	-3,0

5.4.3 Deformation of the ground surface

Stage 1

The results from the analysis of stage 1 are presented in Figure 5.16. It is shown that the left part subsides, while the right part, over pilot tunnel N2 heaves. This is partly due to a shear movement along the structure and the direction of the mica schist. Case 3 (does not include mica schist orientation) and Case 4 (does not include the clay filled structure) show less subsidence. The removal of the surface loads (Case 6) reduces the subsidence greatly and higher horizontal stresses (Case 7) increased the heaving greatly. In the latter case, a smaller peak in the heaving can be seen. This is because the rock mass is consolidated at ground surface near the clay filled structure, see Figure 5.17.

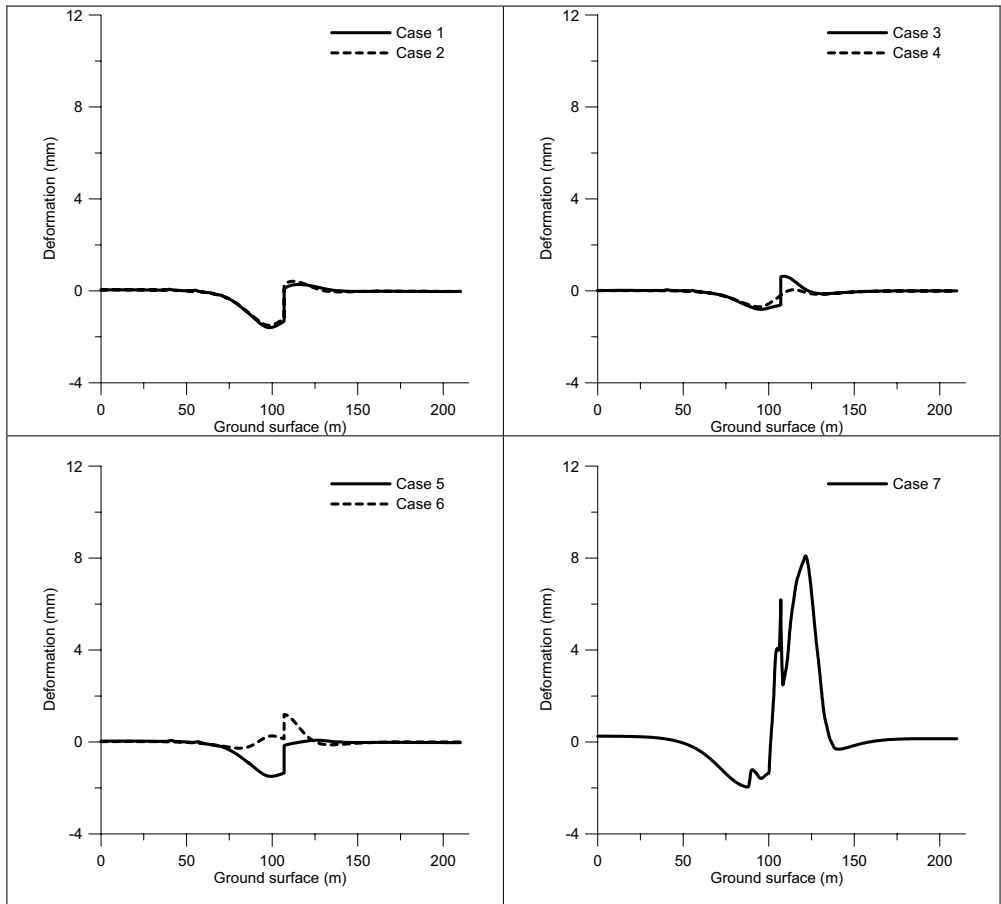


Figure 5.16 Deformation of the ground surface in Stage 1 for cases 1 to 6.

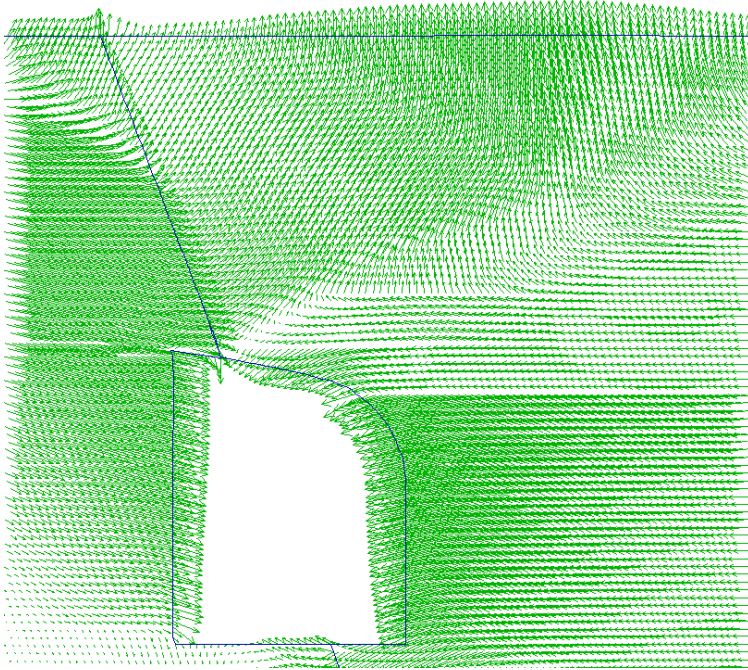


Figure 5.17 Displacement vectors of Case 7, higher virgin state of stress.

Stage 2

The behaviour of the ground surface after stage 2 is similar to that of Stage 1, with the difference that the subsidence is greater, see Figure 5.18. Again, especially case 4 (no clay filled structure) shows less subsidence. Case 6 (no surface loads) shows a tendency of heaving. A notch can be seen in Case 1, Case 4 and Case 6. This is a small part of the rock surface that heaves due to punching of surface load 2 into the ground surface, see Figure 5.19. Case 7 (higher virgin state of stress) shows similar patterns as for the pilot tunnels.

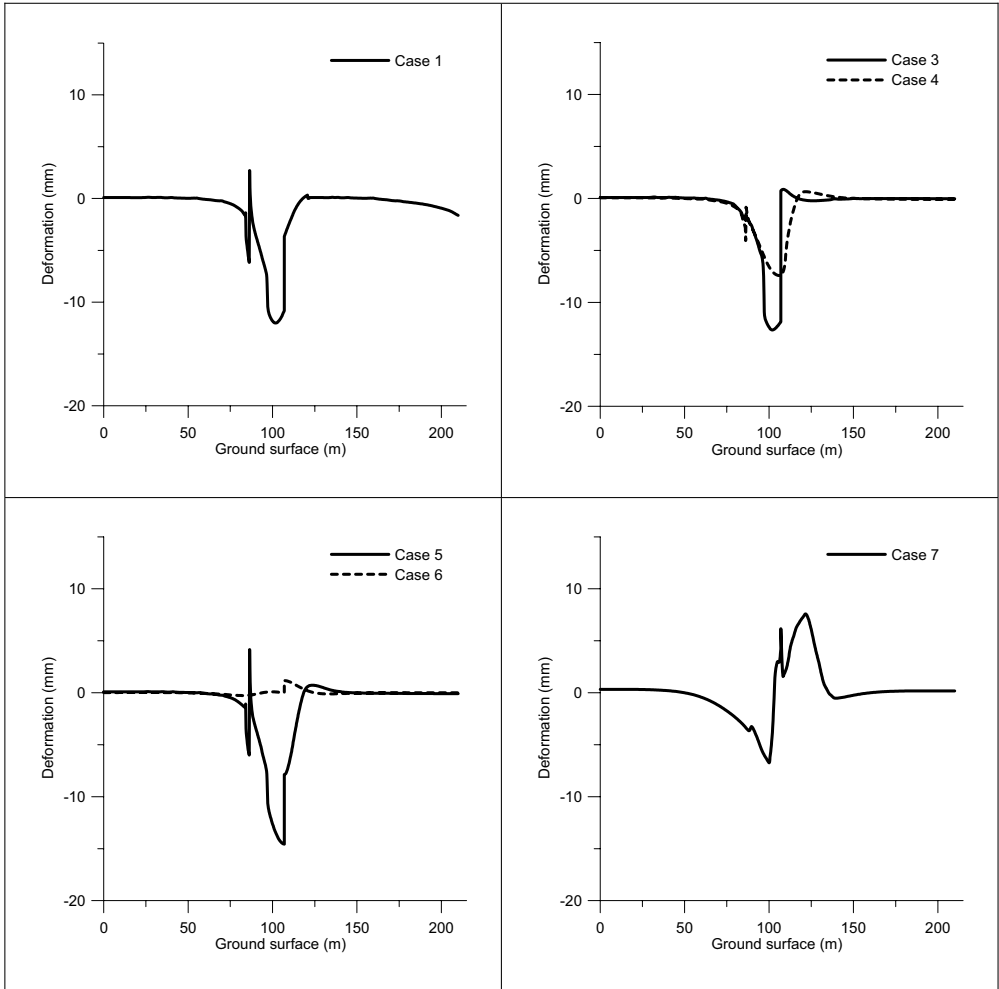


Figure 5.18 Deformations of the ground surface in Stage 2 for all cases for stage 2, except case 2, which fails. Observe the difference in the scale to stage 1.

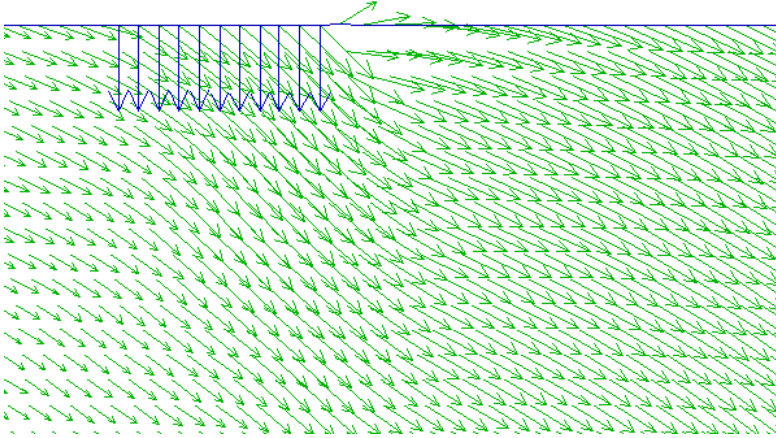


Figure 5.19 Close up on surface load F_2 (blue arrows) and displacement vectors (green arrows) of Case 1.

5.4.4 The area of plasticity

Stage 1

The area of plasticity developed for the different cases of Shuttle station 2 consists mostly of tensile failure, and slip along ubiquitous joints (i.e. slip along the mica schist). Figure 5.20 shows that tensile failure occurs in the wall and abutment of pilot tunnel N2 for all cases. In case 6 (no surface loads) tensile failure can be observed at the wall of pilot tunnel U2 as well. Ubiquitous joint failure can be observed in the pillar and in the wall of tunnel U2 for all cases except case 3 (without ubiquitous joints) and case 4 (no clay filled structure). When the virgin stresses were increased (Case 7) the zone of plasticity increases greatly. The pillar and the tunnel walls have experienced tensile failure, and slip along ubiquitous joints has occurred in the pillar, the left tunnel wall and over the right abutment. A band of shear failure extends from the intersection of the tunnel roof and the structure and up to the ground surface. This can be explained with the displacement vectors in Figure 5.17.

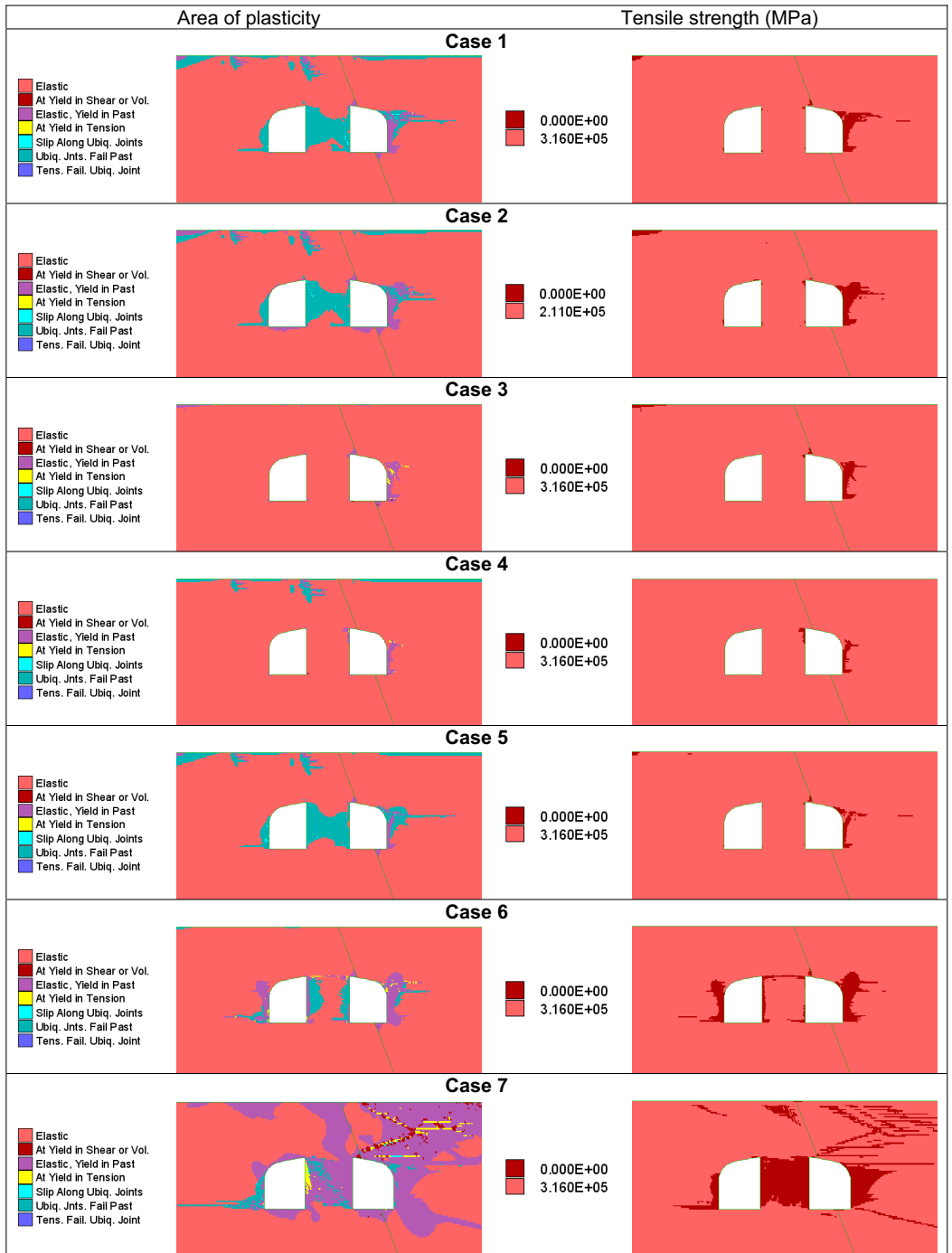


Figure 5.20 Area of plasticity and tensile strength of case 1 to 7 in Stage 1.

Stage 2

The area of plasticity grows after excavating the pillar, see Figure 5.21. Tensile failure can be seen in a region at the right tunnel abutment/roof. This is more or less obvious in all cases, except for case 6 (no surface loads) Furthermore, it shows that the failure consists of tensile failure, shear failure underneath the surface load F2, slip and tensile failure along ubiquitous joints.

Just left of surface load F2, an area of tensile failure can be seen for all cases with a clay filled structure, surface loads and low stresses, i.e. Case 1, Case 2, Case 4 and Case 5. This area originates from a bending motion of the overburden created by slip in the clay filled structure and the surface load, see Figure 5.15 and Figure 5.21. When the overburden bends down along the clay filled structure, tensile failure takes place above the left abutment of the tunnel.

Furthermore, it can be seen that slips along ubiquitous joints occur in the tunnel walls and at the right abutment.

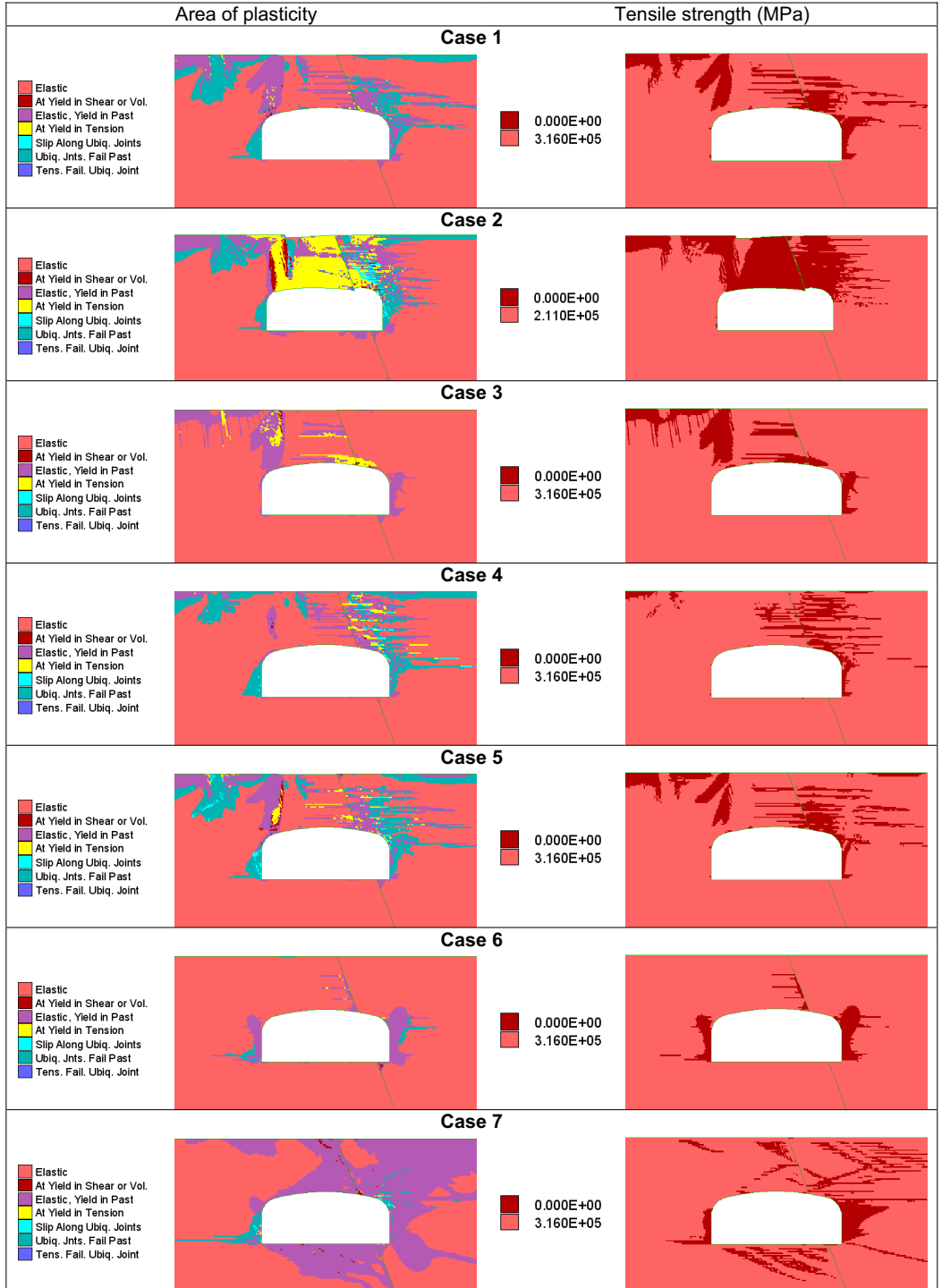


Figure 5.21 Area of plasticity and tensile strength of case 1 to 6 in Stage 2.

5.4.5 Extensometer measurements

Stage 1

Extensometer measurements were conducted when the station was constructed. The expansion and/or compaction of the overburden was calculated from the results of the analyses and compared with real deformations.

Extensometer 1 and the corresponding values from the analyses show similar results, see Figure 5.22. Extensometer 2 shows an expansion of 3 mm above the pillar, where the models show values less than 0.5 mm, except for Case 7 (high virgin state of stress) that has an extension of about 6 mm. Extensometer 3 returns a negative value, i.e. contraction of the overburden. This is not seen in any of the cases. Again, Case 7 shows a great extension, this time almost 9 mm.

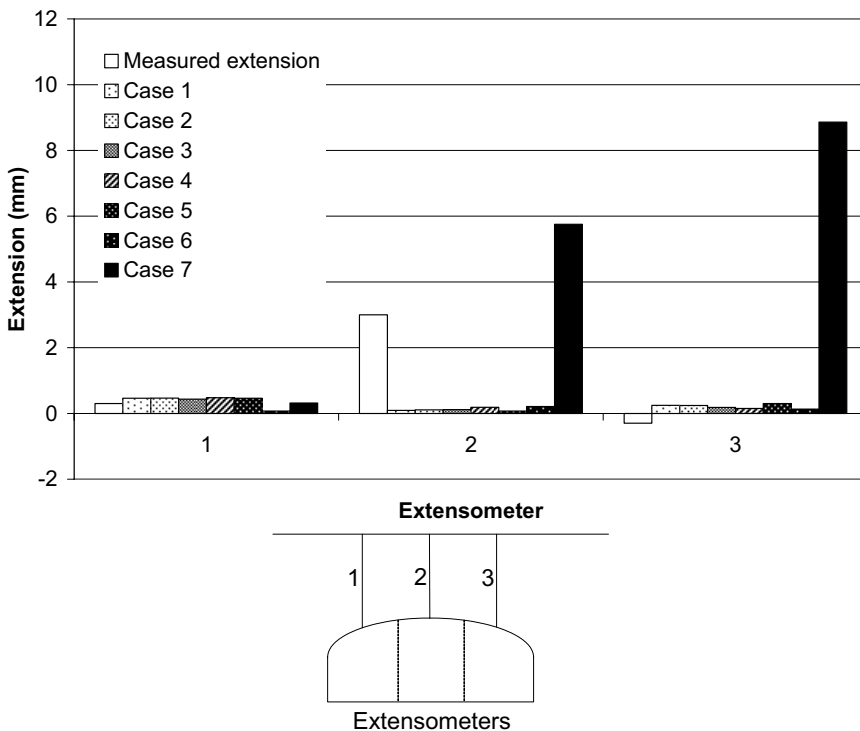


Figure 5.22 Results from extensometer measurements of Shuttle station 2, and calculated values from cases 1 to 7.

Stage 2

In stage 2, extensometer 2 is missing due to excavation of an elevator shaft. Extensometer 1 shows an expansion of approximately 0.5 mm, which is comparable to the modeled data, see Figure 5.23. Extensometer 3 shows an extension slightly greater than 0.5 mm. Cases 1, 4, 5 and most notably Case 7 show much larger expansions of the overburden. Case 3, (no ubiquitous joints) shows a similar extension of the overburden as the one measured in the case study.

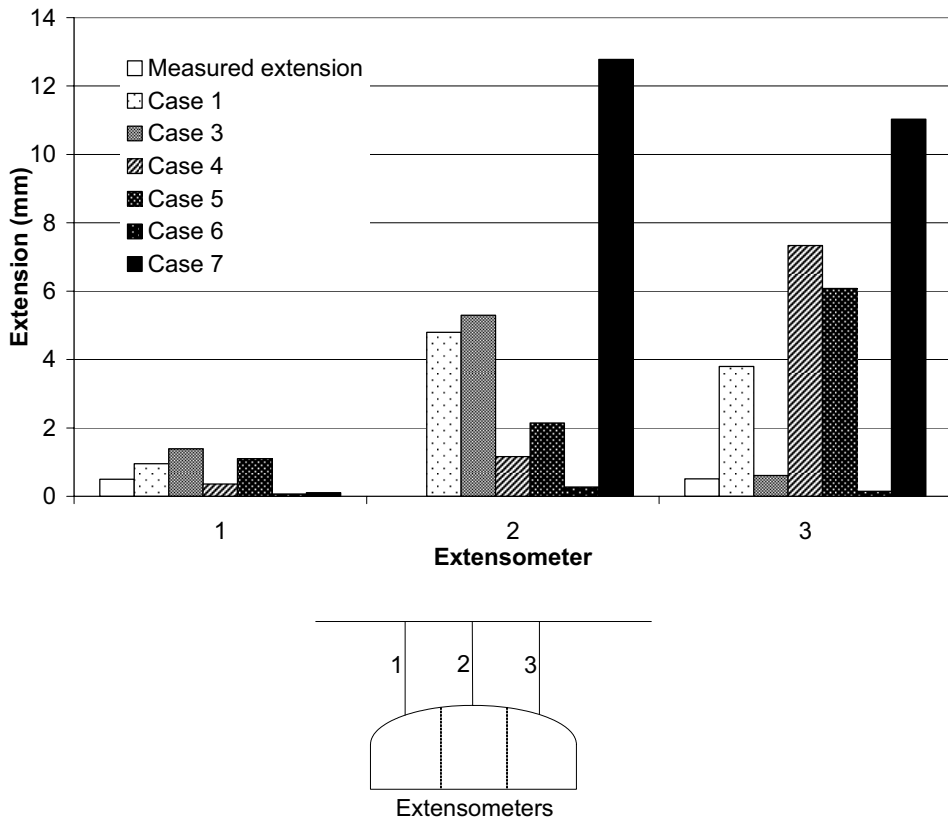


Figure 5.23 Results from extensometer measurements (only extensometer 1 and 3) of Shuttle station 2, and calculated values from all cases except case 2.

6 DISCUSSION

To achieve the objectives of this project, conceptual analyses and analyses of an existing case have been conducted. Important questions are, how can the results be used to describe the behaviour and is it possible to translate the results into an absolute stability prognosis of a real case?

6.1 Conceptual analysis

The procedure of estimating the rock mass parameters for the conceptual models have resembled the established routines for data collection of real cases, i.e. the strength parameters such as cohesion, friction angle, tensile strength and compressive strength and global strength and Young's modulus have been obtained from the intact uniaxial compressive strength and classification systems, in this case, *GSI* and the computer program *RocLab* (RocScience, 2005). The factors have been varied in such a way as to resemble the measurements and estimations of such parameters in real preliminary tunnel investigations. This was done with respect to the precision and uncertainty of methods used to estimate/calculate the parameters. The variation of virgin stress state has been done by using a number of stress versus depth expressions presented in the literature

In the conceptual analysis it was shown that the interval of *GSI* has a great impact on deformations, tangential stresses at and close to the boundary and the extent of the area of plasticity. As shown in Edelbro (2007) the tables, used for *GSI*, may be experienced as inaccurate as they are very basic. This means that the results from a certain site will be subjective and may vary depending on the persons who classify the rock mass.

The area of plasticity in the models showed a fairly similar pattern for all varied factors. Mainly tensile yielding occurred, and took place in the walls and abutments of the tunnel, and propagated into the rock mass. Although, it is impossible to estimate exactly how this affects the stability of the tunnel, it can be assumed that a larger area of plasticity is less favourable than a small area, especially if it reaches to the ground surface. When the area where tensile stresses, or very low compressive stresses, increases, the risk of fallouts may increase. Furthermore, failure of the upper parts of the walls (areas where all stresses are tensile in the elastic analyses) may undermine the abutment, and may lead to larger fallouts.

Since the confining stress is very low, and failure occurs mainly in the form of tensile yielding, the Mohr-Coulomb criteria is vulnerable in accurately capturing the yield process, since it is based on simultaneous mobilization of friction and cohesion (Saiang and Nordlund,

2007). The strength of the rock mass will therefore depend more on the tensile and cohesive strength, than on friction, at least in a continuum model and assuming that intact rock bridges are present.

Since the tensile strength of the rock mass is calculated from the intact uniaxial compressive strength, (σ_{ci}), and GSI , variations in GSI and σ_{ci} will give variations in the tensile strength, which leads to variations in the area of plasticity. This is a rough simplification and the true tensile strength of the rock mass is probably not equal to the calculated tensile strength. The calculated value is an average for the whole rock mass. The true tensile strength is a combination of the intact tensile strength for all points where no natural weaknesses are present. If a discontinuity is present, the true tensile strength is very low or zero depending on filling, intact rock bridges and length of the discontinuity. Moreover, the tensile strength is direction dependent; this includes also the residual tensile strength, which was discussed earlier in Chapter 4. Perpendicular to a discontinuity, the tensile strength is zero, while it may be close to the intact tensile strength parallel to the discontinuity. However, to get this kind of behaviour in numerical models, all discontinuities must be present in the model. Since the structural geology of a rock mass is unique at every cross-section this kind of behaviour could not be studied in the conceptual analysis.

For the conceptual analyses, the only factor that truly indicated instability was the existence of large geological structures. This was so for relatively flatly dipping discontinuities ($\text{dip} \leq 30^\circ$), although no analyses were conducted to determine whether there is a relation between the dip angle and the friction angle. If this is the case, it may be possible to judge the stability by comparing the dip angle and the friction angle. For all other factors in the conceptual analysis, it could only be said that the factors have more or less impact on the stability. It seems that a shallow tunnel in hard rock without larger discontinuities is rather stable, and if excavated and reinforced properly, there should not be any major instability problems.

At shallow depths the induced stresses can be very complex due to the geological conditions and the highly anisotropic state of stress. Anisotropy has not been studied in the conceptual analysis, but can probably affect the stability.

The deformation of the rock mass that can be considered as a continuum surrounding a shallow tunnel appears mainly as heaving of the ground surface and tunnel roof and convergence of the tunnel walls. However, the analyses in this thesis does not show when the deformations occur relative to the tunnel face since the models are 2-dimensional. The reinforcement of the tunnel will be affected differently depending on when it is installed. If shotcrete, for example, is installed immediately after excavation, there is a risk that tensile

stresses will be transferred through the rock-shotcrete interface in the walls and abutments of the tunnel. Compressive stresses might be induced in the tunnel roof. Since this work did not consider the face advance, no recommendation on when reinforcement should be installed can be made.

6.2 Case Study

The data for the Shuttle station 2 analyses comes from mapping, measurements and estimations conducted before and during the construction and excavation of the tunnel. Some of the data was less reliable, like the value for the intact uniaxial compressive strength, σ_{ci} , which comes from a simple estimation of R -values (Brown, 1981) along the tunnel. This is a very rough way of estimating σ_{ci} and data from uniaxial compressive tests or point load tests would have been preferred. Two values of σ_{ci} were chosen for the analyses. The lower value led to collapse of the tunnel. The uniaxial compressive strength did not show great importance in the conceptual analysis but showed to have a major effect on Shuttle station 2. A probable reason why Case 2 fails is that the surface loads induce shear failure in the clay filled structure and a bending failure of the left side of the overburden which leads to tensile yielding over the left abutment, see Figure 6.1. The same kind of behaviour can be seen in the models that include the clay filled structure, surface loads and a low state of stress but with a more limited zone of bending failure in the left part of the overburden. When the intact uniaxial compressive strength is reduced, the tensile strength of the rock mass is also reduced, and this area of tensile yielding reaches all the way from the ground surface to the tunnel roof. The cohesion and friction of the rock mass are also reduced when the intact uniaxial tensile strength is reduced. This, along with the weakened rock mass due to tensile yielding leads to a shear failure, induced by the surface load F_2 , from the load to the left abutment. The whole roof is then pushed down by gravity and the surface load.

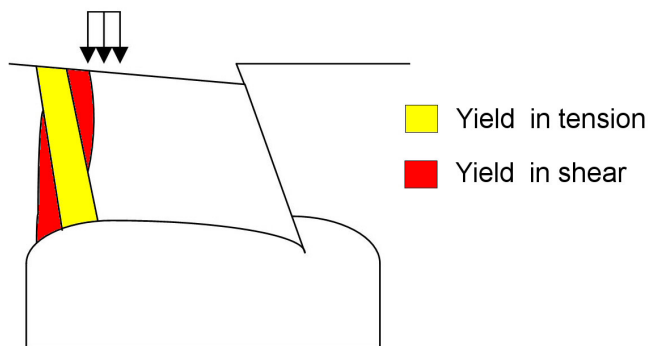


Figure 6.1 A simplification of the failure mechanism of Case 2.

The reason why the intact uniaxial compressive strength has such an impact on the stability of Shuttle station 2, while it has little impact on the conceptual analysis may be due to a variety of many reasons. Firstly, the two values of the uniaxial compressive strength chosen for Arlandabanan differed 50% while they only differed 20% in the conceptual analysis. Moreover, the Arlandabanan values were considerably lower than the values used in the conceptual analyses. The accuracy needed in estimation of data is probably more important for low strength values. Finally, Arlandabanan contained surface loads and anisotropy and a discontinuity while the conceptual analysis did not.

The cross-section used in the analysis was chosen because it included both convergence measurements and extensometer measurements. However, a smaller part of the pillar was left for an elevator shaft in the cross-section, which makes it a 3D problem. Because all earlier analyses were conducted with 2D, this case was also analysed in 2D, and the elevator shaft was neglected. This is a source of error for the pillar extraction stage (stage 2).

Case 3 (no mica schist) and Case 4 (clay filled structure) showed similar behaviour. From this it can be concluded that geological structures and anisotropy can be dealt with in the same way, and that the angle of the weaknesses are the most important parameter.

As for the conceptual analysis, it can be seen that low compressive and/or tensile stresses are present in the walls and in some cases, in the abutments of the tunnel, while they are higher in the roof. The area of plasticity in the conceptual models as well as in the models of Arlandabanan show that tensile failure occurs mostly in the walls and abutments of the tunnel. This can especially be noticed in the right pilot tunnel, N2. When the theoretical and measured cross-sections are studied, tendencies can be seen that support these analysis results. There is a tendency that the theoretical and measured tunnel section differ most in the right side of the tunnel, see Figure 6.2.

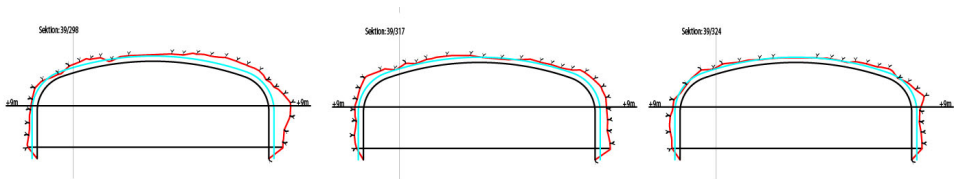


Figure 6.2 Theoretical and measured cross-sections 39/289, 39/317 and 39/324 from Shuttle station 2.

There is a difference between the measured values of the deformations from the tunnel excavation and those calculated in the analyses of the tunnel. The deformations measured by the extensometers and the corresponding deformations obtained in the analyses shows the largest difference, see Figure 5.22. When the pilot tunnels were excavated, there was a difference between the reading of extensometer 2 and the corresponding deformation obtained by numerical analysis. Case 7, with higher horizontal virgin stresses than those measures close to the studied cross-section shows deformations similar to those measured by extensometer 2. Heaving of the tunnel roof inducing tensile failure of the pillar was also observed when the pilot tunnels were excavated. This is also seen in Case 7, see Figure 5.20. One explanation is that the interpretation of the stress measurements was too conservative and that higher stresses are present in addition to the fact that the surface loads may have been overestimated when they were calculated for 2D conditions.

The extensometer measurements of stage 2, the pillar extraction, see Figure 5.23, resemble Case 3 (no mica schist orientation). This shows that the significance of the mica schist might have been over-exaggerated.

6.3 Summary

Yielding in points of the rock mass does not have to mean a stability problem for a tunnel. The behaviour of the tunnel is well described by the tangential state of stress and the deformations. However, it is difficult to translate the results from the conceptual analyses and the Arlandaban case into statements about the stability. It is known that no major instability problems occurred while constructing Shuttle station 2.

Several well known and frequently used tools in rock mechanics have also been tested in this work. First of all, *GRC* (Ground reaction curve) was planned to be used as a way to analyse the stability and behaviour. However, this proved to be impossible, since all models in the conceptual analysis experienced heaving of the overburden and *GRC* is founded on the idea of tunnel roof convergence. Moreover the Factor of safety (*FOS*) function in *FLAC* was also tested. This function calculates a relation between the rock mass strength of the existing tunnel, and the rock mass strength when the tunnel collapses. This proved not to work since the strength had to be reduced to such a degree that the rock mass failed in compressive failure due to the virgin state of stress before the tunnel was excavated.

7 CONCLUSIONS

Based on the conceptual analysis and the case study it can be concluded that:

- The failure that occurred in the conceptual analyses and the case study is tensile which means that the tensile strength of the rock mass is an important factor. Furthermore, the behaviour and stability of a shallow tunnel is more sensitive to variations in the residual tensile strength than the peak tensile strength.
- The structural geology of the rock mass is the most important factor to consider when analysing the behaviour and stability of a shallow tunnel. Moreover, the behaviour and stability of a shallow tunnel is most sensitive to variations in the orientation of the structures. Since the tensile strength of the rock mass depends strongly on the tensile strength of discontinuities, the spacing and the number of joint sets are of great importance.
- The behaviour and stability of a shallow tunnel is highly sensitive to variations of the virgin state of stress. Intermediate stresses are favourable. Low stresses give lower tangential stresses in the boundary of the tunnel, which increases the risk of fallouts. Very high horizontal stresses gives larger deformations and greater tensile stresses in the area of the abutments of the tunnel, under the assumption that the rock mass can be considered as a continuum.
- Since the rock mass strength (compressive as well as tensile) is determined with the help of *GSI* and the intact uniaxial compressive strength, σ_{ci} , it is important to be able to determine these parameters as accurate as possible. *GSI* is more uncertain than the intact uniaxial compressive strength, at least when the latter has been measured with uniaxial compressive tests or point load tests. This means that *GSI* is a more critical parameter in stability analysis.
- It is equally important to know the extent and reduction of strength of the weaknesses of the rock mass (weathering, blast damage etc.) and the rock mass strength.
- The greatest risk of instability of a shallow tunnel, in a rock mass without larger geological structures, is fallouts from the walls and abutments of the tunnel.
- It is recommended that parameter studies are used to investigate the sensitivity of the factors that have larger impact on the behaviour and stability and/or are considered to be more uncertain when conducting a stability analysis of a shallow tunnel.

A general overview over how sensitive the behaviour and stability are to variations of the different factors based on the results from the conceptual analyses and the case study is presented in Table 7.1. The impact of the variations of the different factors has on the instability indicators are divided into three categories, high, medium and low impact.

Table 7.1 The significance level that the different parameter groups have on the different instability indicators.

	σ_ϕ , tunnel boundary	Deformation of tunnel boundary	Subsidence / heaving	Area of Plasticity	Extent of tensile stresses
Virgin state of stress	High	High	High	High	High
σ_{ci}	Medium	Medium	Medium	Medium	-
<i>GSI</i>	High	High	High	High	-
σ_t	High	Medium	High	High	-
Over burden	High	High	High	Medium	Medium
<i>E</i>	Low	Medium	Medium	Low	-
<i>c/φ</i>	Low	Low	Low	Low	-
Weathering	High	Medium	Low	Low	-
<i>EDZ</i>	High	Low	Low	Low	-
Structural geology	High	High	High	High	-
Surface loads	Medium	High	High	Medium	-
Tunnel size and geometry	Medium	High	High	High	-

8 RECOMMENDATIONS FOR FUTURE WORK

This project has shown that stability analyses using software based on the assumption of continuous conditions cannot tell whether shallow underground constructions in hard rock are stable or not. Furthermore, the project revealed some issues which need to be further studied in order to improve the understanding of stability analyses of shallow tunnels. It is recommended that a methodology for geomechanical modelling of shallow tunnels is developed, consisting of

- recommendations for collecting of data,
- a suitable failure criteria,
- proper instability indicators.

Since using *GSI* and σ_{ci} together with *RocLab* was proven to be important, and at the same time fairly uncertain, it is recommended that more research is done in this area. Moreover, the Mohr-Coulomb failure criteria might not be suitable for analysis of shallow tunnels, since tensile failure is the main type of failure of shallow tunnels and the Mohr-Coulomb failure criteria is constructed for mainly compressive failure. This goes hand in hand with the development of more suitable instability indicators for shallow tunnels. The indicators in this work could not quantify the stability of the tunnel in a satisfactory manner.

9 REFERENCES

Amadei, B., Stephansson, O. (1997) *Rock stress and its measurement*. London: Chapman and Hall.

Banverket (2002) *BV tunnel*. Standard BVS 585.40.

Barton, N., By, T.L., Chryssanthakis, L., Tunbridge, L., Kristiansen, J., Löset, F., Bhasin, R.K., Westerdahl, H., Vik, G. (1992) *Comparison of prediction and performance for a 62 m span sports hall in jointed gneiss*. Proc. 4th. in. rock mechanics and rock engineering conf., Torino. Paper 17.

Barton, N., Löset, F., Lien, R., Lunde, J. (1980) *Application of the Q-system in design decisions*. In *Subsurface space*, (ed. M., Bergman), 2, pp. 553-561. New York: Pergamon.

Barton, N.R., Lien, R., Lunde, J. (1974) *Engineering classification of rock masses for the design of tunnel support*. *Rock Mech.*, 6, pp. 189-239.

Berg, S. (2005) *Bergspänningsmätningar på litet djup*. Master thesis 2005:426, Luleå University of Technology, Luleå, ISSN:1402-1617(in Swedish).

Bergsten, K.,Å., Ljungren, C., Söder, P.E., Wikman, A. (1995) *Mätrapport, Bergspänningsmätningar på Arlanda, Arlandabanan, flygstationsområdet*. Vattenfall Hydropower, Internal report (in Swedish).

Bieniawski, Z.T. (1974) *Geomechanics classification of rock masses and its application in tunnelling*. In: *Proceedings of the 3rd International Congress on Rock Mechanics*, Denver, pp. 27-32.

Bieniawski, Z.T. (1976) *Engineering classification in rock engineering*. In: *Proceedings of the Symposium on Exploration for Rock Engineering*, Johannesburg, pp. 97-106.

Bieniawski, Z.T. (1989) *Engineering rock mass classifications*. John Wiley & Sons, New York.

Boussinesq, J. (1883) *Application des potentiels à l'étude de l'équilibre et du mouvement des solides élastiques*. Paris, Gauthier – Villars.

Brown, E.T., Editor (1981) *Rock Characterization, Testing and Monitoring. ISRM Suggested Methods*. Pergamon Press, Oxford, 211 p.

Chang, Y., Hansen, L., Söder, P.E., Hässler, L. (1996) *Arlandabanan, Projektunderlag för permanent bergförstärkning*. Internal report, Linkprojektörerna, Vattenfall Hydropower, NCC Teknik, SIAB Teknik, Tyréns Infrakonsult, (in Swedish).

Chang, Y., Hellstadius, K. (1998) *Shuttle station 2, Arlandbanan – bergprojektering och uppföljning*. In: Bergmekanikdagen 1998, SveBeFo, Stockholm (in Swedish).

Diederichs, M.S. (1999) *Instability of hard rock masses: The role of tensile damage and relaxation*. Doctoral Thesis, University of Waterloo, Waterloo, Ontario, Canada.

Edelbro, C. (2004) *Evaluation of rock mass strength criteria*. Licentiate Thesis 2004:72, Luleå University of Technology. ISSN:1402-1757

Edelbro, C., Sjöberg, J., Nordlund, E. (2007) *A quantitative comparison of strength criteria for hard rock masses*. Tunneling and Underground Space Technology 22 (2007), pp. 57-68.

Edelbro, E. (2003) *Rock mass strength – a review*. Technical report 2003:16, Department of Civil and Mining Engineering, Division of Rock Mechanics, Luleå university of Technology. ISSN:1402-1536

Emsley, S., Olsson, O., Stenberg, L., Alheid, A-J., Falls, S. (1997) *ZEDEX – A study of damage and disturbance from tunnel excavation by blasting and tunnel boring*. Stockholm (Swedish Nuclear and Waste Management CO).

Fairhurst, C. (1986) *In-situ stress determination – an appraisal of its significance in rock mechanics*. In Proc. Int. Symposium on Rock Stress and Rock Stress Measurements, Stockholm, Centek Publ., Luleå, pp 3-17.

Fredriksson, A. (2006) Personal communication

Gaziev, E., Erlikhman, S. (1971) *Stresses and strains in anisotropic foundations*. In: Proceedings Symposium on Rock Fracture, ISRM (Nancy), Paper II-1.

Grimstad, E., Barton, N. (1993) *Updating the Q-system for NMT*. In: Proceedings of the First International Symposium on Sprayed Concrete, Fagernes, Norway 1993, Norwegian Concrete Association, Oslo.

Hoek, E., Brown, E.T. (1980) *Underground excavations in rock*. Revised first edition. London: Institution of Mining and Metallurgy.

Hoek, E., Kaiser, P.K., Bawden, W.F. (1995) *Support of underground excavations in hard rock*. A.A. Balkema, Rotterdam, Brookfield.

Hoek, E., Carranza-Torres, C., Corkum, B. (2002) *Hoek-Brown failure criterion – 2002 edition*. In: Proceedings of the 5th North American Rock Mechanics Symposium and 17th Tunnelling Association of Canada Conference: NARMS-TAC 2002, July 7-10, University of Toronto, pp. 267-271.

Hudson, J.A., Cooling, C.M. (1988) *In situ rock stresses and their measurement in the UK – Part I. The current state of Knowledge*. In: Int. J. Rock Mech. Min. Sci. & Geomech. Abstr., Vol 25, pp. 363-70.

Itasca (2005a) *FLAC* version 4.0. Manual. Minneapolis, ICG.

Itasca (2005b) *UDEC* version 4.0. Manual. Minneapolis, ICG.

Jing, L. (2003) *A review of techniques, advances and outstanding issues in numerical modelling for rock mechanics and rock engineering*. In: Int. J. Rock Mech. & Min. Sci., Vol 40, pp. 283-353.

Leijon, B.A. (1989) *Relevance of point wise rock stress measurements – an analysis of overcoring data*. In: Int. J. Rock Mech. Min. Sci. & Geomech. Abstr., vol 26, pp. 61-8.

Malmgren, L. (2005) *Interaction between shotcrete and rock – experimental and numerical study*, Doctoral thesis 2005:48, Luleå University of Technology. ISSN:1402-1544.

Martino, J.B. (2002) *The excavation damage zone in recent studies at the URL*, The 2002 international EDZ workshop, The excavation damage zone – causes and effects. Edited by J.B. Martino, Atomic Energy of Canada Limited.

Mindlin, R.D. (1939) *Stress distribution around a tunnel*. Transactions American Society of Civil Engineers, reprinted from Proceedings of the American Society of Civil Engineers, Paper no. 2082.

Mindlin, R.D. (1948) *Stress distribution around a hole near the edge of a plate under tension*. Proceedings of the Society for Experimental Stress Analysis V, No. 2, pp. 56-68.

Palmström, A. (1995) *RMi – A rock mass characterisation system for rock engineering purposes*. Ph.D. Thesis, University of Oslo, Norway.

Poulos, H.G., Davis, E.H. (1974) *Elastic solutions for soil and rock mechanics*. New York, John Wiley & Sons.

Ran, J.Q., Passaris, E.K.S., Mottahead, P. (1994) *Shear sliding failure of the jointed roof in laminated rock mass*. Rock mechanics and Rock Engineering, 27 (4), pp. 235-51.

Rock Engineering group (1996) *Examine^{2D} version 6.0, User's guide*. University of Toronto.

RocScience (2006). Program: "RocLab". URL:
<http://www.rocsience.com/products/roclab.asp>

Saiang, D., Nordlund, E. (2006) *Continuum Analysis of Shallow Tunnels in Brittle Rock with Damaged Rock Zone Around Their Boundaries – A Parameter Study*, Luleå University of Technology, Sweden, To be published.

Serafim, J.L., Pereira, J.P. (1983) *Considerations of the geomechanical classification of Bieniawski*. Proceedings Int. Symposium in Engineering Geology and Underground Construction (Lisbon), 1(II), pp. 33-42. Lisbon, SPG, LNEC.

Stephansson, O. (1993) *Rock stress in the Fennoscandian shield*, In: Comprehensive Rock Engineering (ed. J.A. Hudson), Pergamon Press, Oxford, Chapter 17, Vol 3, pp. 445-59.

Stille, H., Eriksson, M., Nord, G. (2004) *Kompendium i bergmekanik*. The Royal Institute of Technology, Stockholm (in Swedish).

Stille, H., Groth, T., Fredriksson, A. (1982) *FEM-analysis of rock mechanical problems with JOBFEM*, Stiftelsen Bergteknisk Forskning – BeFo 307:1, Stockholm.

Stimpson, B., Ahmed, M. (1992) *Failure of a linear Voussoir Arch: a laboratory and numerical study*. Canada Geotech. J., 29, pp. 188-194.

Zoback, M., et al. (1989) *Global patterns of tectonic stress*. Nature, vol 341, pp. 291-8.

